ABSTRACT

POOLE, JOHN OWEN. A Dynamically Polarized Deuteron Target. (Under the direction of Christopher R. Gould.)

A dynamically polarized deuteron target was constructed at the Triangle Universities Nuclear Laboratory for low energy polarized neutron transmission experiments. Theoretical calculations suggested a measurement of the longitudinal spin-dependent total $\vec{n} - \vec{d}$ cross section difference, $\Delta\sigma_L$, would provide evidence of three nucleon force effects.

The target was operated at a temperature of 0.5K with a recirculating ^{3}He evaporation refrigerator and a 2.5T split-pole superconducting magnet which can be mechanically mounted to produce either a longitudinally or tangentially polarized target relative to the beam momentum. The target material consisted of a cube of volume 2.7 mℓ of either partially (D6) or fully (D8) deuterated 1,2-propanediol chemically doped with EHBA-Cr^V to provide the paramagnetic centers for dynamic nuclear polarization with microwaves in the region of 69GHz. Polarization was monitored during the experiment using a continuous wave NMR Q-meter capable of both phase sensitive and magnitude detection. A PC running LabVIEW controlled data acquisition, frequency sweep of the digital frequency synthesizer and a novel background cancellation technique. A pre-recorded background signal was subtracted on a channel by channel basis before the NMR spectrum was sampled.

Polarization was extracted from the NMR spectra by a fit to a theoretical lineshape. Effects of dispersion and signal distortion were considered. The equal spin temperature (EST) hypothesis was used to determine deuteron polarization indirectly by measuring the polarization of the residual protons in the partially deuterated sample. Efforts to improve the system stability and signal-to-noise ratio are discussed along with numerical methods, fitting strategy and evaluation of uncertainties.

Positive and negative deuteron polarizations on the order of 13$\pm$2% were achieved when the target was used for preliminary measurements of $\Delta\sigma_L$, for E$_n$ between 5 and 12 MeV. Future work is discussed in light of these results.

A Dynamically Polarized Deuteron Target

by
John Owen Poole

A dissertation submitted to the Graduate Faculty of
North Carolina State University
in partial fulfillment of the
requirements for the Degree of
Doctor of Philosophy

Physics

Raleigh, North Carolina

2007

APPROVED BY:

Christoper R. Gould, Chair	Paul R. Huffman
Albert Young	Mohamed A. Bourham

Biography

Education

B.S. Electrical Engineering, Clemson University, 1995

Memberships

American Physical Society

Institute of Electrical and Electronics Engineers

Publications

R. Singh, J. O. Poole, K. F. Poole, S. D. Vaidya, "Fundamental Device Design Considerations in the Development of Disruptive Nanoelectronics" J. Nanosci. Nanotech. Vol. 2 No. 3/4, pp. 363-368, June/Aug. 2002.

D. M. Markoff, R. D. Foster, C. R. Gould, D.G. Haase, J. O. Poole, B. W. Raichle and W. Tornow, "Polarized Neutron-Polarized Deuteron Measurements with the TUNL Dynamically Polarized Deuteron Target", Proc. 9th Intl. Workshop on Polarized Sources and Targets, ed. V. Derenchuk and B. von Przewoski (World Scientific, NY, 2002). pp. 344-348.

Contributed Abstracts and Oral Presentations

J. O. Poole, C. R. Gould, D. G. Haase, B. W. Raichle, J. R. Walson, M. L. Seely and W. Tornow. "Nuclear magnetic resonance system for a polarized deuteron target.", Bull. Am. Phys. Soc. **42** 1797 (1997).

J. O. Poole, D. M. Markoff, C. R. Gould, D. G. Haase and W. Tornow, "Development of a dynamically polarized D target at TUNL.", Bull. Am. Phys. Soc. **43** 1541 (1998).

J. O. Poole, D. M. Markoff, C. R. Gould, D. G. Haase and W. Tornow, "Development of a dynamically polarized D target at TUNL.", Bull. Am. Phys. Soc. **44** 1519 (1999).

Co-Authored Abstracts

D. M. Markoff, J. O. Poole, C. R. Gould, D. G. Haase, B. W. Raichle, W. Tornow and D. E. Gonzales Trotter, "Measurement of the spin-dependence of the $\vec{n}-\vec{d}$ interaction at MeV energies.", Bull. Am. Phys. Soc. **43** 1554 (1998).

D.M. Markoff, J. O. Poole, C. R. Gould, D. G. Haase, B.W. Raichle and W. Tornow. "Measurement of the spin-dependent longitudinal total cross section difference $\Delta\sigma_L$ in the $\vec{n}-\vec{d}$ system.", Bull. Am. Phys. Soc. **44** 1407 (1999).

R. D. Foster, C. R. Gould, D. G Haase, D. M. Markoff, J. Messimore,G. Palmquist, E. Pearson; J. O. Poole and W. Tornow, "An upgrade of the TUNL dynamically polarized deuteron target.", Bull. Am. Phys. Soc. **44** 11 (1999).

R. D. Foster, D. G. Haase, C. R. Gould, D. M. Markoff, J. O. Poole and W. Tornow, "Upgrade and testing of the TUNL dynamically polarized deuteron target.", Bull. Am. Phys. Soc. **46** 14 (2001).

D. M. Markoff, R. D. Foster, C. R. Gould, D.G. Haase, J. O. Poole, B. W. Raichle and W. Tornow, "Polarized Neutron-Polarized Deuteron Measurements with the TUNL Dynamically Polarized Deuteron Target", Proc. 9th Intl. Workshop on Polarized Sources and Targets, Nashville, IN, September, 2001.

Acknowledgements

I would like to thank Dr. Gould for being my advisor and for seeing the work through to completion. I would also like to thank Dr. Huffman and Dr. Bourham for their helpful suggestions to improve the document and Dr. Young for his guidance in the data analysis. I would like to thank my parents for their support.

Contents

List of Figures viii

List of Tables x

1 Introduction **1**

1.1 Motivation 1

1.1.1 Refinement of NN potential models 2

1.1.2 Three Body Forces and the Three Body Problem 2

1.1.3 Effective Field Theories 3

1.2 Spin Polarized Nuclei 4

1.3 Polarized Target Technology 5

1.4 Experimental Setup 7

2 Nuclear Scattering Experiment **10**

2.1 Atomic Beam Polarized Ion Source 10

2.1.1 Dissociator 11

2.1.2 Transition Units 11

2.1.3 ECR Ionizer 13

2.1.4 Cesium Oven 13

2.1.5 Spin Filter Polarimeter 14

2.1.6 Wien Filter 15

2.2 Tandem Van de Graaff Accelerator 16

2.3 Beam Transport 17

2.4 Polarized Neutron Production 18
2.5 Neutron Detection 21
2.5.1 Monitor Detector 21
2.5.2 Main Detector 22
2.6 Theory of Measurement and Experimental Protocol 23

3 Polarized Target **25**
3.1 Cryogenic Systems 25
3.1.1 Refrigerator and Cryostat 25
3.1.2 Thermometry 30
3.2 Magnet 31
3.3 Target Material 32
3.4 Dynamic Nuclear Polarization 34
3.4.1 Principles of DNP 34
3.4.2 Microwave System 37

4 Target NMR Polarimetery **40**
4.1 NMR Principles 41
4.2 NMR Hardware and Software 42
4.2.1 NMR Coil and Lambda Cable 43
4.2.2 Signal Quality and Noise 45
4.2.3 Detection of the NMR Signal 46
4.2.4 Hardware Background Subtraction 47
4.3 Extracting the Polarization 48
4.3.1 Area Methods 48
4.3.2 Fit to Theoretical Lineshape 49
4.4 Data Analysis 57
4.4.1 Fit Data 57
4.4.2 Equal Spin Temperature Hypothesis 66

4.5 Observations and Conclusions 68

5 Results and Conclusions **71**

5.1 Nuclear Physics Results 71

5.2 Future Work 75

5.3 Concluding Remarks 78

Bibliography **79**

Appendices **85**

Appendix A. Fortran Code **86**

Appendix B. NMR "Best Fit" Data **125**

Appendix C. Results of NMR Bulk Data Analysis **130**

List of Figures

Figure 1.1 Simplified diagram of the experimental setup. 8

Figure 2.1 The atomic beam polarized ion source. 11
Figure 2.2 Simplified Breit-Rabi diagram for deuterium. 12
Figure 2.3 Low energy (LE) beam transport system. 18
Figure 2.4 High energy (HE) beam transport system. 19
Figure 2.5 Polarized neutron production cell. 21
Figure 2.6 Polarized target and detector setup. 22

Figure 3.1 Polarized target cryogenic system. 28
Figure 3.2 Simplified diagram of the ^{3}He gas handling system. 29
Figure 3.3 Electron spin resonance (ESR) spectrum of doped propanediol. . . . 36
Figure 3.4 Spin temperature theory illustrating mechanism of dynamic nuclear polarization (DNP). 37
Figure 3.5 Diagram of microwave system for dynamic nuclear polarization. . . . 38

Figure 4.1 Block diagram of front end of NMR analog electronics. 43
Figure 4.2 Deuteron quadrupole energy shift. 50
Figure 4.3 Components of the D8 lineshape model. 53
Figure 4.4 Dispersive and absorptive components of the deuteron NMR signal. 54
Figure 4.5 NMR background. 58
Figure 4.6 Deuteron NMR signal before and after residual background subtraction. 59

Figure 4.7 Typical D8 NMR datasets. 61
Figure 4.8 Full fit to "best data". 62
Figure 4.9 χ^2 versus target polarization. 64
Figure 4.10 The relationship between proton and deuteron polarization given by the EST hypothesis. 68
Figure 5.1 Preliminary measurements of $\Delta\sigma_L$ for the $\vec{n}$-$\vec{d}$ system. 72

List of Tables

Table 3.1 Typical operating conditions for refrigerator. 31

Table 4.1 D8 model parameters for full fit to "best data". 65

Table 4.2 Uncertainty in target polarization. 65

Table 4.3 Sensitivity of target polarization to model parameter variation. 66

Table 4.4 Summary of EST hypothesis data for partially deuterated (D6) target. 67

Chapter 1

Introduction

Progress in nuclear physics relies heavily on the interaction between theory and experiment. Dynamics at the nuclear level are dominated by the strong nuclear force which has been studied through observation of nuclear structure, nuclear reactions and scattering experiments. The spin degree of freedom of the strong nuclear force is a significant factor contributing to the difficulty of developing a comprehensive model[1, 2, 3].

Recent advances in both theoretical formalism and computational techniques have made possible high precision calculations of three nucleon scattering observables which can be tested experimentally[4, 5, 6]. Polarized nuclear beams and targets have unequally populated spin states which allows the spin-dependence of the nuclear force to be studied. The interest in low energy, few-body nuclear systems provided the motivation to modify the TUNL polarized proton target[7, 8] to produce a polarized deuteron target suitable for polarized neutron transmission experiments with energies below 20MeV.

1.1 Motivation

The Polarized Target Group at TUNL has successfully measured both $\Delta\sigma_T$ and $\Delta\sigma_L$ for the $\vec{n} - \vec{p}$ system with a dynamically polarized proton target[7, 8]. Adapting the experimental setup to handle a polarized deuteron sample builds on the experience and protocols

developed previously, while the $\vec{n} - \vec{d}$ system provides the simplest non-trivial few-body system. This opens up a rich new set of dynamics which will aid in the careful study of the strong nuclear force. No measurements of $\Delta\sigma_L$ for the $\vec{n} - \vec{d}$ system in this important energy range had been previously reported at the time this work was commenced.

1.1.1 Refinement of NN potential models

Modern realistic high precision nucleon-nucleon (NN) potential models, such as Nijmegen-I, Nijmegen-II[9], Argonne AV18[10] and CD-Bonn[11, 12], based on meson exchange have achieved considerable success in reproducing the NN dataset with a χ^2 per degree of freedom close to 1[9, 13]. This success comes at the expense of roughly 45 free parameters which are determined by a fit to an extensive database of phase-shift data. While quantitatively accurate, these semi-phenomenalogical models have many parameters which have no physical interpretation and ultimately do not lead to a better understanding of the nuclear force at a fundamental level. Continued refinement of these useful computational models requires additional high quality experimental data.

1.1.2 Three Body Forces and the Three Body Problem

The simplest nuclear scattering interaction involves two nucleons. For these systems where the potential governing the interaction is known, an analytical expression for the outcome can be derived. For three or more interacting bodies, there is no analytical solution but using the Fadeev formalism gives a so-called "exact" numerical solution with an error below 1%[14]. For large numbers of nucleons, statistical methods and the shell model have been very successful in understanding nuclear structure and aggregate behavior of collections of nucleons but do not shed much light on the nature of the NN interaction itself[1, 3].

With a binding energy of 2.2 MeV, the deuteron can be considered a quasi-free proton and neutron. The choice of a polarized neutron beam removes effects from the Coulomb interaction which would add a significant contribution to the elastic scattering cross section at these energies.

A three body force results where the quantum numbers describing the state of all three interacting nucleons must be considered simultaneously and the result cannot be duplicated by considering the superposition of forces where particles are taken two at a time[4]. This concept can easily be generalized to N interacting bodies although the strength is generally believed to fall off rapidly for N $>$ 2.

The fact that current NN potential models including only two nucleon force (2NF) adequately describe a wide range of phenomena is evidence that three nucleon force (3NF) is relatively small[4]. At the same time, significant unexplained discrepancies between theory and experiment for several few body nuclear systems exist. The best known example is the underestimate of the triton binding energy by as much as 0.9MeV[15]. In 1933, Wigner recognised that this could only be explained by the more complicated dynamics[16] of which 3NF are now widely believed to be the most likely candidate.

Calculations by Witala, et. al.[5] show that the spin dependent longitudinal cross section difference, $\Delta\sigma_L$ for the $\vec{n}-\vec{d}$ system provides evidence of 3NF effects at the 10% level. These calculations are performed using several modern NN potential models both with and without a Tucson-Melbourne 3NF adjusted to achieve correct binding energy for the triton. It is interesting to note that when the 3NF is adjusted to reproduce the triton binding energy, all NN potential models considered converge in their predictions for $\Delta\sigma_L$ over a wide energy range. The calculated zero crossing of $\Delta\sigma_L$ at 11.8 MeV with NN interactions alone and 12.2 MeV with the TM 3NF, makes it a strong candidate in the search for an experimentally testable 3NF effect.

1.1.3 Effective Field Theories

It is now accepted that quantum chromodynamics (QCD) is the underlying theory of the strong force and therefore the fundamental theory governing NN interactions[17]. However, QCD is non-perturbative at energies below 100 MeV and therefore direct calculations of elastic scattering observables in this energy region are not possible. A new class of theories bridges the gap between traditional nuclear physics and the high energy realm of QCD.

Rather than starting with the natural degrees of freedom in traditional nuclear physics, the nucleons and pions, or the quarks and gluons of QCD, these effective field theories (EFT) construct a Legrangian which preserves the relevant symmetries [18]. This effectively freezes out degrees of freedom not responsible for low energy phenomena.

The most successful of these is chiral perturbation theory (χPT) which preserves the (broken) chiral symmetry of QCD[19]. Besides establishing the connection with a first principles approach to the NN interaction, another important consequence is that N-body forces appear naturally rather than as ad-hoc assumptions and, in particular, the strength comes automatically rather than as an arbitrary adjustable parameter[20]. High precision few body experimental data sensitive to 3NF are now necessary to test predictions made with this new theoretical approach.

1.2 Spin Polarized Nuclei

Spin polarized targets and beams are necessary to study the spin dependence of the nuclear force. A polarized nuclear target is a collection of nuclei with an unequal population of the magnetic substates. Nuclei with non-zero intrinsic angular momentum I have $2I + 1$ magnetic substates m_s. For an $I = 1/2$ particle, such as the proton, this gives m_s of $+1/2$ and -1/2 and for an $I = 1$ particle, such as a deuteron, the possible values for m_s are $+1$, 0 and -1. Polarization of an ensemble of spins is formally defined as

$$P = \langle I_Z \rangle / |I| \tag{1.1}$$

where I_Z is the component of the angular momentum relative to some conveniently chosen axis.

The nuclear magnetic moment is given by $\mu = \gamma \hbar I$ where γ is the gyromagnetic ratio, a constant for each nuclei, and $\hbar$ is Planck's constant divided by 2π. Placing the target material in a magnetic field $\vec{B}$ breaks the energy degeneracy of states with different m_s, providing a method to manipulate or probe spin populations by driving transitions with

RF electromagnetic fields tuned to the energy difference. The $\vec{B}$ field defines the z-axis and determines the Zeeman splitting energy.

For an ensemble of spin 1/2 particles, vector polarization, P_z, is given by

$$P_z = \frac{n_+ - n_-}{n_+ + n_-} = \tanh(\mu B/2kT) \tag{1.2}$$

where n_+ and n_- are the number of particles with $m_s = +1/2$ and -1/2, respectively. For an ensemble of spin 1 particles, in addition to the vector polarization P_z, it is possible to define a tensor polarization, or alignment, P_{zz}, which are given by

$$P_z = \frac{n_+ - n_-}{n_+ + n_0 + n_-} = \tanh(\mu B/2kT) \tag{1.3}$$

$$P_{zz} = \frac{1 - 3n_0}{n_+ + n_0 + n_-} = \frac{4\tanh(\mu B/2kT)}{3 + \tanh^2(\mu B/2kT)} \tag{1.4}$$

where or n_+, n_0 and n_- are the number of particles with m_s =+1, 0 and -1, respectively. P_{zz} is a function only of the population of the $m_s = 0$ state. These populations may be obtained from the Brillouin function which allow the polarizations to be expressed in terms of the magnetic field strength, B, the absolute temperature of the spin system, T, and Boltzmann's constant k[21].

1.3 Polarized Target Technology

The ability to construct practical polarized targets for nuclear and high energy physics experiments has followed advances in cryogenics, superconducting magnet technology, the chemistry of target materials and the understanding of dynamic polarization mechanisms[21]. In general, the ideal polarized target would have a high nuclear polarization and cross section for the nuclei studied. These properties can be expressed as a figure of merit where a higher figure of merit corresponds to less time required to obtain a measurement with the same uncertainty. This can be expressed quantitatively as $(P_T x)^2$ where P_T is the target

polarization and x is the target thickness.

A common method of producing nuclear polarization is known as static polarization. Any nuclei with $I \neq 0$ will have a magnetic moment $\mu = \gamma \hbar I$ which will align, either parallel or anti-parallel, with an external magnetic field. The low energy state is energetically preferred but thermal energy tends to drive the system toward the state of maximum entropy where populations would be equalized. This requires large magnetic fields and low temperatures, usually greater than 5T and less than 50mK, respectively. The equilibrium polarization is approached as $1 - e^{-t/T_1}$ where the spin lattice relaxation time constant, T_1, is on the order of hours for solids at low temperature[7, 8]. To reach a maximum steady polarization requires polarization to grow overnight. The strong temperature dependence and low heat capacities of materials at low temperatures make this method very sensitive to beam heating[21]. The maximum achievable polarization is limited by the magnetic moment of the isotope and in practice for many nuclei, including deuterons, it is not possible to obtain sufficiently high polarization for nuclear physics experiments.

The first practical solid polarized proton target was constructed in the early 1960's using rare earth ions and hydrated inorganic salts[21]. These represented an important breakthrough because of a new technique called dynamic nuclear polarization (DNP). In DNP, microwave energy is used to transfer polarization from the highly polarized electronic spin system to the relatively unpolarized nuclear spin system. DNP produces orders of magnitude increases in polarization over static polarization and allows rapid growth and reversal of target polarization. This reduces the requirements on magnetic field strength and temperature and, the higher polarization results in a smaller systematic error associated with the target. The main requirements are a suitable diamagnetic material and paramagnetic dopant. The mechanism of the transfer depends on the type of material used, in particular the relative width of the nuclear and electronic Zeeman levels. The original inorganic salts had a low density of polarizeable protons and were soon replaced by organic alcohols due to a much larger relative density of hydrogen in the latter[21]. Deep inelastic scattering experiments requiring high radiation resistance for long periods require more durable materials

but this is not the case with the experiments run at TUNL. A microwave source and the additional waveguide access to the cryostat also need to be considered for DNP.

To produce the low temperatures required, a recirculating ^{3}He evaporation refrigeration system was used at TUNL. Pumping on liquid ^{4}He reduces temperatures to 1K. Using ^{3}He, it is possible to reach temperatures as low as 300mK. A ^{3}He -^{4}He dilution refrigerator can produce operating temperatures below 10mK. Beam heating considerations must be included in the loading on the refrigeration system.

1.4 Experimental Setup

The Atomic Beam Polarized Ion Source (ABPIS) provides beams of vector and tensor polarized negatively charged deuterons of arbitrary vector and tensor polarization[22]. This beam is accelerated by a 10 MV tandem Van de Graaff accelerator and passes through an analysing magnet which provides energy selection and directs the beam to the target area. A beam of polarized neutrons is produced directly in front of the target via the polarization transfer reaction ^{2}H$(\vec{d},\vec{n})^3$He which has well known polarization transfer coefficients. The neutrons pass through the polarized target and are detected at zero degrees by a liquid scintillator coupled to a photomultiplier tube. Neutron production is normalized to a small plastic scintillator detector located between the neutron production cell and target to compensate for beam dependent neutron asymmetries. The beam and target polarization was reversed at a rate of 10Hz and every eight hours, respectively, to reduce polarization state dependent systematic errors.

Figure 1.1 shows a simplified diagram of the experiment with longitudinally polarized neutrons passing through a longitudinally polarized deuteron target and being detected by a zero degree detector. In terms of measured quantities,

$$\Delta\sigma_L = \frac{2\epsilon_n}{P_n P_t x} \tag{1.5}$$

where ϵ_n is the neutron asymmetry, P_n is the neutron polarizaton, P_t is the deuteron target

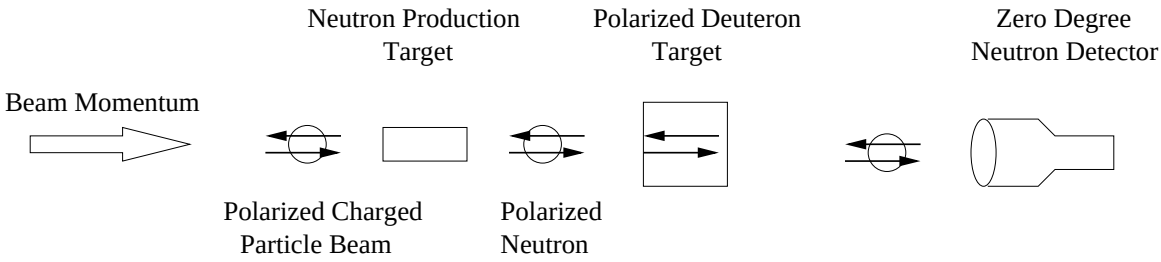

$$\Delta\sigma_L = \left[\ \sigma(\rightarrow\rightarrow) + \sigma(\leftarrow\leftarrow)\ \right] - \left[\ \sigma(\rightarrow\leftarrow) + \sigma(\leftarrow\rightarrow)\ \right]$$

Figure 1.1: Simplified diagram of the experimental setup. The production of polarized neutrons and detection at zero degrees with the solid arrows indicating spin state is shown. The definition of the longitudinal cross section difference, $\Delta\sigma_L$, is represented graphically.

polarization and x is the target thickness.

At the start of the project, the largest uncertainty in measured quantities needed to calculate the polarization observable $\Delta\sigma_L$ was associated with the target polarization. Much of the effort in the modification of the target was therefore devoted to the nuclear magnetic resonance (NMR) system used to monitor the target in real time and the off-line analysis necessary to extract the polarization. This proved much more challenging for deuteron NMR than for proton NMR owing primarily to the much smaller size of the deuteron NMR signal. The measurement of an absolute polarization with NMR, which was previously used to measure relative changes in the target polarization, placed additional requirements on the analysis of the NMR data.

The TUNL experiment used a target of either partially (D6) or fully (D8) deuterated 1,2-propanediol doped with EHBA-Cr^V complex in a 2.5T magnetic field and operated at 0.5K. Under these conditions an average deuteron vector polarization $P_z = 13 \pm 2\%$ was obtained with a microwave frequency of approximately 69GHz. Preliminary measurements of $\Delta\sigma_L$ for the $\vec{n} - \vec{d}$ system have been performed for neutron energies E_n = 5.0, 6.9, 8.9 and 12.3 MeV. The discrepancies with theoretical predictions are discussed. This experience laid the groundwork for future measurements and provided the insight required to proceed

with the upgrade of the refrigeration system. In order to increase the target polarization by reducing the operating temperature, the decision was made to upgrade to a dilution refrigerator for future work[23].

Chapter 2

Nuclear Scattering Experiment

The experimental measurement of $\Delta\sigma_L$ requires a source of variable energy spin-polarized neutrons, a polarized deuteron target and neutron detectors. The Atomic Beam Polarized Ion Source (ABPIS), the tandem Van de Graaff electrostatic accelerator, along with the beam transport and production of the polarized neutrons through the ^{2}H($\vec{n}$,$\vec{d}$)^{3}He polarization transfer reaction will be discussed. The spin filter polarimeter (SFP) was used to measure charged particle polarization which is used to calculate neutron polarization. A discussion of neutron detection and the associated data acquisition electronics will be followed by a brief overview of the theory of the measurement of $\Delta\sigma_L$ focusing on experimental protocol and sources of experimental uncertainties.

2.1 Atomic Beam Polarized Ion Source

The TUNL Atomic Beam Polarized Ion Source (ABPIS)[22] is used to produce the primary beam of negatively charged deuterons with arbitrary vector and tensor polarization. Due to the importance of a polarized beam, the physical principles underlying the operation of the source will be discussed. The integrated SFP which provides charged beam polarimetry used to calculate neutron polarization will also be discussed. The ABPIS is capable of producing charged beams of protons and deuterons with arbitrary polarization about an

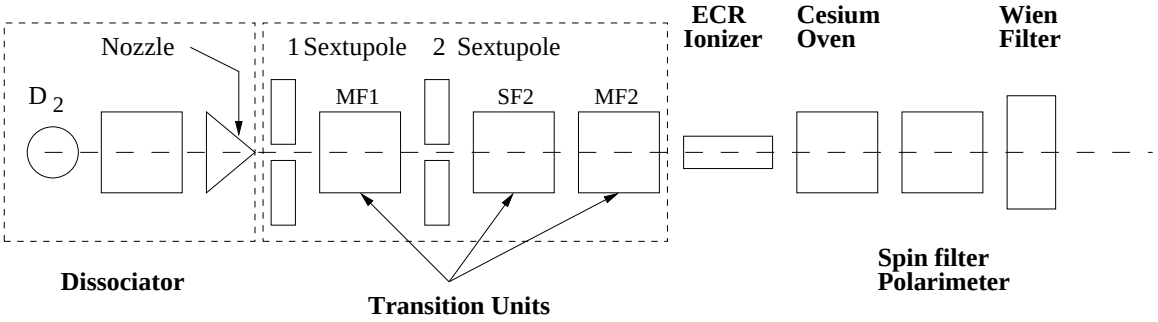

Figure 2.1: The atomic beam polarized ion source. Six functional blocks: dissociator, transition units, ECR ionizer, Cesium oven, SFP and Wien Filter, are shown.

arbitrary polarization axis. The source can be divided into six functional blocks as shown in Figure 2.1. The core of the ABPIS consists of the transition units which are responsible for the nuclear spin polarization. These produce a neutral beam which must be converted to a negatively charged beam for acceleration in a tandem Van de Graaff accelerator. Since only a negatively polarized deuteron beam is necessary for this experiment, the discussion will be limited to relevant topics.

2.1.1 Dissociator

High purity deuterium gas, produced at TUNL by the electrolysis of heavy water, is dissociated in a plasma generated by a 13.56 MHz RF field. The resulting monatomic beam was cooled and slowed as it passed through a copper nozzle held at a temperature of 30K and covered by a layer of N_2 gas to reduce recombination. This was followed by a narrow aperture which removed atoms with a large component of radial velocity leaving a well-focused atomic beam.

2.1.2 Transition Units

A series of three separate tuneable transition units and two iron-core electromagnet sextupoles produced a nuclear spin polarized beam via the hyperfine interaction. Each sextupole selectively focuses atoms with electronic spin $m_S = +1/2$ while defocusing $m_S = -1/2$

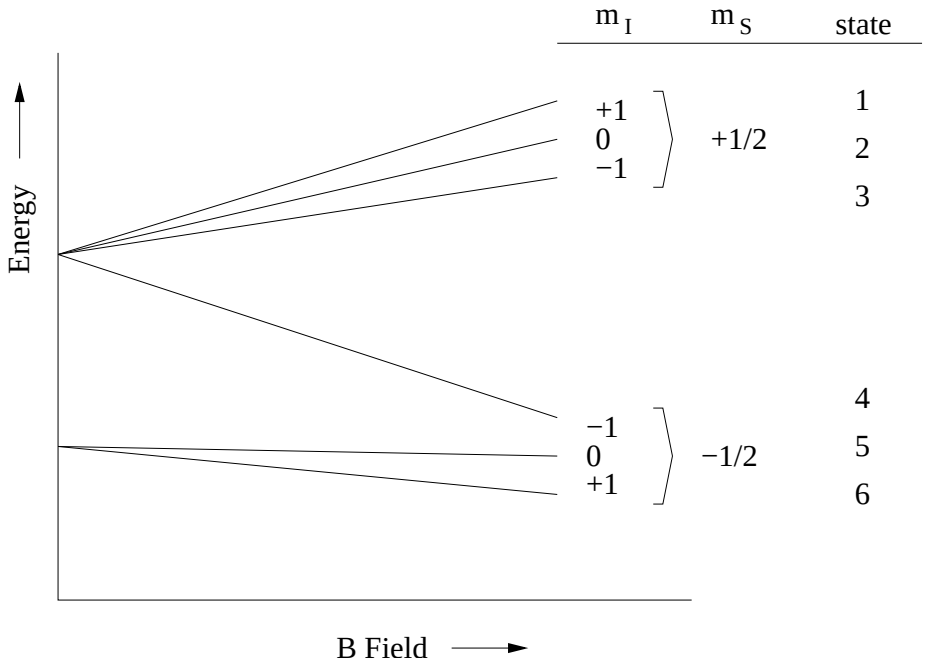

Figure 2.2: Simplified Breit-Rabi diagram for deuterium. This shows the hyperfine splitting as a function of magnetic field. States are labeled with nuclear and electronic quantum numbers as discussed in the operation of the ABPIS transition units.

in the radial direction. The unfocused component of the beam is then removed by four high speed turbo pumps. Specific hyperfine transitions are driven by the RF transition units. There are three sets of transition units: two medium field (MF1 and MF2) and one strong field (SF) where the field strength is relative to the critical field, B_c, necessary to provide all possible polarization states for protons and deuterons.

To discuss this in concrete terms, it is necessary to refer to Figure 2.2 which shows deuterium with energy levels labeled according to the quantum numbers m_I and m_s for the nuclear and electronic spin states, respectively. The starting unpolarized atomic beam has equal populations in all six states. Consider producing a beam with $P_z = +1$. The first sextupole removes states 4, 5 and 6 resulting in an electronically polarized beam but still no net nuclear polarization. The MF1 transition unit then drives the transition from state 3 to 4 and the component of beam in state 4 is then removed by the second sextupole, leaving states 1 and 2. To maximize P_z, the SF transition unit drives the transition from state 2

to 6, leaving the final beam in states 1 and 6. To produce a beam with $P_z = -1$, the first sextupole removes states 4, 5 and 6 after which MF1 drives the transition from states 3 to 4. Next, the second sextupole removes state 4, leaving states 1 and 2. MF2, operated in the weak field mode, drives transitions from states 1 to 4 and 2 to 3. The resulting beam contains deuterons in states 3 and 4. In both cases, the process of polarizing the beam reduces intensity by a factor of 3.

The transition units can be set manually when tuning the source or by a 10Hz pulser through the TUNL spin-state controller to produce a beam of rapidly changing polarization states. Data collection was vetoed for 10ms after a change to allow the source and beam optics to reach a steady state.

2.1.3 ECR Ionizer

For acceleration in a tandem Van de Graaff accelerator, a negatively charged ion beam is needed to allow a change in polarity of the beam as it passes through the terminal. This must be done in a two step process to maintain nuclear polarization of the beam. The first step in this process requires stripping the electrons from the deuterium atoms to produce positively charged ions. This is accomplished by collisions with high-energy electrons in a magnetically confined nitrogen plasma in the electron-cyclotron resonance (ECR) ionizer. A traveling wave tube amplifier (TWTA) was used as the source of microwave power to produce the nitrogen plasma.

2.1.4 Cesium Oven

The second step to produce a negatively charged beam is to add two electrons to the bare deuteron. Cesium metal is heated under vacuum to produce a vapor, and the density of the vapor is controlled by adjusting the temperature to a nominal operating temperature of 200 °C. Negatively charged deuterium ions are produced with approximately 10% efficiency. The meta-stable $2S_{1/2}$ ions that only pick up a single electron to form neutral atoms provide a convenient method to monitor nuclear polarization of the beam by the SFP. Any beam

that is not negatively charged will be removed by pumps in the source or beamline on the LE side of the accelerator.

2.1.5 Spin Filter Polarimeter

Direct measurement of neutron polarization through nuclear scattering techniques is both difficult and time consuming. Therefore it is standard practice to measure charged particle polarimetery and to calculate neutron polarization using well known polarization transfer coefficients[24].

The ABPIS was upgraded to include an integrated SFP[25]. This was useful for tuning the transition units as well as making absolute measurements of charged particle polarization at periodic intervals during an experimental run. Without the SFP, hours of accelerator time must be devoted to obtaining maximum beam polarization before each experimental run and these measurements could not be repeated frequently to detect any drift in the source. Since several parameters need to be carefully adjusted simultaneously and because of the hysteresis in the iron pole pieces of the sextupoles, careful tuning of the source is necessary. Each experiment requires different polarization states and the previous parameters can only be used as a rough estimate.

The SFP is physically located between the cesium charge exchange region and the Wien filter. It relies on the neutral atoms in the metastable $2S_{1/2}$ states created as a by-product of the charge exchange collisions in the cesium vapor. The Lamb shift between the $2S_{1/2}$ and $2P_{1/2}$ states provides a mechanism to drive the long-lived metastable state to the ground state.

The spin filter is a RF cavity tuned to allow only a single hyperfine state to pass. These metastable atoms in the selected state are then quenched to the ground state by a 1KV difference across the quenching electrodes and, the resulting photons are detected by a photomultiplier tube sensitive to UV. A SFP measurement involves scanning the magnetic field and recording the counts detected by the photomultiplier tube as a function of magnetic field.

First, a scan is taken with all of the transition units off to establish the background. With the RF transition units on, a second scan is taken. The peaks corresponding to each hyperfine state are gated manually using the SFP control console and both the tensor and vector polarization is calculated from the area under each peak.

SFP measurements, which take about 30 seconds, can be conveniently made during the time required to reverse the polarization state of the target. Extensive use of the ABPIS and SFP by many experimental groups at TUNL has provided a high level of confidence in the ability to measure the absolute polarization of a deuteron beam to within $\pm 3\%$. Making the measurement at the source rather than at the target has likewise been validated. When the source is providing beam for experiments, the SFP acts as an electrostatic lens.

2.1.6 Wien Filter

The transition units produce nuclear polarization relative to an axis parallel to the beam momentum but an experiment may require arbitrary polarization at the target. In addition, for a longitudinally polarized beam, the energy analyzing magnet and magnetic steerers rotate the plane of polarization as the beam travels from the source to the target. It is most convenient to compensate for these issues by applying the necessary correction to the polarization axis at the source. Since the dynamically polarized target is located on the 59° beamline measured relative to the axis of the accelerator, for a longitudinally polarized beam with the same axis at the target, the Wien filter must compensate for the sum of the shift due to the inflection magnet and the analyzing magnet.

The Wien filter consists of a set of perpendicular electric and magnetic fields where a magnetic field precesses the spin and the electric field is applied to counteract the deflection of the beam. The Wien filter can be physically rotated to produce polarization relative to any desired axis.

The frame of the source is held at -80KV relative to ground to provide sufficient energy to transport the beam to the low energy end of the accelerator.

2.2 Tandem Van de Graaff Accelerator

The energy of the nuclear spin polarized deuteron beam from the ABPIS is boosted by a FN model 10 MV tandem Van de Graaff electrostatic accelerator[26]. The negatively charged beam enters at the low energy (LE) end and is attracted towards the positively charged terminal at the center of the tank. Inside the terminal, a carbon foil strips two electrons as the beam passes through it, changing the beam polarity from negative to positive. The positive beam is then accelerated away from the terminal for a total increase in energy of $2|e|V_T$ where V_T is the terminal voltage and e is the elementary unit of charge. Two high voltage (HV) power supplies at the high and low energy ends transfer charge to the pelletron chain. A pelletron charging chain consisting of alternating stainless steel and nylon insulators mechanically transfers charge to the terminal. The pelletron system offers several advantages over belts including higher operating speeds, larger charging currents, longer life and dust-free operation which reduces the need for the accelerator tank to be periodically opened and cleaned.

The column which houses the beamline consists of glass sections which are supported under compression. A uniform electric field gradient is provided by a series of column resistors that connect the terminal to the grounded tank. All electrical power required inside the terminal is generated by an alternator driven off the pelletron chains. Control signals required at the terminal are carried by a fiber optic cable.

The steel tank is pressurized to 15-20 atm with a mixture of CO_2, SF_6 and N_2 dielectric buffer gas to minimize breakdown and arcing between the terminal and tank wall under high electric fields. The terminal potential controls the energy gain of the beam and therefore must be adjustable to allow the accelerator to produce a stable beam at the required energy. The energy resolution is a function of both the intrinsic spread in the beam as well as the stability of the terminal voltage. Several mechanisms control the terminal potential and provide the feedback necessary to maintain a constant beam energy. The terminal is a large stainless steel structure with a high capacitance so the terminal potential is directly

proportional to the charge on it. At the basic level, the terminal voltage is set by the difference in the charge transferred to the terminal by the pelletron and charge removed by several other processes.

The corona needles are arranged on a grid in front of a grounded electrode. The needles are connected to ground through a triode which acts as a variable resistance. This corona needle assembly can be moved in the radial direction to provide sufficient corona current so that the triode operates over a range of 30KV. The assembly is placed closer to the terminal for lower terminal voltages and closer to the tank wall for higher terminal voltages.

The terminal potential stabilizer (TPS) can be operated in either slit or generating volt meter (GVM) mode with GVM used primarily when there is no beam or intermittent beam through the accelerator and slit mode is used when beam is on target. Slit mode operates on the difference in beam current between two slits at the exit of the 20-70 analyzing magnet. The terminal voltage is adjusted to minimize the difference by providing feedback to control the corona current.

2.3 Beam Transport

Due to the shared nature of a facility like TUNL, the beam must be able to be directed to multiple experiments in different target rooms. Beam transport deals with guiding and focusing the beam between the source and the accelerator and the accelerator and target. Low energy (LE) beam transport between the source and accelerator shown in Figure 2.3 is accomplished by holding the frame of the ABPIS at -80KV relative to ground. An inflection magnet directs the beam from the ABPIS to the accelerator.

From the high energy (HE) side of the accelerator the beam is steered by magnetic dipoles and focused by magnetic quadrupoles as shown in Figure 2.4. Automated feedback is provided by several pairs of slits coupled to magnetic steerers which compensate for small instabilities and keep the charged particle beam centered on the neutron production cell.

Beam current can be measured at various points along the beamline by inserting Faraday

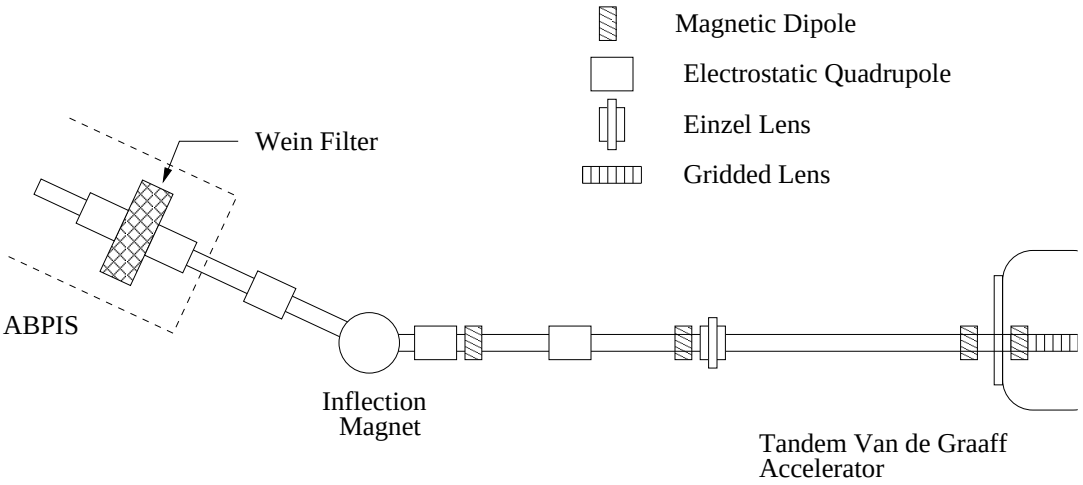

Figure 2.3: Low energy (LE) beam transport system. TUNL LE steering and focusing beam optics between ABPIS and input of the tandem Van de Graaff accelerator.

cups which block the beam and record the integrated current. This was done during the initial startup of the source and accelerator and when beam energy was changed. Upstream of the neutron cell a beam profile monitor provides a two-dimensional cross section of the beam.

The 20-70 magnet, a water-cooled iron core electromagnet stabilized by feedback from a NMR probe, provides the primary energy analysis and also serves to direct the beam from the accelerator to the appropriate experimental area. The dynamically polarized target is located on the 59° beamline. The final length of the charged particle beamline is shielded by soft iron pipe and layers of μ-metal to prevent deflection from the target magnetic fringe fields.

The beamline is maintained at a pressure below 10^{-4} Torr by several diffusion pumps located along the beamline between accelerator and target to minimize loss of beam through scattering with residual gas molecules.

2.4 Polarized Neutron Production

Neutrons cannot be accelerated or steered so they must be produced directly in front of the target through a polarization transfer reaction. The $^2H(\vec{d},\vec{n})^3$He reaction has a Q-value

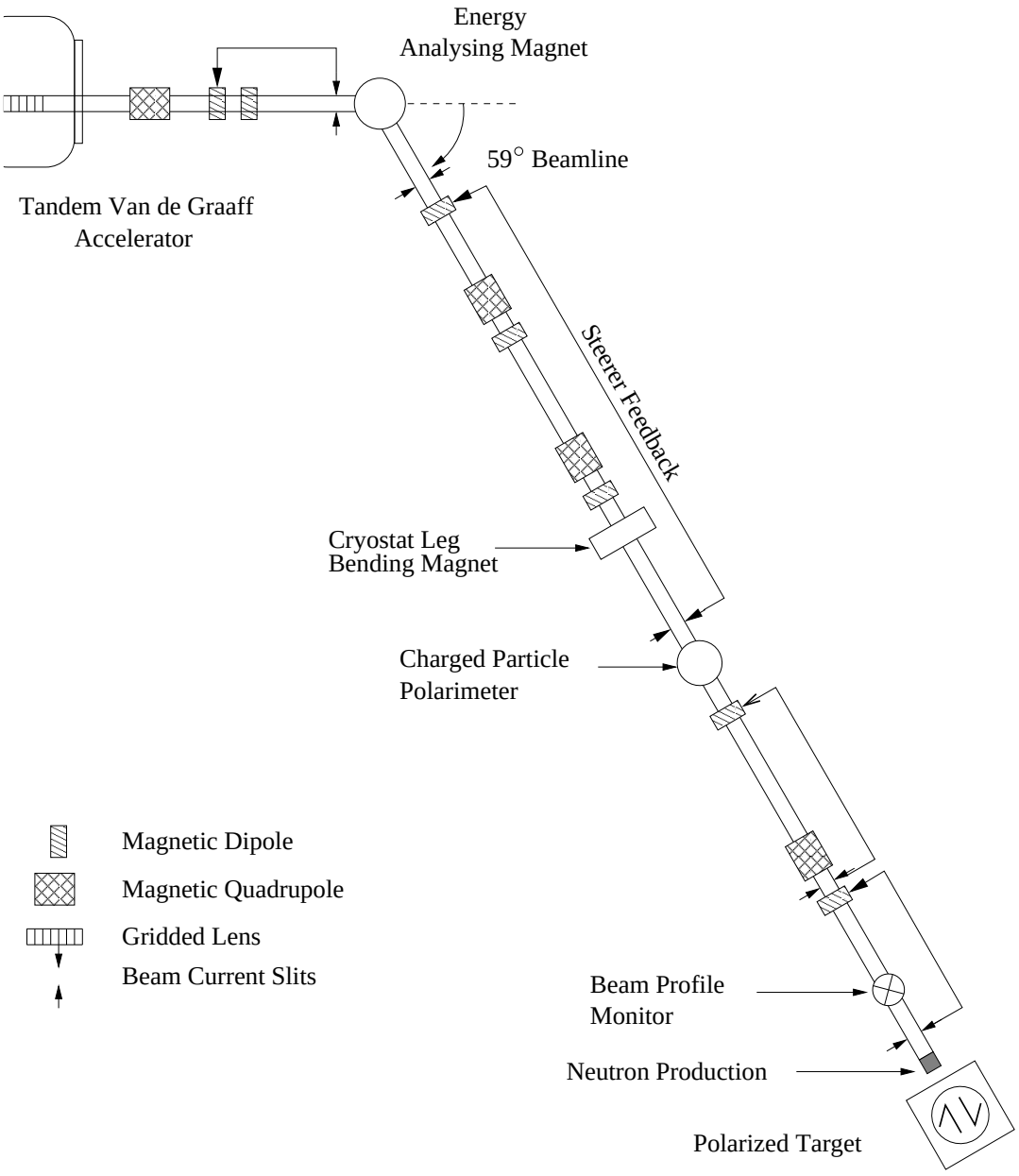

Figure 2.4: High energy (HE) beam transport system. TUNL HE beam transport including the 20/70 energy analysing magnet and the 59° beamline to the dynamically polarized target area.

of 3.27 MeV with large relatively energy independent polarization transfer coefficients and is suitable for production of polarized neutrons with $4 < E_n < 20$ MeV[24]. This favors production of neutrons with forward momentum distributed narrowly around 0°.

Neutron polarization is related to both the tensor and vector polarization of the deuteron beam by the expression

$$P_n(0^\circ) = \frac{\frac{3}{2} P_z K_y^{y'}(0^\circ)}{1 + \frac{1}{2} P_{zz} A_{yy}(0^\circ)} \tag{2.1}$$

where $K_y^{y'}(0^\circ)$ and $A_{yy}(0^\circ)$ are the 0°vector and tensor polarization-transfer coefficients and P_z and P_{zz} are the vector and tensor polarization of the deuteron beam, respectively.

The neutron production target, see Figure 2.5, is a cylinder 6.0cm in length by 1.9cm in diameter filled with high purity deuterium gas to a pressure of 2 atm. This is located at the end of the beamline directly in front of the target cryostat. Forced convection with compressed air is used to cool the outside of the gas cell to prevent overpressure and rupture of the havar window separating the entry side of the production cell from beam line vacuum. Havar foil, a high-strength non-magnetic alloy, provides minimal energy dispersion while maintaining the integrity of the vacuum. A 0.5mm tantalum beam stop at the exit of the production cell prevented any unreacted deuterons leaving the cell.

The neutron production cell is electrically isolated from the beamline which allows the charge to be collected and thus the beam current to be measured by the beam current integrator (BCI). Both the tantalum beam stop and aluminum cryostat housing have small neutron cross sections.

Energy loss due to the havar window and deuterium gas was calculated using the computer code BABEL[27]. The computer code RKIN[28] was used to calculate the neutron beam energy given the energy of the deuteron beam at the center of the production cell. An estimated 10% spread in neutron energy resulted primarily from the production of neutrons along the entire length of the production cell.

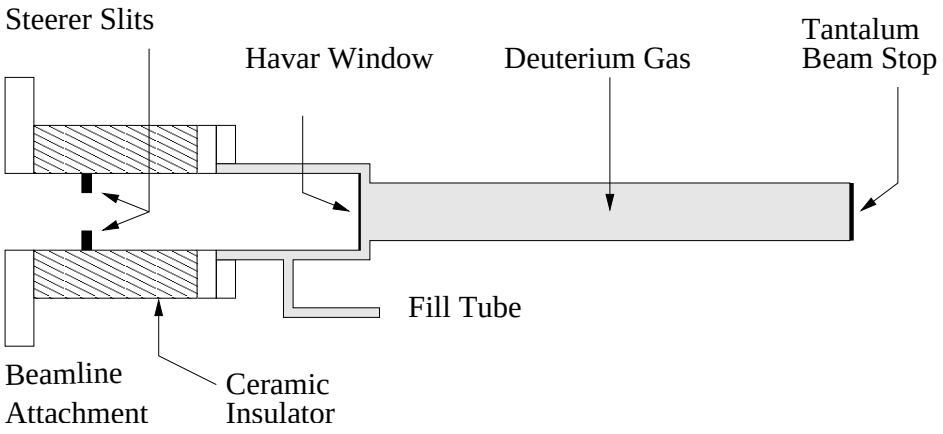

Figure 2.5: Polarized neutron production cell. Polarized neutrons are produced in the polarization-transfer reaction between the deuteron beam and deuterium gas.

2.5 Neutron Detection

Neutrons are detected by a scintillating material which produces photons. These photons are converted to an electrical signal and amplified in a photomultiplier tube. Neutrons can be distinguished from gamma rays in some scintillating materials due to the difference in pulse shape by a technique referred to as pulse shape discrimination (PSD). This was done by setting a threshold for pulse rise and fall times to exclude gamma rays which have shorter pulse rise and fall times than neutrons. The main detector, monitor detector and polarized target are shown in Figure 2.6.

2.5.1 Monitor Detector

The monitor detector is a 2.5cm long plastic scintillator with a rectangular cross section of 2.5cm x 1.3cm. This was optically coupled to a photomultiplier tube through a 1.0m light pipe to allow the photomultiplier tube to be placed far enough away to minimize effects from the target magnet. The scintillator is located directly after the neutron production cell to compensate for any production dependent neutron asymmetry.

Output from this detector was energy discriminated to remove low energy neutrons from n-d breakup and gamma ray events. Pulse shape discrimination was not possible because

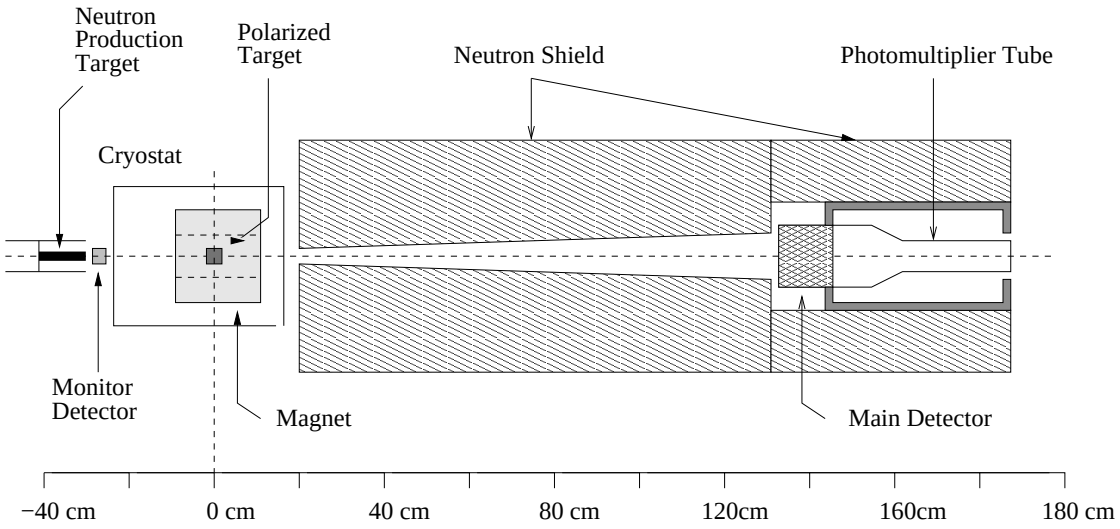

Figure 2.6: Polarized target and detector setup. This shows the placement of the polarized target relative to neutron production target, the monitor and main detectors. The photomultiplier tube for the monitor is at the end of a 1m light pipe (not shown).

the count rate was too high and the plastic scintillator does not produce a distinguishable response for protons and gamma rays. Counts in the monitor detector are assumed to be proportional to the neutron flux incident on the target.

2.5.2 Main Detector

The main detector consists of a 12.7cm long by 12.7cm diameter cylinder filled with BC-501 liquid organic scintillator. The front and cylinder walls are silvered and the back is optically coupled to a photomultiplier tube. This detects neutrons that pass through the target. The path behind the target is shielded by a polyethylene collimator which effectively blocks neutrons reaching the detector other than by passing directly through the target. The bias voltage on the photomultiplier tube was adjusted between -1300V and -2000V to produce a sufficiently strong signal. The base of the photomultiplier tube is transistorized to reduce count rate dependent effects because of overloading of the final stage dynodes at high count rates.

Pulse shape discrimination was used to differentiate between neutrons and gamma rays.

Gamma rays from neutron activation provide the primary source of background but neutrons from n-d breakup are also a concern. All electronics associated with processing detector signals consisted of standard NIM modules housed in the TUNL control room. A VAX microcomputer and XSYS[29] was used for data acquisition and monitoring progress of the experiment.

2.6 Theory of Measurement and Experimental Protocol

The core of the measurement of $\Delta\sigma_L$ involves the measurement of the difference ΔN between two measured quantities, N_+ and N_-, where ΔN is orders of magnitude less than either N_+ or N_-. Extreme care must be taken to avoid asymmetries unrelated to spin-dependent elastic scattering. The expected $\Delta N/N$, where N is the average number of counts, is on the order of 10^{-4}.

The calculation of $\Delta\sigma_L$ from measured quantities can be expressed as

$$\Delta\sigma_L = \frac{2\epsilon_n}{P_n P_t x} \tag{2.2}$$

where ϵ_n is the neutron asymmetry, P_n and P_t are the neutron beam and deuteron target polarizations, respectively, and x is the target thickness. In the case of a D6 partially deuterated target, the contribution due to the polarized protons cannot be neglected, leading to a correction,

$$(\Delta\sigma_L)_d = \frac{2\epsilon_n}{P_n(P_t x)_d} - \frac{(P_t x)_p}{(P_t x)_d}(\Delta\sigma_L)_p \tag{2.3}$$

where the subscripts indicate proton and deuteron respectively.

Data is collected in 16 runs of 1024 sets of data. Each data set consists of 8 flips of the beam polarization, four up and four down. The beam polarization is flipped at a rate of 10Hz and the target polarization is reversed approximately every eight runs which which occurs every 4 hours. An eight-step spin flip, $+--+-++-$, sequence is designed to

eliminate up to second order drifts associated with beam and target instrumentation. A veto signal inhibits data collection if beam current is below threshold. Offline data analysis discards all data from any incomplete 8 step sequence or for which the raw asymmetry exceeds a preset threshold.

Raw neutron asymmetry, ϵ_n, is the difference in the total number of neutrons counted in the parallel and anti-parallel states. This must be corrected for asymmetries arising from the effects of tensor polarization of the beam, beam current, count rate and detector dead time.

The dead time correction was determined by the difference between counts from a 100KHz pulser gated by the PSD "live-time" output and the ungated signal from the same pulser[7]. The first step was to apply this correction to the raw neutron asymmetry. The beam current integrator (BCI) asymmetry, ϵ_I, is the difference in total charge collected on the neutron production cell for different spin states of the charged particle beam. A linear fit to the dead-time corrected neutron asymmetry, as a function of BCI asymmetry, gives ϵ_n for $\epsilon_I = 0$ as the y intercept and the sensitivity is given by the slope. An asymmetry is determined in a similar manner for the monitor detector and subtracted to compensate for any neutron production dependent asymmetry, most importantly differences between deuteron beam tensor polarization for the $+P_z$ and $-P_z$ states.

The uncertainty in neutron asymmetry is predominantly from the uncertainty in the counting statistics which follows a Poisson distribution and therefore scales as $1/\sqrt{N}$ where N is the total number of neutrons counted. Statistical error is reduced by increasing N and the minimum length of an experimental run is set by the need to reduce the counting error to acceptable levels. Systematic error is inherently more difficult to detect and remove. A standard approach is to make a differential measurement in such a way that systematic error will appear with opposite sign and cancel out. Flipping beam and target polarization as discussed is the primary method to accomplish this.

To arrive at an uncertainty for $\Delta\sigma_L$, the standard rules for error propagation are applied to each term in Equations 2.2 and 2.3.

Chapter 3

Polarized Target

The dynamically polarized deuteron target is composed of several distinct subsystems necessary to produce a spin polarized target suitable for nuclear physics experiments. This includes the cryogenic system, a superconducting magnet, deuterated target material, the microwave system and the NMR Q-meter used to measure the polarization. This chapter discusses dynamic nuclear polarization (DNP) and provides details of the first four polarized target subsystems mentioned above. The NMR hardware and off-line analysis of the NMR spectra will be covered in Chapter 4.

3.1 Cryogenic Systems

3.1.1 Refrigerator and Cryostat

The cryogenic system consists of the three concentric modules shown in Figure 3.1 and a gas handling system. The primary component is a recirculating ^{3}He evaporation refrigerator based on a versatile design developed at PSI[30] with modifications to handle a larger amount of target material and to accommodate a superconducting magnet mounted in multiple orientations. The liquid ^{4}He (LHe) stage serves to condense the circulating ^{3}He gas, which is in turn pumped on to reduce the temperature to 0.5K. The cryostat and refrigerator are constructed of non-magnetic materials, primarily aluminum, brass and non-

magnetic stainless steel to avoid introducing any magnetic field inhomogeneity.

LHe was purchased commercially in 100ℓ dewars and consumed at a rate of approximately 1.2ℓ/hr when the refrigerator was operating at 0.5K. The liquid level within the cryostat was monitored by a superconducting level gauge that controlled an automated filling system to transfer LHe from the storage dewar to the cryostat when the level fell below a preset minimum. The solenoid valve controlling the fill was replaced with a pneumatically actuated valve when interference was noted in the NMR system at the beginning of fill cycles. A second microcontroller maintained the pressure of the LHe dewar between 12 and 15 psi. This was to ensure a high enough pressure for a fast and efficient transfer from floor level to the top of the cryostat but not high enough to cause excess loss due to boiloff in the dewar.

A small area of the surface of the LHe bath was pumped on with a mechanical pump to reduce the temperature from 4.2 to 2.2 K. This results in a non-uniform temperature profile across the LHe bath. The temperature gradient does not affect the primary function of the LHe bath to act as a heat sink. The pumping rate is controlled by a needle valve, referred to as the 2K valve, which is adjusted to maintain stable operation with minimal cryogen consumption. The volume of ^{4}He gas was measured by a Singer dry gas meter to keep a running estimate of the cryogen consumption.

At 2.2K ^{4}He undergoes a phase transition which is accompanied by a significant decrease in vapor pressure. The practical limit which can reached by pumping is 1.2K. Liquid ^{3}He does not exhibit this limitation until a much lower temperature. A simplified functional diagram of the closed loop ^{3}He gas handling system is shown in Figure 3.2. The entire ^{3}He gas system, including the storage tanks, is held below atmospheric pressure to minimize the potential loss of gas should a leak develop. Room temperature ^{3}He gas enters at the top of the cryostat after passing through an activated carbon absorption filter cooled by liquid nitrogen (LN_2). This removes any water vapor, nitrogen or oxygen which may freeze and cause blockages inside the narrow passages within the cryostat. The gas is then condensed in a cylindrical continuous heat exchanger which is in thermal contact with the 2K bath.

The ^{3}He needle valve located after the heat exchanger provided a variable flow impedance which was adjusted to provide sufficient back pressure to condense the ^{3}He gas. Liquid ^{3}He collects in the ^{3}He cup in which the target material is suspended. The low molecular weight of ^{3}He makes it difficult to pump efficiently. Two roots blowers, rated at 140 ℓ/s and 80 ℓ/s at STP, maintain sufficiently high pumping rates at low pressures to handle the required heat load. The refrigerator has two stable operating points. Figure 3.2 shows the series connection of the two roots blowers and sealed rotary pump in the ^{3}He line. With the roots blowers turned off and the sealed rotary pump running, the stable operating temperature is 1K. With all three pumps operating, a stable operating temperature of 0.5K can be achieved.

The refrigerator operates on the principle that heat is removed from the target as He undergoes the phase change from a liquid to a gas. An estimate of the cooling power of either stage can be made from

$$\frac{dQ}{dt} = L\frac{dn}{dt} \tag{3.1}$$

where dQ/dt is the cooling power, L is the enthalpy of vaporization and dn/dt is the molar flow rate. A typical ^{3}He flow rate of 0.6 mmol/s gives a cooling power of 15mW [7] which is sufficient for reliable operation over extended periods of time. Conduction and radiation from the surroundings at 300K are both difficult to quantify and at the same time provide the dominant heat input. Other sources of heat include beam heating, excess microwave power and mechanical vibrations.

The target insert goes into the ^{3}He space and holds the target material, the NMR coil, coaxial cable, 10 Torr ^{3}He baratron port and microwave waveguide. This step occurs when the refrigerator is stable at 4.2K and before ^{3}He gas is introduced. Several copper disks along the length of the target insert act as radiation baffles. An insert is necessary to allow insertion and removal of the target material while the refrigerator is at LHe temperatures.

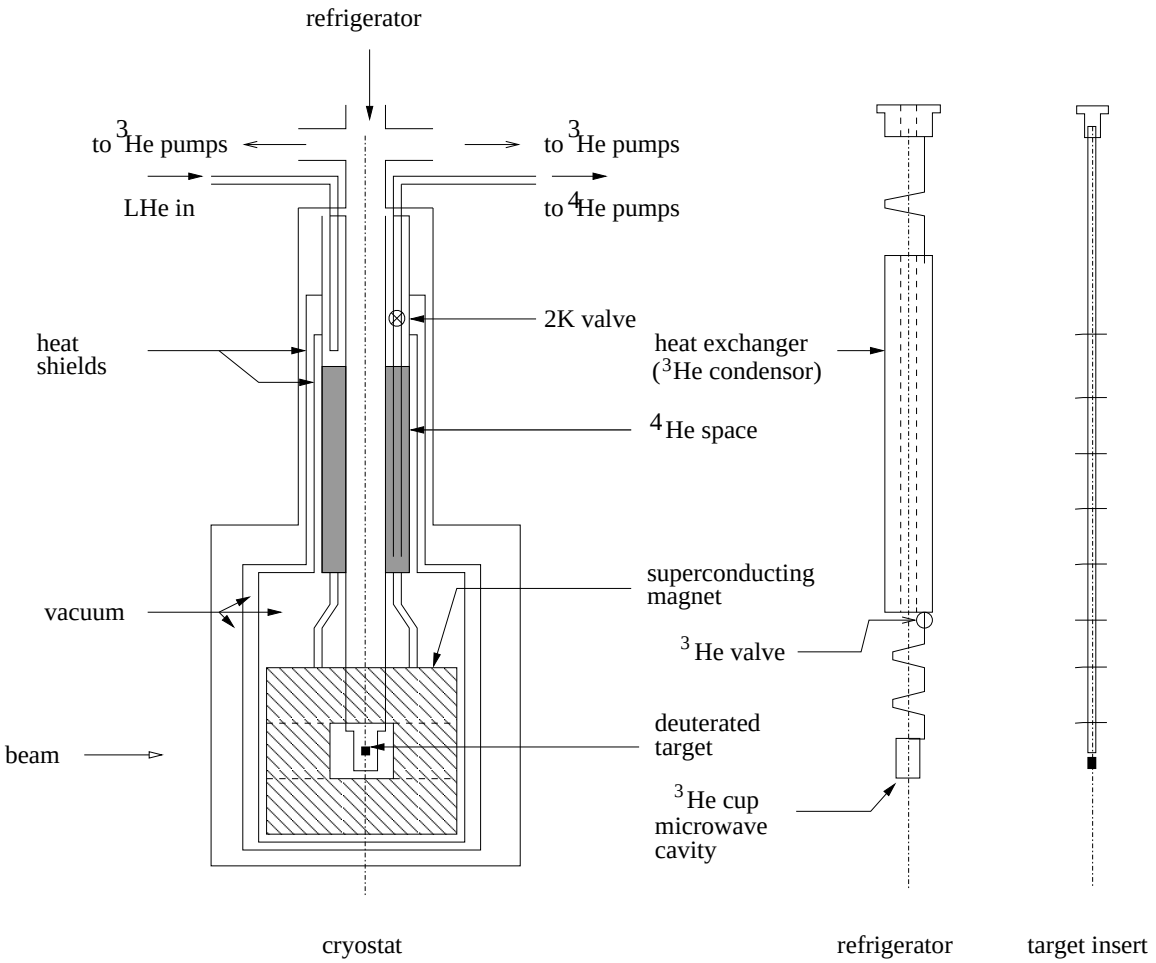

Figure 3.1: Polarized target cryogenic system. Diagram shows the target insert which fits down the center of the refrigerator. The combined target and refrigerator fit down the center of the cryostat. The external ^{3}He gas handling system is shown in Figure 3.2.

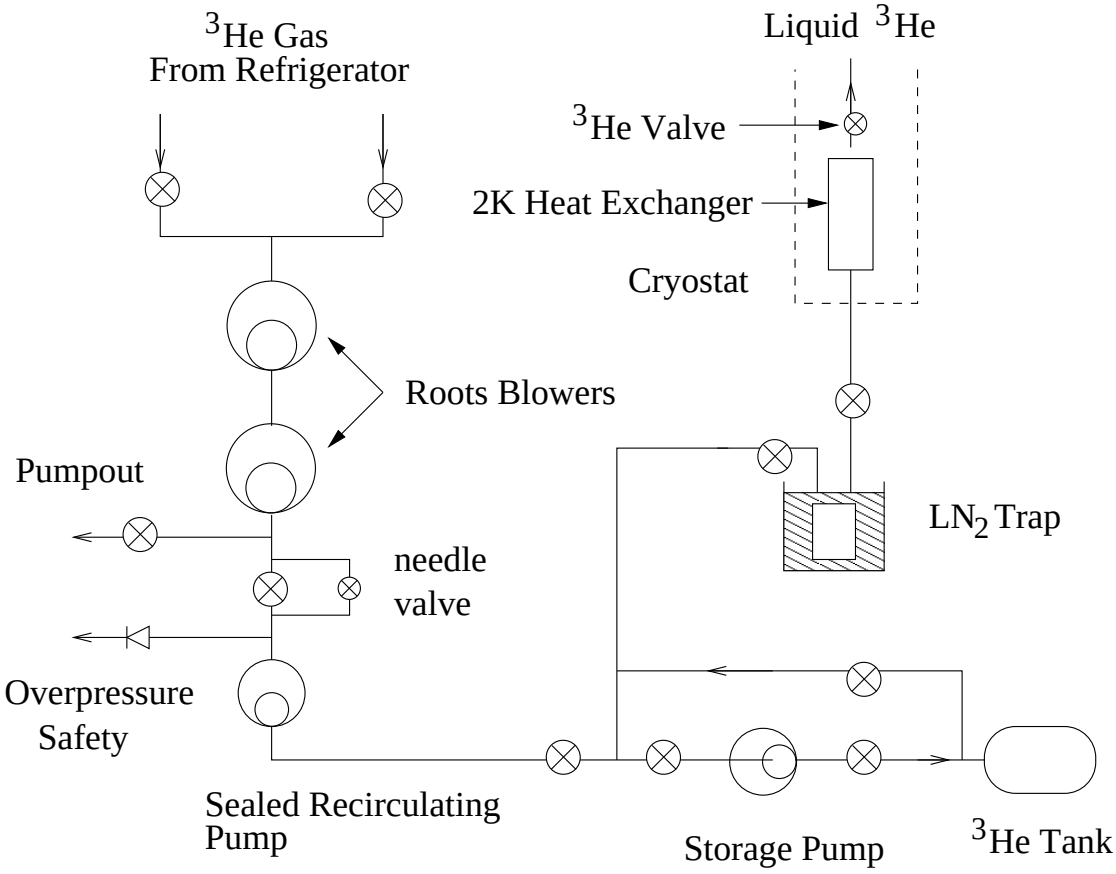

Figure 3.2: Simplified diagram of the ^{3}He gas handling system. Gas panel and pump rack components are shown. The liquid phase of ^{3}He inside the cryostat (not shown) completes the closed loop.

3.1.2 Thermometry

Temperatures are monitored using electrical resistance sensors during the cooldown and operation of the refrigerator. Resistance measurements, using a 4-wire bridge technique, are used to monitor the initial cooldown and for refrigerator diagnostics. Accurate techniques are necessary at low temperature for calibration of the NMR system when using thermal equilibrium (TE) methods.

Two 1000Ω platinum resistors anchored to the top and bottom of the magnet enclosure are useful during the initial LN_2 cooldown, over the temperature range between 300 and 70K. For LHe temperatures, a 220Ω Speer, and a 1KΩ carbon-glass resistor anchored to the condenser provided temperature measurements useful for monitoring the operation of the ^{4}He stage.

RuO and Ge semiconductor sensors were mounted on the ^{3}He cup to provide temperatures of the ^{3}He in the system. The RuO sensor is calibrated against the Ge sensor but it is not sensitive to magnetic fields which makes it useful when stabilizing the refrigerator with the magnet energized. Both are affected by microwaves and therefore provide only reference values rather than temperature while the target is in the dynamically polarized state.

At temperatures below 1K, the vapor pressure of ^{3}He exhibits a strong temperature dependence which can be used for thermometry. This is standard practice in low-temperature physics as a passive measurement which is both sensitive and reproducible. The baratron gauge head is connected to the cryostat by a 1m long x 1mm diameter stainless steel tube. The temperature differential along the tube is 300K. Under these conditions the baratron reading must be corrected for the thermomolecular effect[31]. This phenomena is responsible for a pressure gradient along the tube. All thermometry data was digitized and recorded once every minute along with the NMR data. Table 3.1 provides typical values of parameters observed during the experiment.

Table 3.1: Typical operating conditions for refrigerator. Locations of sensors and gauges are given along with typical values when the refrigerator is operating at 0.5K without DNP.

parameter	value	sensor location
Speer	2.2 K	condensor
CG-1000	1280 Ω	condensor
RuO	520 mK	^{3}He cup
Ge	520 mK	^{3}He cup
^{4}He valve pressure	0.2 torr	^{4}He pump line
condensor pressure	220 torr	^{3}He gas cryostat input
^{3}He static pressure	580 mtorr	^{3}He cup
^{3}He flow rate	0.35 mmoles/s	^{3}He gas return

3.2 Magnet

A 2.5T Nb-Ti split-pole superconducting magnet is housed inside the cryostat and can be mechanically mounted to produce either a longitudinally or transversely polarized target relative to the beam momentum. Since the polarization axis is determined by the direction of the magnetic field, which is in turn determined by magnet geometry, any change other than a 180° shift can only be achieved by a physical rotation of the magnet coils. The magnet is surrounded by a LHe jacket which is fed internally from the bottom of the ^{4}He bath. Because of this arrangement for maintaining the magnet in a superconducting state, an audio alarm and telephone autodialer are triggered if the level of LHe should fall below a critical minimum. A magnet quench could potentially cause catastrophic damage to the target.

At the rated operating current of approximately 80A, the magnet provides a static magnetic field of 2.5T. Manufacturer specifications gives the field homogeneity as better than 1 part in 10^4 over the target volume. The importance of a homogenous field is to ensure uniform polarization across the entire target volume.

To center the NMR signal within the fixed frequency sweep, it was necessary to accurately set the magnetic field to 2.5T. The current is set by measuring the voltage across a brass shunt while operating the magnet in the non-persistent current mode. While taking data with beam on target, the magnet is operated in the persistent mode for long term field

stability and reduced heat load.

3.3 Target Material

Propanediol provides a high density (10% by weight) of polarizable deuterons and can be combined with a convenient chemical dopant to provide the free radicals for DNP[21, 32]. Radiation hardness of the target material is not a concern for low energy, low beam current and short experimental runs at TUNL. Research into suitable combinations of organic materials and stable paramagnetic dopants[33] is an active field. However, taking into account the constraints of the system, 1,2-propanediol doped with a complex of 2-ethyl-2-hydroxy-butyric acid (EHBA) and Cr^V provides a comparable level of performance to the newer and more exotic materials[33, 34].

Deuterated 1,2-propanediol is commercially available in two forms. The partially deuterated form $CD_3CD(OH)CD_2OH$ is known as D6 and the fully deuterated form $CD_3CD(OD)CD_2(OD)$ is known as D8. Both D6 and D8 had isotopic enrichment above 98%. Experimental data was obtained with both D6 and D8 targets and the merits of each are discussed in Chapter 4. EHBA-Cr^V complex was produced at TUNL from from EHBA and $K_2Cr_2O_7$ using methods described in the literature[35]. The EHBA-Cr^V was added in quantities of 0.360g per 10mℓ of propanediol to obtain a mixture with an estimated spin concentration of 10^{20} spins/mℓ. This process was carried out at room temperature under partial vacuum in a light tight container. The liquid was then rapidly frozen by dropping it into a bath of LN_2 to form spherical beads with a diameter of approximately 2mm. Bead size was controlled by a constant flow rate of the liquid through a hyperdermic needle held at a potential of 2500V relative to the LN_2 bath. The potential served to produce a smaller bead size than would have been possible with gravity alone due to the viscosity of propanediol. This technique combined with the non-conductive nature of the beads required them to be degaussed with a grounded sieve prior to use. The rapid cooling resulted in some spontaneously shattered beads. This material was separated out and used for tests of the

NMR system.

The target material is stored in LN_2 to maximize the lifetime of the dopant. The target material was loaded into the target cup after the refrigerator was cooled to LHe temperatures. Care was taken to minimize ice formation by flowing He gas over the beads during transfer to the cryostat.

Ensuring a uniform temperature profile across the target was important. Small beads immersed in liquid ^{3}He offer the highest probability that the temperature will be uniform. A solid cube, on the other hand, offers far less surface area for heat removal and, is less likely to exhibit a uniform temperature if beam heating is an issue.

A meaningful calculation of beam heating effects is not possible due to the low intrinsic thermal conductivity and low heat capacities of the materials involved. An upper limit of the heat load due to the beam can be established by assuming that the entire energy of the beam is deposited in the target. A 10 MeV beam of 10^5 neutrons per second produces a heat load of 0.16μW. A comprehensive model taking into account factors such as the heat transfer across boundaries, knowledge of local variations in temperature, and order of magnitude uncertainty in parameter values at 0.5K, makes any prediction unreliable. A measurement of $\Delta\sigma_L$ consistent with a lower target polarization than measured by NMR would be an indication of beam heating but this was not observed. A careful measurement of $\Delta\sigma_L$ as a function of the length of time the beam is on target would also uncover beam heating effects, should this be an issue.

From geometrical considerations, assuming one bead occupies a cube with side equal to the bead diameter, an approximate packing fraction can be calculated. The packing fraction obtained using this approach is η=0.52. The cost of reduced thickess x is significant because $\Delta\sigma_L$ scales linearly with x (see Equation 1.5). The amount of target material was measured by melting and weighing the target material at the end of an experimental run. Assuming uniform packing, the thickness was determined by dividing the total mass of target material by the molecular mass of propanediol to determine moles and then multiplying by the number of deuterons per molecule of propanediol. This was then expressed as the number

of deuterons per unit area by dividing by the area of the face of the target cup perpendicular to the beam. For D6 and D8 targets, typical values of thickness were 5.2 x 10^{-3} and 6.5 x 10^{-3} deuterons/b, respectively. The accuracy of this method relies on the target cup being full of beads which is difficult to achieve in practice. This difficulty is responsible for the greatest uncertainty in determining target thickness. Nuclear scattering experiments which calculate $P_T x$, the product of target polarization and thickness, provide an advantage over this method in that the amount of target material in the path of the beam is correctly accounted for.

3.4 Dynamic Nuclear Polarization

Dynamic nuclear polarization (DNP) refers to transferring the high polarization of the electronic spin system to the nuclear spin system using an alternating electromagnetic field in the microwave spectrum. The orders of magnitude gain in polarization, increased temperature stability, and ability to grow and reverse target polarization on a short time scale all justify the added complexity. The ability to reverse target polarization quickly and without changing the static magnetic field significantly reduces a potential source of systematic error associated with the target.

3.4.1 Principles of DNP

In a 2.5T magnetic field and at a temperature of 0.5K, the electronic polarization of the Cr^V ions is greater than 99% while the deuteron polarization is only 0.1% due to the large difference ($\mu_e/\mu_d = 2144$) in magnetic moments as shown by Equations 1.2 and 1.3. The requirements for a candidate material are a suitable combination of high deuteron density and quasi-free electrons. The quasi-free electrons are usually provided by paramagnetic impurities intentionally added to the target material. The spin-lattice relaxation time constants, which govern the timescale on which a spin system will return to its equilibrium state, should be such that $T_{1e} \ll T_{1n}$ in order to allow a single electron spin to relax quickly

and be available to flip another deuteron. This requirement is easy to meet with T_{1e} less than 10ms and T_{1n} on the order of hours under conditions present in the TUNL target. Uniform nuclear polarization across the bulk is achieved by spin diffusion.

In 1,2-propanediol, unpaired electrons are provided by the highly paramagnetic Cr^V ions stabilized in an EHBA complex. Optimium doping concentrations have been determined by others[32]. In the original polarized proton target materials such as Nd:LMN·$24H_2O$, DNP was explained by the well-resolved solid effect[21, 36] Here, the hyperfine interaction splits the electron-nucleon energy levels into distinct states each with a unique quantum number m_e and m_n. A "forbidden" transistion, meaning the simultaneous flip of an electron and nuclear spin, was driven with microwaves. The electron would then revert back to its equilbrium state on a time scale much shorter than the nucleon and therefore was available to repeat the process and drive the deuteron population to a new equilibrium value. With the well-resolved solid effect, the maximum obtainable polarizations can be calculated from rate equations and the frequencies at which the maximum positive and negative polarizations occur can be determined from an energy level diagram.

A two level system such as a spin 1/2 particle will be given as an example, as the generalization to three levels introduces m=0 which only complicates the picture without providing any new physics. The only difference is that in the spin 1 case we can change the populations of the m=1 and m=-1 levels independently because of angular momentum selection rules which limit changes in angular momentum to ± 1 whereas in a spin 1/2 system, the m=1/2 and m=-1/2 are linked.

The concentration of paramagnetic centers is high enough to cause spin-spin dipole interactions that result in the broadening of the electronic Zeeman levels which cannot be ignored. When the width of the electron spin resonance (ESR) spectrum becomes comparable with the nuclear Larmor frequency, this results in a quasi-continuous band rather than discrete energy levels with mixed nuclear spin states as seen if Figure 3.3. In this case, rather than attempting to keep track of individual energy levels, the population of the nuclear spin states is best described by a Boltzmann distribution with a temperature T_{ss}.

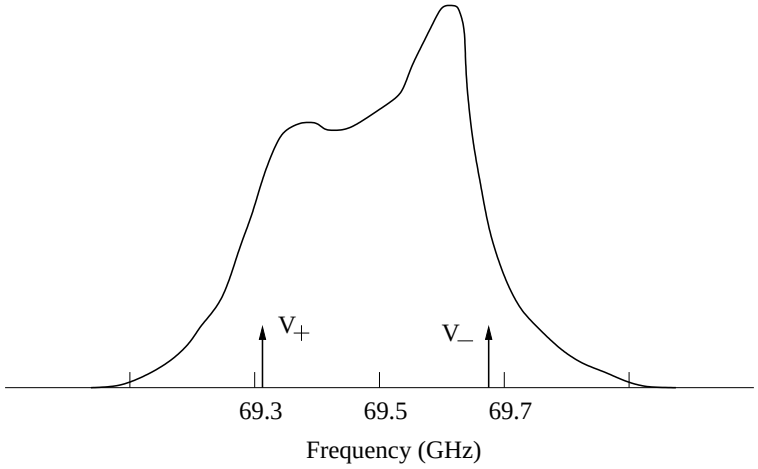

Figure 3.3: Electron spin resonance (ESR) spectrum of doped propanediol. General shape of the ESR absorption spectrum for 1,2-propanediol doped with EHBA-Cr^V complex in a field of 2.5T and at a temperature of 0.5K. This shows the frequencies for maximum positive and negative nuclear polarization.

As the spin-spin interactions are still weak relative to the electronic Zeeman interactions, the population of these electronic spin states are still described by a temperature T_z.

The concept of a spin temperature has been successful in the theoretical description of many magnetic resonance phenomena in solids and is useful in understanding the closely related mechanism of DNP.

Figure 3.4 is useful in explaining the mechanism of DNP in frozen propanediol by example. Panel (a) shows thermal equlibrium conditions where both the nuclear and spin systems are described by a common spin temperature, T_s, equal to the lattice temperature. The system has a small polarization determined by the strength of the magnetic field and temperature of the sample. Positive dynamic polarization occurs in (b) when nuclear spins in the bottom of the upper distribution move to the top of the lower distribution. While the transitions in both directions are driven at the same rate, the much larger number of deuterons in the lower Zeeman band result in a net gain for the positive nuclear spin state. This changes the distribution described by T_{ss} which corresponds to positive nuclear polarization. In contrast, the opposite change in the population described by T_{ss} is illustrated in panel (c), resulting in negative polarization.

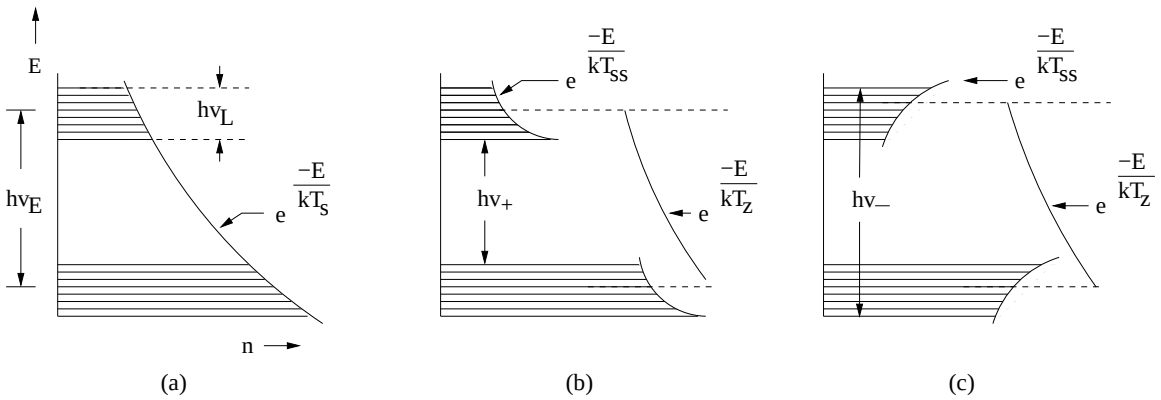

Figure 3.4: Spin temperature theory illustrating mechanism of dynamic nuclear polarization (DNP). Population (a) thermal equilibrium with common spin temperature T_s, and after microwaves with $T_z \neq T_{ss}$ for the cases of (b) positive and (c) negative polarization.

The need for spin temperature theory to understand the mechanism for DNP has other consequences, the most important of which is the equal spin temperature (EST) hypothesis. Under equilibrium conditions, all polarizable nuclei species are described by a common spin temperature which means that we can choose to measure the polarization of the most convenient species and use this to calculate the polarization which is more difficult to measure directly. The EST hypothesis also sets an upper limit on the maximum polarization because the difference depends only on magnetic moments and the number of magnetic substates, both intrinsic properties of individual nuclei.

3.4.2 Microwave System

DNP requires a source of microwaves to polarize the target. The frequency of the microwaves is determined by the electronic spin resonance (ESR) frequency of propanediol in a 2.5T magnetic field. A Varian reflex klystron with a maximum power output of 5W was used as a tuneable source of microwaves in the region of 69-70 GHz. Coarse tuning was accomplished by mechanical adjustment of the resonance cavity using a rotary micrometer which served as a reference to allow previously optimized settings to be quickly reproduced. The klystron reflector voltage provided the fine control of frequency. Both forward and reverse microwave

power was monitored with microwave power meters for the purpose of optimal tuning of the klystron. The klystron was operated at the reflector volage which produced the second peak in forward power.

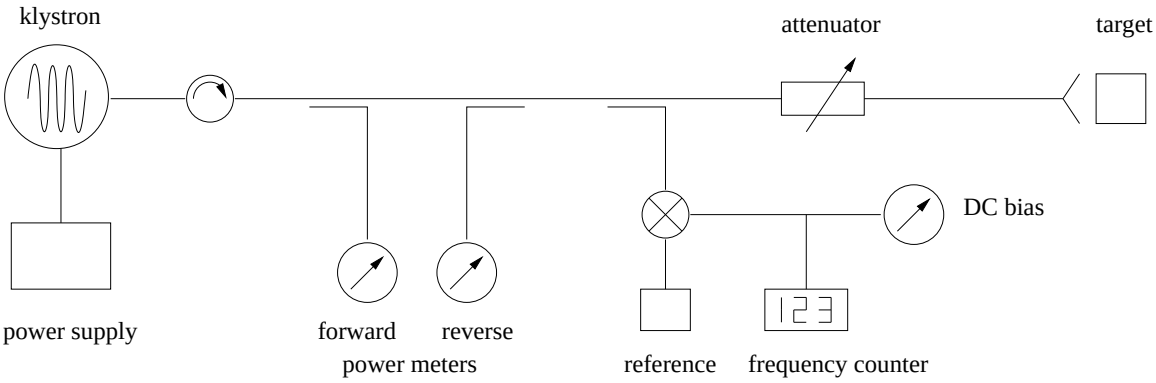

Figure 3.5: Diagram of microwave system for dynamic nuclear polarization.

The microwave frequency was measured by mixing the output of the klystron with a stable 11.5006 GHz reference. The 6th harmonic of 11.5006 GHz is 69.0036 GHz which is the approximate microwave frequency required to polarize the target. This produces a beat frequency in the 40-600 MHz range. A digital frequency counter provided a convenient way to monitor this. Maximum positive and negative polarizations were observed at beat frequencies of 90MHz and 520MHz respectively.

The beat frequency is the difference in frequency between the microwave source and 69.0036GHz. The beat frequency is not sufficient to uniquely determine the microwave frequency. Maximum negative polarization will occur at a frequency higher than the frequency for positive polarization which leaves 69.524 GHz as the only possibility. The ambiguity for maximum positive polarization is removed by considering the difference between the frequencies for the positive and negative states determined by others[37] under similar conditions. This gives 69.097 GHz as the microwave frequency producing maximum positive polarization.

A variable attenuator reduced the microwave power reaching the target with the optimal setting determined experimentally. Total microwave power reaching the target was

estimated at 6mW [7] by comparing resistive and microwave heating using the RuO sensor anchored to the ^{3}He cup. The current through a 1KΩ resistor attached to the ^{3}He cup provided a well defined heat input for this purpose.

The waveguide was terminated in a conical microwave horn located directly above the target. The copper ^{3}He cup served as a resonant cavity. Maximum target polarization was reached after 20 minutes of irradiation with microwaves at the frequency for the desired polarization state. Reversing target polarization involved both a mechanical adjustment of the klystron as well as retuning the reflector voltage.

Many factors including the preparation and storage of the target material, changes in operating temperature and drift in the microwave source affect the target polarization. Hence, the only reliable method of determining target polarization is by measurement. This is accomplished using a series tuned constant current NMR Q-meter. A detailed discussion of how to determine the target polarization is the subject of the next chapter.

Chapter 4

Target NMR Polarimetery

Target polarization is one of the quantities that must be accurately determined for the measurement of $\Delta\sigma_L$. A series tuned constant current Q-meter nuclear magnetic resonance (NMR) technique was used to monitor target polarization during the experiment. Several approaches to the offline analysis of the NMR spectra to extract deuteron polarization were investigated.

The characteristic double peaked structure resulting from the interaction of the deuteron quadrupole moment with the molecular electric field gradient in frozen propanediol, can be used to obtain polarization directly from the enhanced signal without the need for a separate calibration step. The focus of this chapter will be on deuteron NMR, but proton NMR will be discussed in the context of the equal spin temperature (EST) hypothesis. The EST hypothesis provides a method that takes advantage of the relative ease of measuring proton polarization to determine deuteron polarization indirectly.

Two separate analog front ends were used for proton and deuteron NMR because it was not practical to construct a RLC circuit, that could be easily tuned over the frequency range required, using a single box. Challenges involved in the measurement of the small signal involve supression of the circuit background, stability over time, sources of noise and signal distortion due to the electronics. Target polarimetery, consisting of the hardware and software of the NMR system and offline data analysis, represents a significant investment

of time and effort in the development of a polarized deuteron target.

4.1 NMR Principles

Nuclear magnetic resonance was discovered independently by Block and Purcell in 1945. A large static magnetic field breaks the energy degeneracy between the nuclear Zeeman levels so that transitions can be driven by a RF field applied perpendicular to the static magnetic field. The energy absorbed or emitted is proportional to the difference in the populations of the magnetic substates and hence the polarization of the target material. The RF frequency required, known as the Larmor frequency, is determined by the gyromagnetic ratio of the nuclei of interest and the strength of the static magnetic field. In practice, the frequency response is broadened by small variations in the local magnetic field but, as the term resonance implies, the response is negligible outside of a narrow frequency band centered around the Larmor frequency.

The net absorption or emission of electromagnetic radiation by the nuclear spin system can be modeled macroscopically as the imaginary component of complex magnetic susceptibility, $\chi(\omega) = \chi'(\omega) + i\chi''(\omega)$. The vector polarization, P_z, can be written as

$$P_z \propto \int_0^\infty \chi''(\omega)\, d\omega \tag{4.1}$$

which forms the basis for the area methods used to determine polarization as described in Section 4.3.1. To measure $\chi''(\omega)$, the target material is placed in the bore of a coil so that the inductance L is given by

$$L = L_0[1 + 4\pi\xi\chi] \tag{4.2}$$

where L_0 is the inductance of the empty coil and ξ is a geometric filling factor. This relationship shows how target polarization modifies the inductance. A RLC circuit constructed to resonate at the Larmor frequency of the target nuclei provides initial amplification of

the NMR signal. Off resonance, the imaginary impedance of the pickup coil is reduced by the impedance of the capacitor. The RLC resonance condition $f_0 = 1/(2\pi\sqrt{LC})$ places a practical upper limit on the inductance. Although a larger inductance is beneficial because the NMR signal scales linearly with L_0, the choice of the fixed capacitance C must be large enough to dominate stray capacitance present in the system.

The Q-meter technique originated from the ability to make very sensitive measurements to determine the change in ratio of the real and imaginary impedances of a tuned circuit. The quality factor, or Q, of any resonant system characterizes the sharpness of the resonance and can be expressed in many equivalent ways. For a RLC circuit at resonance, the most convenient for our purposes is $Q = 2\pi f_0 L/R$. The NMR signal modifies the Q of the tank circuit by absorption or emission of energy which changes the effective value of R.

To clarify nomenclature, the term "NMR signal" will be used to refer to the component of the voltage response as a function of frequency due to the polarization of the material. Proton NMR is less challenging than deuteron NMR in frozen propanediol for several reasons. Higher polarization resulting from the larger dipole moment produces a larger NMR signal and, the lack of quadrupole splitting results in a smaller signal bandwidth.

4.2 NMR Hardware and Software

The NMR system consisted of several modules of both standard components and custom electronics. The analog front end electronics, see Figure 4.1, is based on the Liverpool Q-meter module[38] which has become the *de facto* standard for polarized nuclear target work. Designed for dynamically polarized proton targets with a 2.5T magnetic field, it operates at 106 MHz with the key features being a large dynamic range, excellent linearity, long term stability, magnitude and phase sensitive detection. This hardware has been adapted for use with deuteron NMR at 16.35 MHz by changing the capacitance in the tank circuit and the frequency of the external RF source.

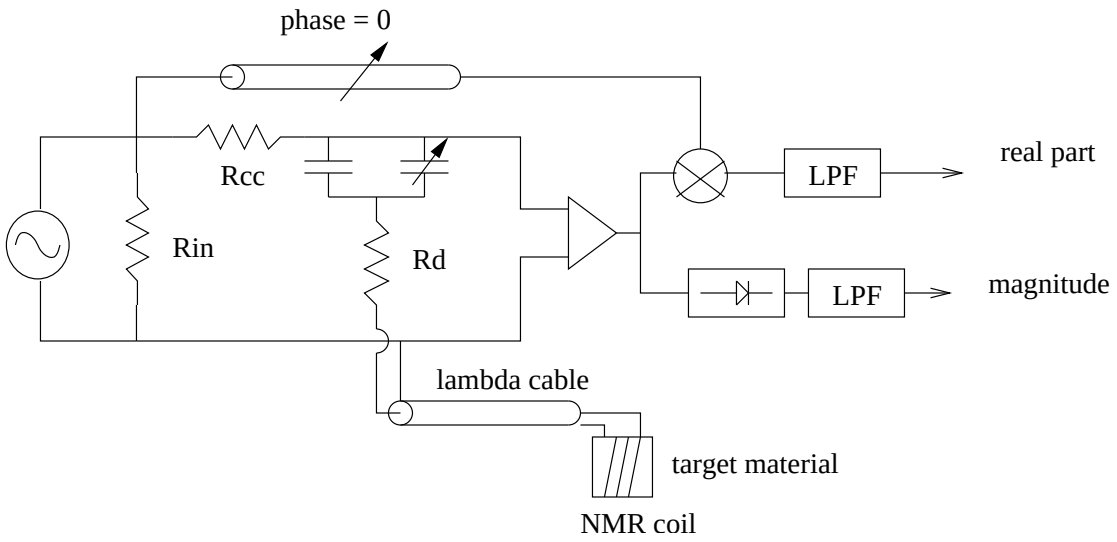

Figure 4.1: Block diagram of front end of NMR analog electronics. The series tuned Q-meter with real part and magnitude outputs is shown.

4.2.1 NMR Coil and Lambda Cable

The NMR coil is 24 gauge bare copper wire wrapped around the outside of the Kel-F target cup in grooves to maintain a fixed geometry. For proton NMR, a 2 turn coil of $L_0 = 0.8\mu H$ was the maximum inductance possible within the constraints imposed by resonance and acceptable values of capacitance. In initial tests with a 2 turn coil an enhanced deuteron signal was observed but, the signal to noise ratio (SNR) was insufficient for quantitative measurements. A 4 turn coil maximized the SNR and maintained the value of C in a practical range. It was physically impossible to place two coils around the target cup. In the absence of a single coil solution, proton NMR and the EST hypothesis were used for the D6 targets and deuteron NMR was used for the D8 targets (see Section 3.3).

The capacitor in the RLC circuit consisted of a high frequency dipped silver mica capacitor in parallel with a mechanically variable capacitor. The primary source of stray capacitance is the copper ^{3}He cup in close proximity to the NMR coil on three sides. In addition to stray capacitance, this also reduces the Q due to eddy current losses. This is important because the Q of the tuned circuit provides the initial amplification of the NMR

signal and in CW NMR spectrometers is typically on the order of 100. There is a tradeoff between increased amplification due to higher Q and distortion caused by non-uniform gain across the spectrum as the Q-curve becomes sharper.

The NMR coil located at the bottom of the cryostat is connected to the room temperature electronics by a semi-rigid UT-85C coaxial cable of length of $n\lambda/2$ where, λ is the wavelength at the Larmor frequency and, n was the smallest integer which provided a cable long enough to connect the coil to the Liverpool module located outside. This condition on the length of the cable comes from transmission line theory which gives that, at these lengths, the cable will contribute a purely resistive impedance to the circuit. For proton NMR, this requirement was satisfied by a λ cable of length 1.971m and deuteron NMR by a $\lambda/2$ cable of length 6.418m. The cable contributes an imaginary, frequency dependent component to the impedance as a direct result of sweeping the frequency.

The cable is the dominant source of NMR background and is also indirectly responsible for the instability over time. Sweeping the magnetic field rather than the RF source driving the RLC circuit, as is the standard practice with NMR spectrometers, is not possible with a fixed frequency microwave source used for DNP as this would result in reduced target polarization.

The voltage measured across the tuned circuit will give the frequency response of the circuit if the current remains constant as the frequency of the RF source is swept. The constant current condition is approximated by placing a 1KΩ resistor, R_{cc}, in series with the RF source. The 1KΩ resistor is two orders of magnitude larger than the impedance of the RLC circuit, including the lambda cable, around the resonant frequency. A damping resistor, R_d, is necessary to prevent oscillation by maintaining a net positive real impedance in the tank circuit when the target transfers energy from the target material to the coil as the frequency is swept through resonance.

A Wavetek Model 5135A phase continuous ultra fast switching frequency synthesizer provided a controllable RF frequency source. This was driven by BCD coded inputs and terminated into a 50Ω load.

Frequency sweeps of ±250KHz and ±300KHz in steps of 1KHz around the Larmor frequency were sufficient to record the entire NMR signal with adequate resolution for proton and deuteron NMR, respectively. This frequency range deliberately included enough channels to the left and right of the NMR signal to easily judge the quality of the background subtraction. A sampling rate of 15KHz was sufficiently slow to allow the frequency synthesizer and DAC output to settle as well as achieve maximum resolution with the ADC. The frequency sweep, background subtraction and data acquisition was controlled by a Windows based PC running LabVIEW.

4.2.2 Signal Quality and Noise

A standard measurement of the quality of an analog signal is the signal to noise ratio (SNR). Quantization error associated with the ADC and DAC should be the dominant source of random noise and be reduced as $1/\sqrt{N}$ where N is the number of data points averaged per channel. No improvement in the NMR signal SNR was evident beyond N=100 after trials with N = 100, 500, 1000 and 10000. Increasing sensitivity through signal averaging to observe the deuteron TE signal would still involve significant improvements in system stability.

Coherent noise refers to features which are constant over time and are therefore reinforced, rather than reduced, by signal averaging. Candidates identified as possible sources of coherent noise include phase noise from the frequency synthesizer and "sticking" bits in the DAC used for background subtraction. The output of the DAC did not change when least significant bits changed. This failure mode was observed in the DAC output of other NI-DAQ boards used at TUNL.

Care was taken to provide good signal hygiene. The Liverpool module was supplied with separate power to the low and high frequency circuits by inductive low pass feedthroughs. The low and high frequency sections were constructed on separate circuit boards and isolated internally in separate shielded compartments within the copper box. Cables carrying analog signals were all coaxial with a grounded shield and the signal was digitized in differential

mode. Analog signal cabling was kept to a minimum length to avoid loops and isolated from power and digital lines. These were routed away from sources of electrical noise and high currents, at right angles if possible, to prevent inductive pickup.

Electronics modules associated with the analog NMR were moved to a separate instrumentation rack to isolate these from digital noise. The entire cryostat was electrically isolated which included insulating couplers inserted into vacuum lines. This was necessary because the copper shield on the coaxial return from the NMR coil was in contact with the cryostat at many points. A 10°C recirculating water system was installed to maintain the λ cable and Liverpool module at a constant temperature.

4.2.3 Detection of the NMR Signal

Detection involves a measurement sensitive to small changes in the amplitude of a RF voltage. Magnitude detection was implemented using full wave diode rectification followed by a low pass filter to produce a DC voltage proportional to the amplitude of the RF signal. This is a simple circuit which requires minimal tuning but a large background contribution from the frequency response of the cable is present. It also results in instability because a large component of shift in background is due to changes in the imaginary impedance of the cable as the teflon dielectric responds to variations in temperature along the length of the cable[39, 40]. The magnitude detection output was used to adjust the variable capacitance in the RLC circuit to achieve resonance at the Larmor frequency.

Phase sensitive detection is an improved technique which provides discrimination between the NMR signal and imaginary impedance of the circuit elements by selecting only the component of the voltage response that is in phase with the driving RF source. This technique was implemented with a doubly balanced mixer where the reference signal was mechanically adjusted through an external length of UT-85C coaxial cable to provide a 0° reference. A tradeoff between phase sensitive and magnitude detection is reduced sensitivity due to losses in the passive mixer. Difficulty in adjusting the external delay line and lack of a method to verify the value of the resulting reference phase at the input to the

mixer has raised questions about the reliability of this method in the present system. The implication is that the signal measured contains an arbitrary mixture of absorptive and dispersive components[41].

4.2.4 Hardware Background Subtraction

To record, average and analyze the NMR signal it was digitized with a NI-DAQ AT-MIO-16X 16-bit ADC. Prior to digitization, hardware background subtraction was necessary. This step removes the frequency dependent circuit response which is orders of magnitude larger than the NMR signal. Background spectra were NMR spectra acquired with the static magnetic field shifted $\pm 5\%$ around nominal operating current to move the entire NMR signal outside of the frequency range swept by the RF source. Sets of backgrounds were recorded as a function of the LHe level over several LHe fill cycles. Over short periods of time it was found that reproducible variations in the backgrounds were synchronized with the LHe level. This was explained by the change in the temperature gradient along the lambda cable as it passed through the region of the cryostat in thermal contact with the 2K bath.

In principle, the best possible sensitivity is obtained by subtracting the response of the entire system without the signal present from the response with a signal. The usefulness of this technique relies on the stability of the system over a period of hours to days. This method did perform well for proton NMR.

After background subtraction, the signal was fed to the digitizer. An on-board amplifier automatically chose the maximum gain possible without saturating the ADC to achieve the optimum resolution of the digitized signal. All analog signals were digitized using differential mode to negate the effects of ground loops or other sources of pickup.

4.3 Extracting the Polarization

There are several methods used to determine target polarization from the recorded NMR spectra. The first step common to all methods removes any residual background that remained after the hardware subtraction. The source of this residual parabolic background was slow drift in circuit parameters in the tuned circuit dominated by the lambda cable. A second order polynomial fit to data at the edge of the spectrum, well outside the range of the NMR signal, was subtracted from the signal to remove the residual background. The deuteron signal analysis used data from the flat regions indicated in Figure 4.6. This choice provided sufficient data well outside of the NMR signal to provide a reliable fit while discarding the first and last channels which often were corrupted. This rather simple phenomenological approach proved very effective in producing the desired flat background on either side of the NMR signal as long as the residual background was small.

4.3.1 Area Methods

The magnitude of the NMR signal is proportional to the difference in spin state populations which is in turn proportional to the polarization of the target material. The simplest method to quantify the magnitude of a complex spectrum is to calculate the total area under the NMR signal. This area is linearly proportional to vector polarization of the target material but some method will be required to determine the constant of proportionality. A common calibration technique referred to as the thermal equliblibrium (TE) method, uses the fact that at a known magnetic field and temperature, the polarization of the nuclei can be calculated from Equation 1.2. This method is very sensitive to the linearity of the system over a large range of signal size since the calibration point is often much smaller than the polarization expected with DNP. An effective area was measured by a simple Riemann sum.

The area method with a TE calibration is used for proton NMR but due to a lack of sensitivity, the deuteron system failed to detect the TE NMR signal at either 1K or 0.5K. A detailed discussion of the protocol of this method will be presented in Section 4.4.2 when

discussing proton NMR in the context of the EST hypothesis.

Low polarization under TE conditions and hence small signal mean the uncertainty in the measured polarization of the target is dominated by the uncertainty in the value of the ratio of polarization to area (P/A). To reach TE conditions the target must remain at a constant temperature, with the microwaves off, for several times the spin lattice relaxation time constant, T_1. This corresponds to about 8 hours at 0.5K and, when combined with the time required to acquire the TE data, adds significant length to experimental run time.

Another calibration method is a low-energy neutron transmission experiment E_n=1.18MeV where $\Delta\sigma_L$ is calculated using the CD-Bonn NN potential model [42]. When $\Delta\sigma_L$ is taken as a known, Equation 2.2 can be inverted to obtain $P_T\,x$. This calibration method needs a low energy source of polarized neutrons which would require a different production reaction such as $^3\mathrm{H}(\vec{p},\vec{n})^3\mathrm{He}$. To implement this would require a polarized proton beam as well as physically changing the neutron production target from a deuteron gas cell to a tritiated foil.

Besides simplicity, the area methods for determining polarization are also much less sensitive to frequency-dependent distortion than methods such as the fit to a theoretical model.

4.3.2 Fit to Theoretical Lineshape

A common method of extracting information from a complex set of data such as spectra, involves fitting to a theoretical model where the parameter of interest is allowed to vary. The interaction of the deuteron quadrupole moment with the molecular electric field gradient shifts the m=±1 substates producing two peaks corresponding to the m=-1 to m=0 and m=0 to m=1 transitions, as shown in Figure 4.2. In an amorphous material such as rapidly frozen propanediol, molecules are randomly oriented relative to the external static magnetic field causing an asymmetric broadening of the peaks.

Defining r as the ratio of intensities of these transitions, we can relate this to the population differences of the Zeeman levels by

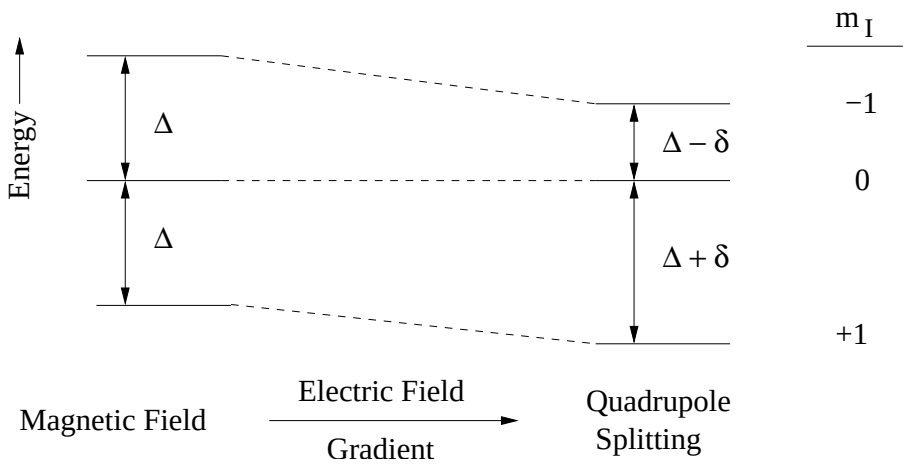

Figure 4.2: Deuteron quadrupole energy shift. Energy level diagram of the deuteron in a magnetic field showing the shift in the m_I =+1, -1 levels resulting from the interaction between the quadrupole moment and an electric field gradient. This is responsible for the double peaked NMR signal in frozen 1,2-propanediol.
.

$$r = \frac{I_-}{I_+} = \frac{n_0 - n_-}{n_+ - n_0} \tag{4.3}$$

The vector and tensor polarizations, P_z and P_{zz} respectively, can now be expressed in terms of r as

$$P_z = \frac{n_+ - n_-}{n_+ + n_0 + n_-} = \frac{1 - r^2}{r^2 + r + 1} \tag{4.4}$$

$$P_{zz} = \frac{1 - 3n_0}{n_+ + n_0 + n_-} = \frac{r^2 - 2r + 1}{r^2 + r + 1} \tag{4.5}$$

Since the peaks corresponding to the two transitions overlap, the only reliable method to separate the contributions is by fitting the NMR data to a theoretical model of the single lineshape. This method has the advantage that polarization is obtained directly from the dynamically polarized signal without the need for a calibration reference. It also eliminates the time spent acquiring and analyzing TE data to extract P/A.

Lineshape Model

The details of the theoretical lineshape for deuteron in frozen propanediol developed by Hamada, et. al. [43] will be reviewed given the central importance of this model. This will also provide insight into the parameters of the model which must be fixed prior to extracting polarization.

To first order, the quadrupole frequency shift, $\Delta\nu$, is given by

$$\Delta\nu = -(m - 1/2)\nu_Q\lambda(\theta, \phi) \tag{4.6}$$

where ν_Q is the deuteron quadrupole frequency and $\lambda(\theta, \phi)$ is a factor that accounts for the dependence of the quadrupole shift on orientation of the molecules relative to the magnetic field.

A normalized frequency x defined by

$$x = \frac{2(f_D - f)}{\nu_Q} \tag{4.7}$$

is introduced to make the model independent of the Larmor frequency, f_D.

A readable derivation of the transition intensities is given by Slichter[44] in a discussion of powder NMR which has the same form due to the similarity between the randomly oriented domains in a finely granulated solid and a polycrystalline material.

The transition intensities are convolved with a phenomenological broadening function $f(x)$ to model the dipole-dipole interactions of the deuterons and the paramagnetic centers. $f(x)$ is chosen to be a bell shaped function. A spin-packet width parameter σ controls the shape of the bell. There are several possible contributions to σ including magnetic field inhomogeneity and bond anisotropy but, in this case, both of these are negligible relative to the broadening due to the high concentration of Cr^V in the target material. The transition intensity is given by

$$F(x) = \frac{1}{p}\int_q^s f(x-\rho(1-t^2/2))K[(q/p)g(t)] + \frac{1}{q}\int_p^s f((x-\rho(t^2-1-\eta))/2)K[(p/q)g(t)] \quad (4.8)$$

where

$$p = \sqrt{2\eta} \qquad q = \sqrt{3-\eta} \qquad s = \sqrt{3+\eta} \quad (4.9)$$

$g(t) = \sqrt{(s/t)^2 - 1}$ and $K(x)$ is the complete elliptical integral of the first kind. The electric field asymmetry parameter, η, is defined as

$$\eta = \frac{V_{yy} - V_{xx}}{V_{zz}} \quad (4.10)$$

where V_{xx}, V_{yy} and V_{zz} are the principle components of the molecular field gradient tensor. F(x) and F(-x) are proportional to the transition intensities I_- and I_+, respectively. The complete NMR lineshape is the sum of the transition intensities for both transitions $m = 0 \rightarrow -1$ and $m = 1 \rightarrow 0$. These are symmetric about $x = 0$ in the limiting case of zero polarization.

Partially deuterated (D6) propanediol contains only the C-D bond while fully deuterated (D8) propanediol contains both C-D and O-D bonds. This lead to two sets of model parameters labeled as η_{OD}, η_{CD}, ν_{QOD}, ν_{QCD} and the ratio ρ where $\rho = |\nu_{QOD}|/|\nu_{QCD}|$.

The complete NMR lineshape is

$$\sum_{i=CD,OD} C_i(rF_i(x) + F_i(-x)) \quad (4.11)$$

where i is the bond type and C_i is the fraction of deuterons in these bonds. The relative components which make up the D8 lineshape model are shown in Figure 4.3.

The vector polarization P_z is proportional to the absorptive part of the NMR lineshape derived from transition intensities as discussed above. With magnitude detection, the NMR signal contains both absorptive and dispersive contributions (see Figure 4.4). The Kramers-Kronig equation gives the relationship between the dispersive (χ') and absorptive (χ'')

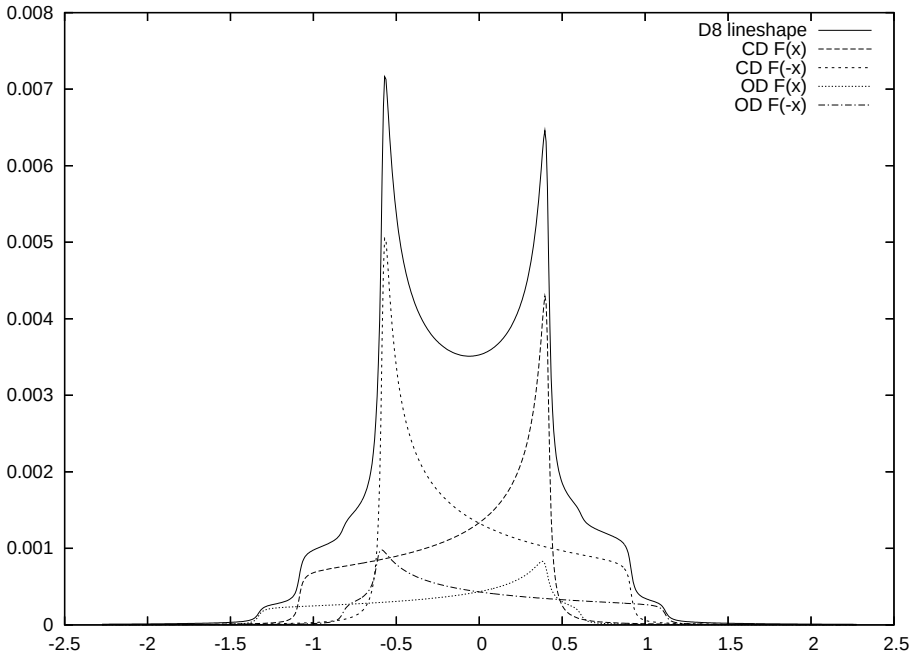

Figure 4.3: Components of the D8 lineshape model. The components of the lineshape model are plotted separately to illustrate the contribution of the two transitions and bond types to the overall lineshape. F(x) and F(-x) correspond to the m_I transitions -1 to 0 and +1 to 0, respectively with the larger F(-x) indicating a positive polarization in this example. Summing the contributions produces the D8 signal shown as a solid line.

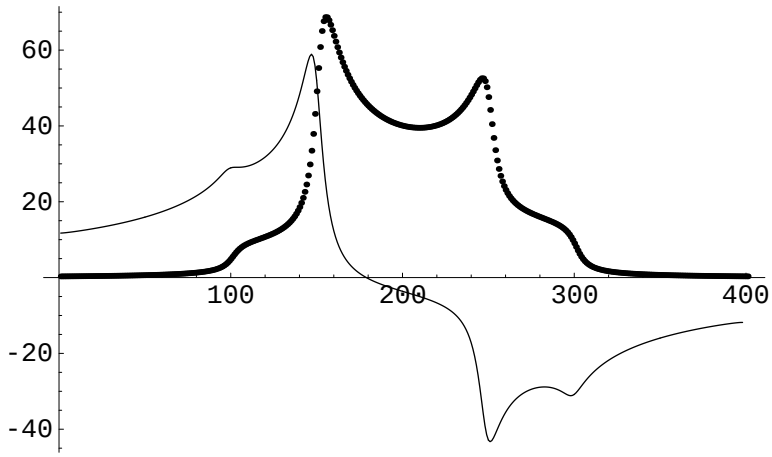

Figure 4.4: Dispersive and absorptive components of the deuteron NMR signal. The dispersive component (solid line) of the deuteron NMR signal was calculated using discretely sampled points of the absorptive component.

components of the magnetic susceptibility

$$\chi'(\omega) = \frac{2}{\pi} \int_0^\infty \frac{\chi''(\omega')\omega' d\omega'}{\omega'^2 - \omega^2} \tag{4.12}$$

It is important to note that this dispersive contribution cannot be removed by the hardware background subtraction although in principle, real part detection should not be sensitive to it. For NMR signals obtained with magnitude detection, the dispersive contribution should, in theory, be included in the lineshape model. Since the NMR signal is negligible outside of a small region surrounding the Larmor frequency, the dispersive component may be calculated with good accuracy from Equation 4.12.

Numerical Methods

Numerical methods will be discussed due to the practical difficulties with evaluation of the theoretical model and the fitting routines. The analysis was done using a program written in Fortran 77 with PGPLOT[45] routines to produce graphical output. LAPACK[46] routines were used for the linear fit and MINPACK[47] routines for nonlinear least squares fitting. Mathematica 5.1 was used to rapidly develop numerical integration, signal process-

ing, regression and graphical output as a benchmark for comparison. Emphasis was placed on developing robust methods rather than on computational efficiency in an effort to avoid spurious results.

Evaluation of the Theoretical Model

Numerical evaluation of the two integrals in Equation 4.8 requires care as the integrands in both cases approach infinity at the upper limit of integration where $K(k) \rightarrow \infty$ as the argument $k \rightarrow 1$. The general problem of integration with a singular integrand at one endpoint can be approached several ways but the simplest is a variable transformation of the form

$$\int_a^b f(x)dx \quad \longrightarrow \quad \frac{1}{1-\gamma} \int_0^{(b-a)^{1-\gamma}} f(b - t^{1/(1-\gamma)})dt \tag{4.13}$$

for $a < b$ and $0 \leq \gamma < 1$. The choice of $\gamma = 1/2$ was sufficient to produce a rapidly converging integrand suitable for Romberg integration.

The choice of the phenomenological broadening function $f(x)$ as a Lorentzian,

$$f(x) = \frac{\sigma}{\pi(x^2 + \sigma^2)} \tag{4.14}$$

leads to a convenient variable substitution[48] resulting in a smooth peak in the integrand as the denominator passes through a minimum.

Evaluation of the dispersive component of the NMR signal using equation 4.12 is a computationally intensive task. It requires multiple evaluations of the lineshape and, it is not numerically well behaved because of the singularity at $\omega' = \omega$ in the integrand. Since the NMR signal is measured at discrete points, it is only necessary to compute the dispersion term at the same set of points. This observation along with the uniform spacing of these points, leads to a simple approximation that considerably reduces the computational cost of calculating the dispersion term [48].

The integral can be written as the sum of two integrals by the method of partial fractions

giving

$$\int_0^\infty \frac{\chi''(\omega')\omega' d\omega'}{\omega'^2 - \omega^2} = \frac{1}{2}\int_0^\infty \frac{\chi''(\omega')d\omega'}{\omega' - \omega} + \int_0^\infty \frac{\chi''(\omega')d\omega'}{\omega' + \omega} \tag{4.15}$$

The first integral was further divided into three regions and the integrand was approximated as a second order polynomial. These integrals can then be evaluated in terms of the values of χ'' at the sampled points and the spacing between the points. The second integral can be expressed as a sum.

Fitting Methods

If the model depends linearly on parameters, the global minimization required to find the least squares fit is reduced to solving a set of linear equations. The only complication that can arise is flat regions in χ^2. Nonlinear fitting, on the other hand, is an inherently difficult problem because no automated procedure for finding global minima exists. This reduces all methods to an iterative process. The only difference between methods is the manner in which the next choice of parameters is made.

This technique requires guidance most often in the form of initial estimates of parameter values. The need for good starting values for the fit parameters is exaggerated when qualitative features of the model and data do not agree. For this reason, a qualitative understanding of effects of the parameters on the lineshape is helpful before attempting a semi-automated fit based soley on minimizing the chosen metric.

The offset parameter for centering the NMR signal requires a non-linear fit because the lineshape function, $F(x)$, is a non-linear function. The broadening parameter σ reduces peak height and rounds the features of the signal. The asymmetry parameter η moves the position of the peaks with smaller values moving them closer together. In the limit of a symmetric bond($\eta = 0$) the two transitions converge to a single peak. Fundamental quantities, such as the deuteron quadrupole moment which have been measured with much greater precision by others and are not affected by the target conditions, could be taken as known constants. The quadrupole coupling constant depends on the molecular electric

field gradient for propanediol, but this has not been determined.

Methods such as n-point smoothing have been used by others[48] simply because they reduce the number of data points by a factor of n. This is useful in the initial stages of data analysis when multiple parameters are allowed to vary and computation time is long. The disadvantage is that n-point smoothing adds distortion. Smoothing data is not generally considered necessary or advisable when using a method such as least squares which, by design, is equipped to provide the best estimate of model parameters in the presence of noise.

Ideally, the parameter of interest should show a strong relationship to polarization and be insensitive to small uncertainties in the other fixed parameters. The aim of the method was to fix η, σ, and ρ, allowing only r and the overall magnitude to vary. The reliability and reproducibility was extensively tested using simulated data with additive Gaussian distributed noise to confirm that parameter values returned from a fit were were in agreement with those used to generate the simulated data. Statistical tests to determine reasonable ranges for the model parameters were carried out to establish the overall uncertainty in target polarization.

4.4 Data Analysis

The two main experimental procedures used to determine the target polarization and the results will be discussed in this section. The first procedure is to extract the polarization by fitting the D8 deuteron NMR data to a theoretical model and the second method uses the EST hypothesis to determine polarization from the D6 proton NMR data.

4.4.1 Fit Data

Figure 4.5 shows the D8 signal prior to hardware background subtraction. Note that the response of the tank circuit and lambda cable dominate and it is not possible to distinguish the enhanced deuteron signal on top of this background.

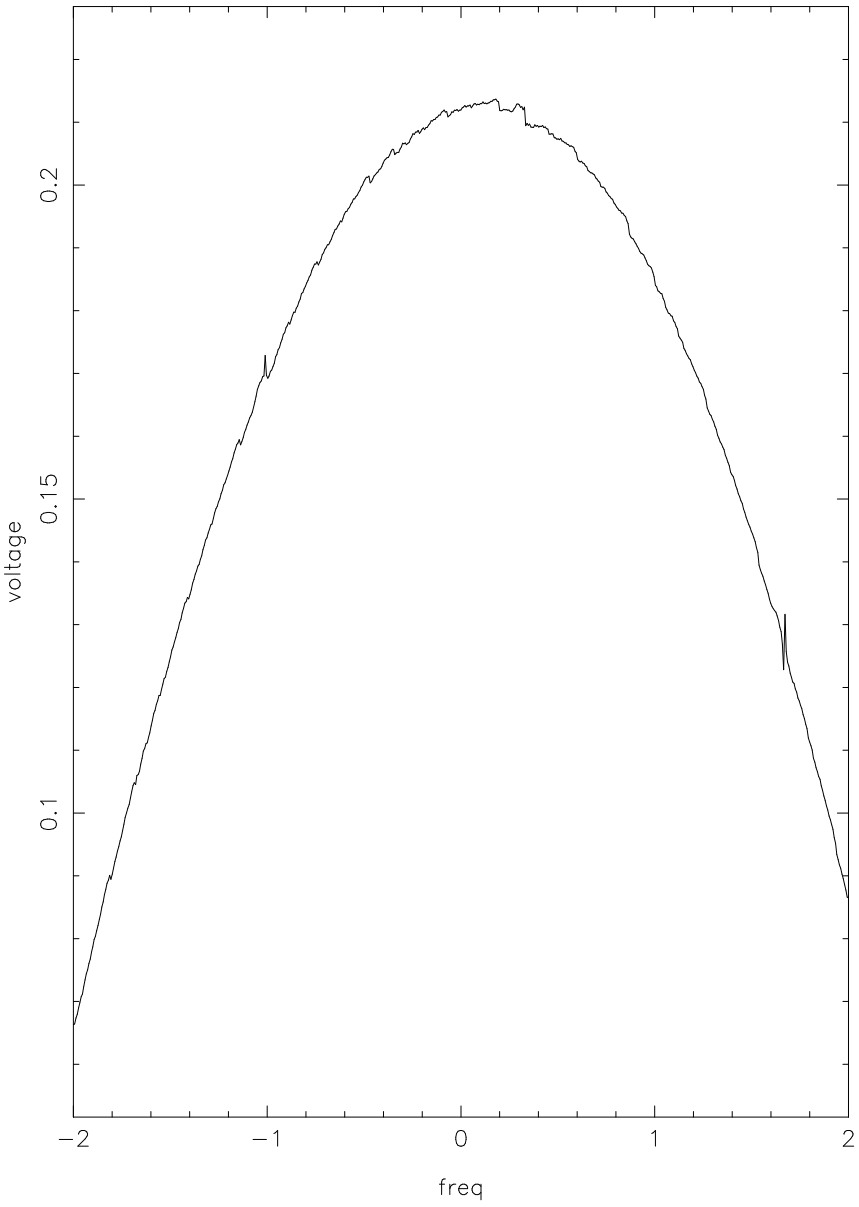

Figure 4.5: NMR background. The enhanced deuteron D8 signal without hardware background subtraction.

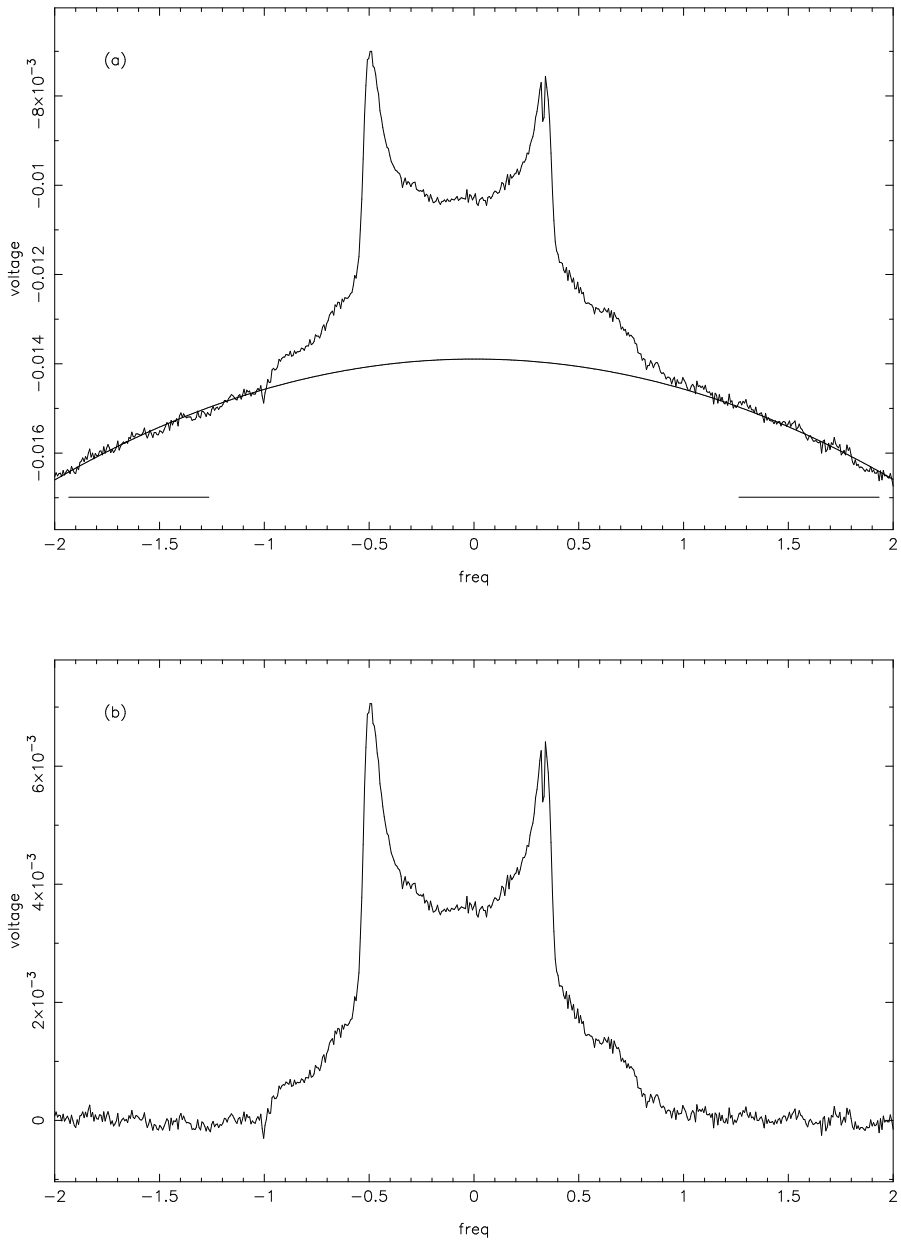

Figure 4.6: Deuteron NMR signal before and after residual background subtraction. (a) Original deuteron NMR signal with fitted quadratic background. The horizontal lines indicate region of signal used to generate quadratic fit. (b) NMR signal after background subtraction. The voltage scale in arbitrary units and the frequency is the normalized frequency (see Equation 4.7).

Figure 4.6 (a) shows a good quality NMR signal obtained after hardware background subtraction and the characteristic shape is now clearly evident. It is necessary to remove the remaining background using a quadratic fit to the edges of the signal, and this is shown in Figure 4.6 (b). This signal with a flat baseline is now suitable for lineshape fitting.

The development of the lineshape fit was done using the best quality data. Examples of poor quality data included NMR signals with large residual backgrounds where, a quadratic fit no longer produced a result suitable for lineshape fitting. This is indicative of a drift in system parameters over hours of operation.

The outliers seen in the data shown in Figure 4.7 were caused by "sticking" bits on the DAC output used for the hardware background subtraction. These were consistent between multiple data sets and provided the most severe examples of coherent noise. In order to fit these signals, individual points that varied more than 10% from each neighboring point were discarded prior to fitting as the least squares method is negatively influenced by outliers.

The procedure followed to fit the model and extract the parameters will be discussed using the high quality data set shown in Figure 4.8. The initial parameter sets for the automated fitting routines were determined by a visual fit. To fit the D8 data, it was recognised that the OD parameters contribute only a small amount to the overall lineshape, primarily to the pedestals, and therefore the first step involves estimating the CD parameters alone. The overall amplitude and the frequency offset were first approximated by eye. The quadrupole coupling frequency, ν_{QCD}, which controls the separation of the two peaks, was chosen by visual inspection. The model was found to be very insensitive to the η_{CD}. The initial value of η_{CD} was chosen to be consistent with values used by others as it is a constant set by the symmetry of the CD bond. With an initial value of P_z estimated from the difference in peak heights, σ was varied to obtain the correct ratio of peak to trough heights. It was necessary to allow the amplitude to vary while determining sigma because sigma has a significant effect on the overall size of the lineshape. Once sigma was chosen, the final adjustment involved simultaneously fitting the transition intensity ratio parameter, r, and the overall amplitude to determine P_z.

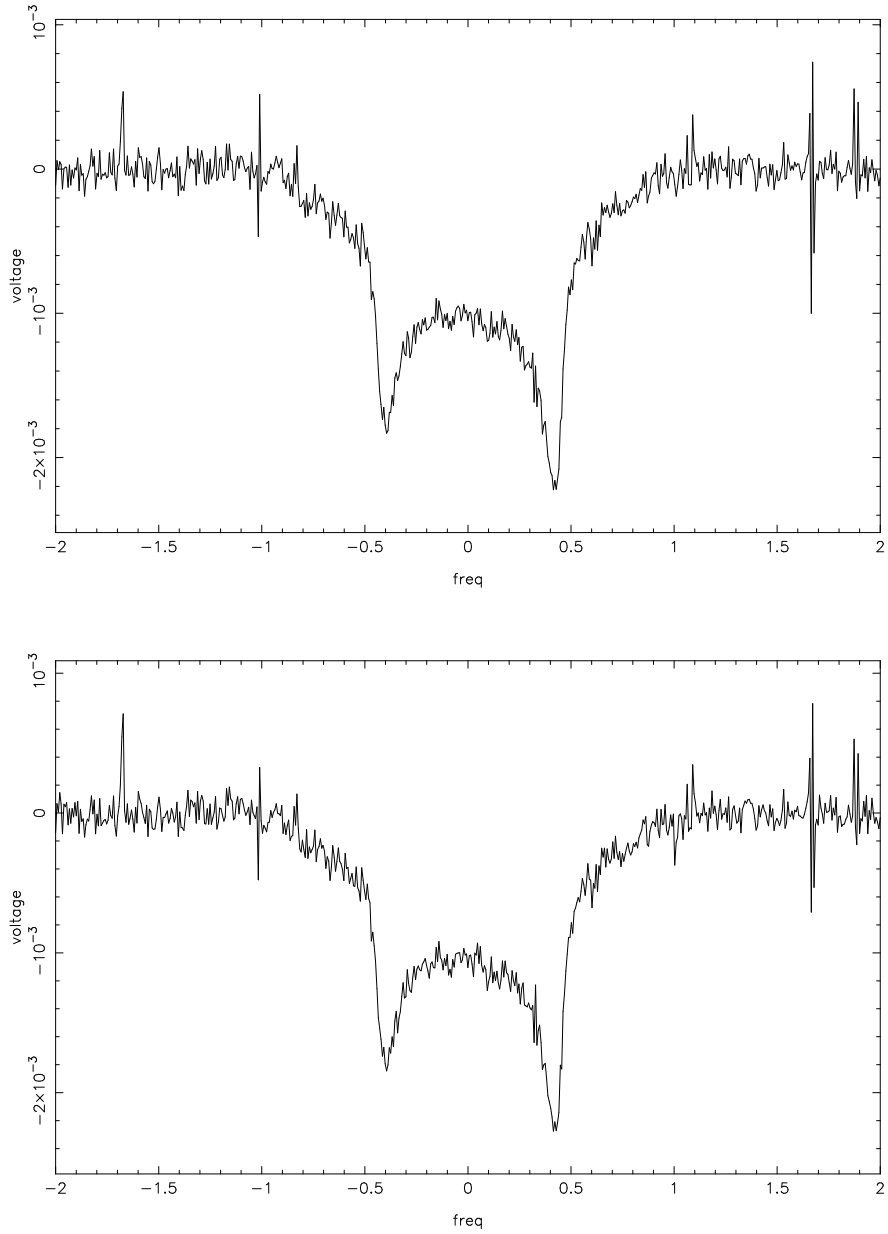

Figure 4.7: Typical D8 NMR datasets. Two of the typical NMR datasets used to produce Table 4.2. The distortion termed "coherent noise" is visible as similar features outside of the NMR signals in both spectra. This clearly demonstrates that these patterns are not random and therefore will not benefit from additional signal averaging.

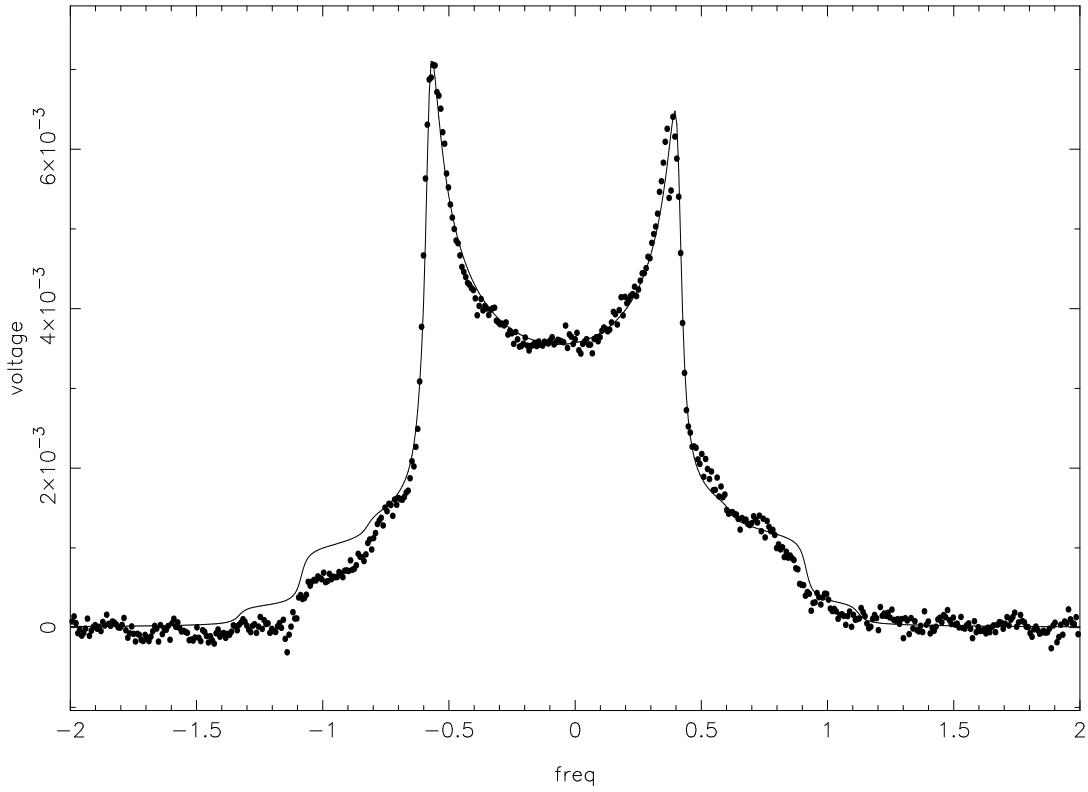

Figure 4.8: Full fit to "best data". Non-linear fit of deuteron signal to theoretical lineshape with all parameters allowed to vary. The polarization $P_z = 11\%$ with other fit parameters are listed in Table 4.1, fit run 1. The voltage scale in arbitrary units and the frequency is the normalized frequency.

The starting point for determining the two parameters specific to the OD bonds was to recognize that the model is insensitve to η_{OD} and therefore, like the case for η_{CD}, this was set to the value determined by Hamada. The final parameter ν_{QOD} is known to be larger than ν_{QCD} and by varying it over a range of several KHz, the best fit to the pedestals was used to establish a final value. Once all fundamental parameters were fixed, a slightly better overall fit could be obtained by allowing small variations in σ, amplitude and r to arrive at the final set of parameters and a value for P_z as shown in Figure 4.8.

The best fit parameters determined by this procedure are shown in Table 4.1 fit run 1. Fit runs 2, 3 and 4 in Table 4.1 show the value obtained for P_z is insensitive to reasonable changes in σ, η_{CD} and ν_{QOD}, respectively. For fit run 2 all parameters were held constant and P_z was determined by fitting. A similar procedure was followed for η_{CD} and ν_{QOD}.

The goal of the fitting to the lineshape is to reliably determine the target polarization[49, 50]. To this end, a simplified approach is to look at the sharpness of the minima of χ^2 as a function of P_z with all other parameters held constant at their best fit values as shown in Figure 4.9. This analysis led to the observation that if the initial fit is not sufficiently close to the best fit parameters, it was possible that χ^2 would not exhibit a minima in the range of physically reasonable values of target polarization. This was particularly evident when the model and the data exhibited qualitative differences attributed to distortion. This emphasizes the need to fit by eye to obtain an initial parameter set before an automated fit based on χ^2 is attempted.

The standard definition of χ^2,

$$\chi^2 = \frac{1}{N\Delta d}\sum_{i=1}^{N}(y_i - d_i)^2 \tag{4.16}$$

where N is the number of data points, y_i is the predicted value corresponding to the ith data point, d_i and Δd is the measurement uncertainty. For all datasets, N = 599. Setting $\chi^2 = 1$ for the best fit set of parameters and inverting Equation 4.16 yields $\Delta d = 1.73$ x 10^{-4}. This estimate of a uniform uncertainty for measured points that make up the signal is

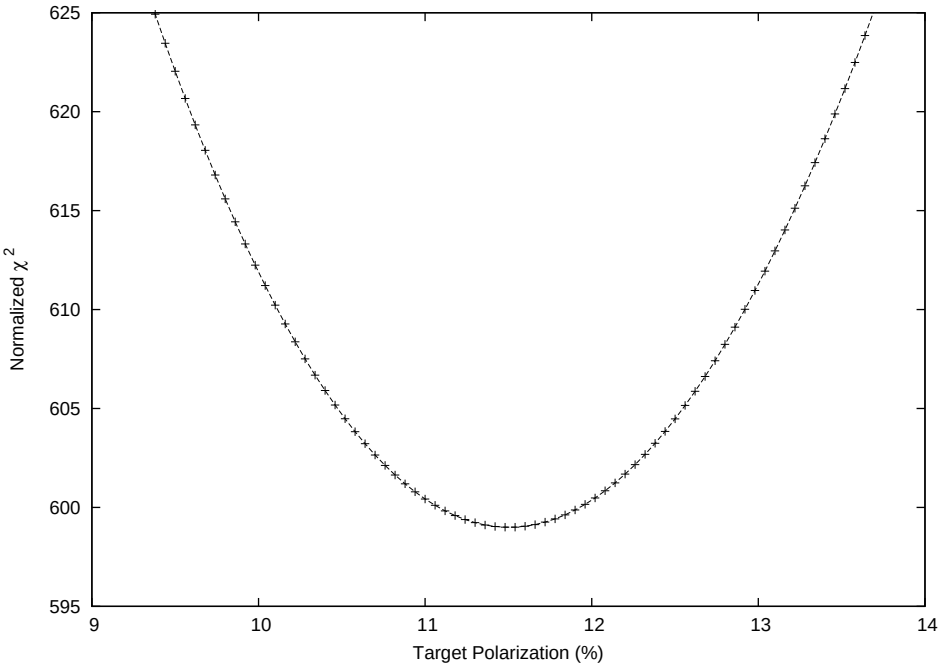

Figure 4.9: χ^2 versus target polarization. This shows the dependence of χ^2 on P_z over the range of physically reasonable target polarization with all other model parameters held constant at their best fit values. χ^2 was normalized to χ^2 for $P_z = 11\%$ with N=599.

approximately equal to the peak-to-peak height of the coherent noise.

To determine a quantitative estimate of the uncertainty in the value of P_z obtained from lineshape fit, values obtained from multiple data sets are compared. The target polarization can be expected to remain constant when the NMR data sets are taken over a short period of time relative to T_1. With T_1 on the order of hours, a set of five NMR spectra collected at intervals of less than two minutes should return the same polarization within measurement uncertainties. While such a small data set is not ideal for statistical analysis, the standard deviation of the values of P_z is given in Table 4.2 as the statistical error.

Table 4.1: D8 model parameters for full fit to "best data".
The parameters used to generate Figure 4.8 are shown as fit run 1. Fit runs 2, 3 and 4 show the effect on P_z as a result of varying one parameter.

fit run	r	P_z	ν_{QCD} (KHz)	ν_{QOD} (KHz)	η_{CD}	η_{OD}	$\sigma(KHz)$	ρ
1	0.85	11.0	1.75	2.150	0.025	0.17	2.48	0.92
2	0.86	10.0	-	-	-	-	2.6	-
3	0.83	12.9	-	-	0.027	-	-	-
4	0.85	11.2	-	2.40	-	-	-	-

Table 4.2: Uncertainty in target polarization. Error estimate for target polarization from fit to multiple data sets.

data set	A	B	C	D	E	F
P_z (%)	-15.2	-15.4	-14.9	- 15.1	-0.152	-0.152
ave. P_z $\pm$ std. dev.	**-15.13 $\pm$ 0.12**					

The acceptable ranges for P_z induced by model parameters varying over their 90% confidence interval are given in Table 4.3.

The data analysis above has focused on understanding the fit to the model using a limited number of specifically chosen data sets. To evaluate the usefulness of the lineshape fitting method as a technique for measuring target polarization, an analysis of 643 spectra acquired over five days in February 1999 is presented below. One of the better spectra was selected based on a visual inspection of the SNR. The standard procedure was followed to obtain a best fit set of model parameters. This set of parameters, except for r and

Table 4.3: Sensitivity of target polarization to model parameter variation.

parameter	best fit	90% conf. interval		P_z(%)	
	value	lower	upper	lower	upper
P_z (%)	14.9	-	-	13.3	16.6
σ (KHz)	2.52	2.41	2.64	14.8	15.0
ν_{QCD} (KHz)	176.1	175.8	176.3	14.2	14.2
ν_{QOD} (KHz)	459.6	389.6	559.6	14.3	14.1
η_{CD}	0.00523	0.00443	0.00603	14.1	14.3
η_{OD}	0.104	0.0545	0.173	14.0	14.2

amplitude, are a function of the target material and should be the same for all 643 spectra. Using this set of parameters, a linear least squares fit, allowing r and amplitude to vary, was performed on each one of the 643 spectra. This determined the best fit value of target polarization. To evaluate the quality of the fit, the uncertainty in this best fit value of target polarizaton was evaluated as follows. χ^2 was normalized to 599 (N=599) with this best fit set of parameters for each spectra. The parameter r was systematically varied above and below the best fit value, simultaneously allowing amplitude to vary, until χ^2 increased by 2.7. This gave the upper and lower bounds on the 90% confidence interval for P_z.

Signals with the highest SNR were more consistent with uncertainties in the $\pm 2.4\%$ range. A $\pm 2\%$ absolute uncertainty corresponds to a $\pm 13\%$ relative uncertainty for a nominal target polarization of 15%. Using an uncertainty of less than 2% as a criterion, only 19% of the data was satisfactory. The fluctuations in target polarization and the uncertainty at the 90% confidence level are summarized as a sequence of plots included in Appendix C.

4.4.2 Equal Spin Temperature Hypothesis

The equal spin temperature (EST) hypothesis states that under equilibrium conditions the distribution of populations of the magnetic substates of nuclei of different species can be described by a common spin temperature. As a consequence, deuteron polarization can be determined indirectly from a measurement of proton polarization. The proton signal is

on the order of 500 times larger due to the larger proton dipole moment and the narrower bandwidth.

The phenomena of EST is a result of the mechanism of DNP in frozen propanediol. The validity of the ESTH has been confirmed experimentally for protons and deuterons in D6 1,2-propanediol by groups[37] with instrumentation capable of measuring both proton and deuteron polarization simultaneously. Another result is that maximum polarization will be achieved by all nuclear species at the same microwave frequencies.

TE data was collected at 0.5K and 1K but the final values shown in Table 4.4 were determined from the 0.5K data, due to the improved SNR and resulting decrease in uncertainly of the calibration constant. Temperatures were determined from ^{3}He vapor pressure thermometry. The measured pressures were corrected for the thermomolecular effect which resulted in an increase in temperature on the order of 2%. The correspondence between ^{3}He vapor pressure and temperature was determined by a linear interpolation from a set of values tabulated in steps of 0.5K. Areas were calculated by a simple Riemann sum after residual background subtraction was performed.

Uncertainties were determined by the standard deviation in the values of P/A. The typical uncertainty in P/A was ±5%. This spin temperature was used to calculate the deuteron polarization.

Table 4.4: Summary of EST hypothesis data for partially deuterated (D6) target.

Run	T(mK)	P/A	P_z(P)	P_z(D)
July 98	532	0.042	0.54	0.15
June 99	543	0.016	0.60	0.16
August 99	537	0.038	0.59	0.16

Based on previous experience with the TUNL dynamically polarized proton target which achieved proton polarization in the range of 65–70%[7, 8] , the EST hypothesis predicts deuteron polarization in the range 17–19%. Figure 4.10 shows the relationship between deuteron and proton polarization. These values of target polarization are at the high end of the range observed.

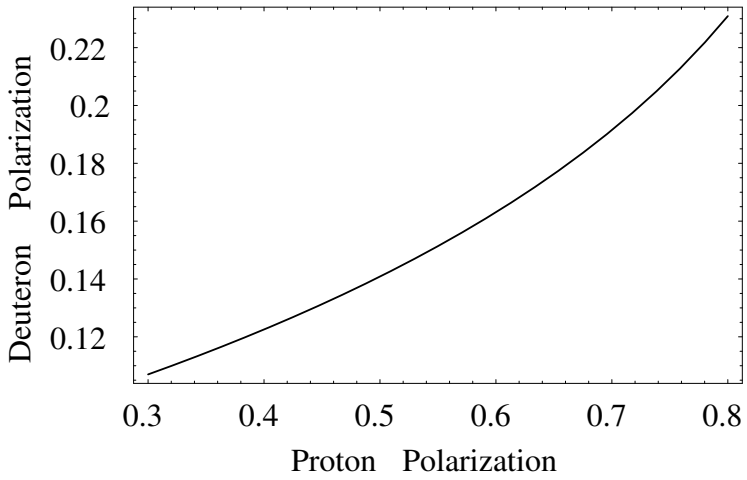

Figure 4.10: The relationship between proton and deuteron polarization given by the EST hypothesis. This plot was generated by inverting Equation 1.2 to give T as a function of proton P_z and then substituting this expression for T into Equation 1.3 to give deuteron P_z in terms of proton P_z.

This method was used for D6 targets but the increase in uncertainty in $\Delta\sigma_L$ due to the remaining protons in the OH groups was too high to observe the zero crossing in $\Delta\sigma_L$ at 12 MeV. In high purity D8 targets, there are not enough residual protons to make an accurate proton TE measurement and, it has been suggested that in very dilute systems, the EST may not hold.

4.5 Observations and Conclusions

As discussed in section 4.1.1, P_z was extracted from NMR spectra by fitting the model developed by Hamada. A large number of simulations were performed with different constraints on the parameters. The sensitivities of the parameters were investigated with limiting conditions providing deuteron polarizations in the 11 - 15% range. An optimum fit to high quality data shown in Figure 4.8 gave $P_z = 11\%$. Automatic curve fitting was allowed to adjust parameter values over a small range after initial parameters were determined by visual inspection. NMR spectra collected over a period of time when the target polarization was expected to be stable were used to determine the standard deviation for

P_z. Consistent results were obtained for $P_z = -15.2\%$ with a standard deviation of 0.12%. However, 81% of the NMR data had an absolute uncertainty greater than $\pm 2\%$ and was considered unsatisfactory.

Attempts to fit showed consistent qualitative differences between the theoretical lineshapes and the data. Reasons for these qualitative differences included large shifts in the background, which could not be adequately compensated for by background subtraction, and instrumentation distortion of the signal. An extensive effort was made to identify the source of the qualitative differences but this was inconclusive. For example, cooling the lambda cable as discussed in Section 4.2.2, improved system stability but did not entirely resolve the problem. The consistent differences between the theoretical model and data were most obvious in the pedestals. The large differences between the model and lineshape in certain parts of the spectrum have an influence on the fit in the least squares method, potentially reducing the sensitivity to the parameters of interest.

There is very little difference between the NMR data obtained using magnitude and phase sensitive detection which tends to indicate either the phase sensitive detection system was malfunctioning or the dispersive component is negligible. It is clear from looking at the data and fitted lineshape that the addition of the dispersive component of the magnetic susceptibility will only make this fit worse and tend to reduce the peak asymmetry and hence value of polarization obtained. This is unexpected from the theoretical calculation but these results are in agreement with those of Hamada who was able to obtain far better fits without including the dispersive component in the lineshape model.

The values obtained for the quadrupole coupling constants (ν_{QCD} and ν_{QOD}) and bond asymmetry parameters (η_{CD} and η_{OD}) are in good agreement with those obtained by Hamada. This is expected because these are physical parameters determined by the molecular structure of propanediol. The significantly lower value of σ is potentially an indication that the true concentration of Cr^V in the target material is lower than that determined by stoichiometric ratios. This is corroborated by the lower than expected polarization obtained by fitting to the "best data". Since the oxidation state of the Cr^V ions in the EHBA-Cr^V

complex is inherently unstable, this possibility should be investigated.

Chapter 5

Results and Conclusions

A dynamically polarized deuteron target was constructed at TUNL and successfully used for preliminary measurements of the spin-dependent cross section difference $\Delta\sigma_L$ for the $\vec{n}$-$\vec{d}$ system. These results are presented along with a brief discussion of future work based on the analysis of this data and the experience gained from the initial runs of the experiment.

5.1 Nuclear Physics Results

Preliminary values of $\Delta\sigma_L$ obtained from the March 1999 data are plotted as a function of neutron energy in Figure 5.1. The two theoretical predictions shown were obtained by using the CD-BONN NN potential model, with and without the Tucson-Melbourne 3NF[5]. The 3σ discrepancy between the measured values and theoretical predictions renders the original goal of searching for comparatively small 3NF effects unattainable. While not providing insight into the 3NF problem, these results provide an opportunity for closer examination of the design of the experiment and the possibility of new physics.

Several key features of this discrepancy must be noted. Measured values are consistently larger than, but follow the same trend as, the theoretical predictions. The difference is energy dependent and proportional to the size of $\Delta\sigma_L$. A simplified, top-down search for the source of this disagreement looks at the individual measurements which combine

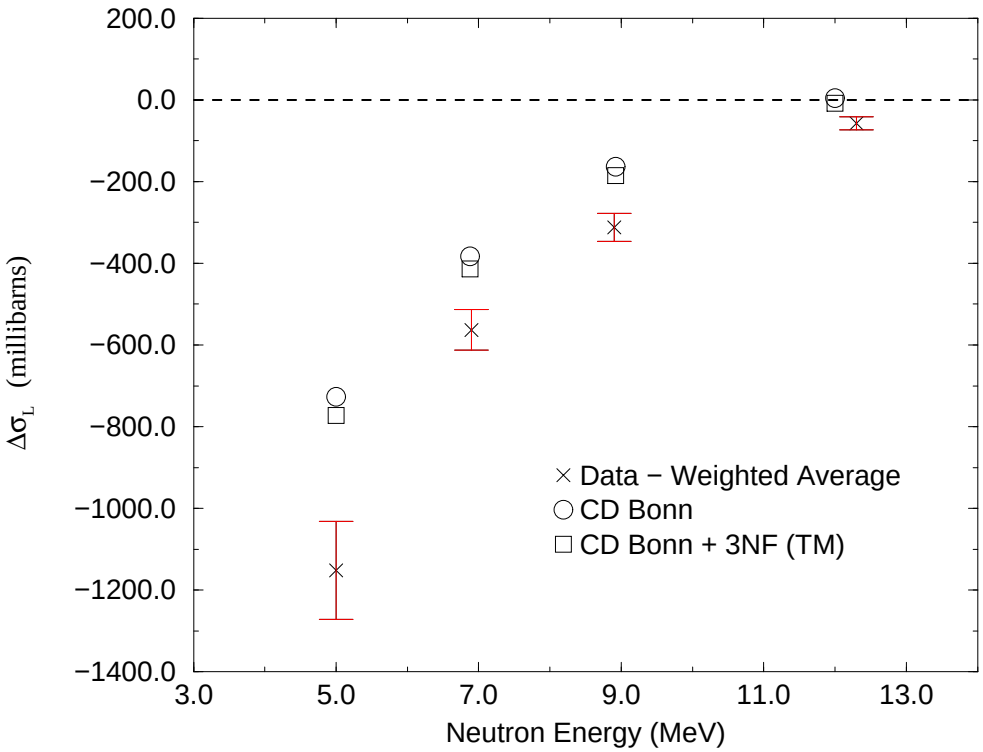

Figure 5.1: Preliminary measurements of $\Delta\sigma_L$ for the $\vec{n}$-$\vec{d}$ system.

to determine $\Delta\sigma_L$ and, does not rule out that more than one factor may be responsible. It is important to note that the difference cannot be explained by a constant offset or a multiplicative factor alone. The quantities needed to calculate $\Delta\sigma_L$ are ϵ_n, P_n, P_T and x.

The neutron asymmetry, ϵ_n, is determined from the y-intercept of a linear fit to the measured neutron asymmetry in the main detector as a function of the BCI asymmetry as discussed in Chapter 2. This result is corrected by removing an asymmetry calculated in a similar manner for the monitor detector upstream of the target. The difference between ϵ_+ and ϵ_- is too small relative to either ϵ_+ or ϵ_- to suspect count-rate dependent detector effects. There is no known evidence of a spin-dependent detection asymmetry from an organic scintillator coupled to a photomultiplier tube. There is no measured asymmetry

when the beam spin state is held constant but the data acquisition is toggled as if the beam spin state was flipping. Likewise, runs with an unpolarized target produced a measured asymmetry consistent with zero. When the polarization axis of the beam is rotated 90° relative to the polarization axis of the target, a $\Delta\sigma_L$ consistent with zero is measured. These tests rule out a constant systematic shift from any source as a partial explanation of the discrepancy.

Issues related to neutron and gamma discrimination cannot be checked retrospectively because the pulse shape information is not stored. The consistency of the results along with the oversight in setup of the PSD electronics make this an unlikely problem. This would likely only be a problem if there is some large beam steering dependence on the polarization state.

Sparking in the cesium oven of the ABPIS proved to be a problem during much of the time experimental data was collected. While the experimental protocol is designed to compensate for the inevitable fluctuations in the beam, abrupt changes such as sparking, may introduce artificial asymmetries in a manner not easy to detect or isolate. To best address this possibility, the data was heavily cut to remove data immediately before and immediately after obvious disturbances in the beam. The random timing of the sparks add to the likelihood that any effects not directly removed would be averaged out over the length of an experimental run. No significant difference in the calculated value of $\Delta\sigma_L$ is obtained between original and more heavily cut data.

Multiple groups at TUNL rely on the integrated ABPIS spin filter polarimeter for accurate determination of charged particle polarimetry and therefore much effort has been devoted to the validation of these measurements. For deuteron beams, the polarization measured by the spin filter polarimeter has been found to be in good agreement with polarization measured independently by scattering experiments in several experimental areas. The polarization transfer coefficients used to calculate P_n from charged particle polarization are well established. This leaves little reason to suspect that P_n is inaccurate.

The same experimental setup and protocol was used when making the measurements of

$\Delta\sigma_L$ and $\Delta\sigma_T$ for the $\vec{n}-\vec{p}$ system and both these values are several times smaller than the values expected for the $\vec{n}-\vec{d}$ system.

This analysis was complicated by the use of D6 on the initial run because of the need to subtract the non-negligible contribution of the residual protons. Subsequent runs with D8 produced results consistent with the D6 runs, ruling out this correction as the source of the error. Contamination of the high purity target material with other polarizable isotopes is unlikely. The common isotopes of other significant elemental components of propanediol, ^{12}C and ^{16}O , are not polarizable because both have nuclear spin I=0. $\Delta\sigma_L$ for $\vec{n}-\vec{p}$ shows a similar trend with opposite sign as $\vec{n}-\vec{d}$ so contamination with polarized protons (see Section 2.6) would produce an effect opposite to that observed.

There is no reason to believe the polarization of the target would have been significantly different for the measurements with different neutron energies although this does raise the question of beam heating of the interior of the target material. Localized beam heating within the target would result in a lower P_T as seen by the beam but not necessarily measured by the NMR technique. The NMR method produces a polarization consistent with the average polarization over the target volume although it is more sensitive to material closer to the NMR coil. Beam heating would produce a smaller value of $\Delta\sigma_L$ than expected which excludes this possibility.

The poor quality of the deuteron NMR data, in particular the qualitative differences between theoretical model and the lack of an independent calibration, leave this as the most obvious source of error in the measurement of $\Delta\sigma_L$. A higher target polarization than measured, consistent with expectations of the EST hypothesis and previous experience with the polarized proton target, would reduce the value of $\Delta\sigma_L$ and offer at least a partial explanation of the discrepancy. While an increase in the target thickness x would shift the value in the same manner, this measurement is less likely to be incorrect. A reduction of any systematic error associated with the polarization of the target could be reduced by increasing the figure of merit of the target. This can be achieved by increasing target polarization, target thickness, or both. A better fit to the NMR data is required for a more

reliable determination of P_T. To improve the quality of the NMR data, the hardware needs to be upgraded.

5.2 Future Work

The preliminary nature of the results presented indicate that additional work is needed. A sensitive measurement involving as many complex subsystems as this experiment, has multiple potential sources for error and therefore the process of arriving at a trusted result will involve iteration and refinement. Taking into account the data analysis, experience gained with deuteron NMR, and overall knowledge of the experiment, the following suggestions are offered for improving future runs. The comments in this section will focus on improvements to the deuteron NMR system as the measurement of target polarization is the largest known factor contributing to the uncertainty in the determination of $\Delta\sigma_L$. Due to the difficulties encountered when attempting to extract deuteron polarization from a fit to the NMR spectrum, as discussed in Chapter 4, it is not possible to achieve a high confidence in the results obtained for this critical parameter. Most importantly, a systematic underestimation of target polarization could potentially go a long way towards explaining the observed discrepancy in measured and predicted values of $\Delta\sigma_L$.

The primary problems with the NMR system are long-term stability and signal-to-noise ratio (SNR) which includes distortion of the lineshape from sources not accounted for by the theoretical lineshape model. An increase in the size of the NMR signal offers the highest potential to improve matters by reducing the impact of these problems. This can be achieved by several methods. The most obvious involves increasing the polarization of the target material although this is the more difficult to implement. Measurement of proton polarization in the presence of the same noise and instabilities highlights the fact that a larger signal significantly reduces the sensitivity to problems experienced in the measurement of deuteron polarization.

An increase in the NMR coil current by reducing R_{cc} would increase the size of the

NMR signal but care needs to be taken not to drive the equilibrium target polarization down or operate in a region where the constant current assumption no longer holds and circuit nonlinearities distort the spectra. In NMR spectroscopy for molecular structure analysis it is routine to completely depolarize the sample to achieve a better SNR, but this is obviously not an option in the case of target polarimetery. It is necessary to optimise the tradeoff between increased signal size and the reduction of the equilibrium polarization.

The primary reason for using a solid cube of target material rather than beads would be to increase target thickness. This would double the amount of material in the NMR coil and therefore double the size of the NMR signal. The main concern would be beam heating effects which might be difficult to detect. Beam heating gives rise to non-uniform polarization and, since the NMR technique provides an average polarization, the results obtained by this method are only valid if the assumption of uniform polarization holds. The target cup or NMR coil geometery would need to be modified to allow this to be loaded. One option would be to freeze the liquid directly in the target cup if the phase change did not produce enough of a volume change to damage the cup.

Investigation of alternative methods to remove or suppress the circuit background could potentially improve both SNR as well as stability. Schemes that involve either a matched cable or remove the lambda cable entirely would be the most difficult to implement given the geometrical constraints of the TUNL target.

When the spectrometer is operated at a single frequency the lambda cable adds a constant contribution across the entire spectrum. If, instead of acquiring the NMR spectrum by sweeping the frequency, the magnetic field was scanned, background subtraction would not be necessary. Sweeping the magnetic field at a fixed frequency was a common practice in CW NMR spectrometers. Varying the magnetic field could be accomplished relatively easily by shim coils in a Helmholtz configuration outside of the cryostat. If this were attempted, it would be necessary to retune or turn off the microwave source for dynamic polarization to avoid actively depolarizing the target while collecting NMR data. The time required to acquire a NMR dataset is very small compared with the spin lattice relaxation

constant so the decay in polarization would be negligible. A point to note is that klystrons take time to reach stable operating conditions after applying power. The option to turn microwave power on and off would require switching the klystron output from the target to a dummy load.

Phase sensitive detection should, in theory, eliminate most circuit and cable background effects. A comparison of the NMR signals acquired by magnitude detection and those obtained by phase sensitive detection, failed to demonstrate ideal behavior. The mechanical phase adjustment was unexpectedly sensitive and this might have been the underlying cause of why the phase sensitive detection did not perform as well as expected. Since it is not possible to measure the phase of the reference at the input of the mixer directly, the accuracy of this setup is questionable. An electrically variable reference phase might be more reliable.

Time stability of the system would need to be improved for a dynamic tuning approach such as synchronous resonance tuning (SRT) [51]. Stability would also be critical for calibrating the NMR using a thermal equilibrium method. The ability to determine an absolute polarization from both the lineshape asymmetry as well as an area based method would boost confidence in the reliability of the polarization measurement. Finding and removing the source of coherent noise observed in the NMR spectra would also improve matters.

An increase in the size of the ^{3}He cup would move the copper walls further from the NMR coil and result in an increased quality factor for the tuned circuit. Metal is essential to ensure structural integrity so that it can withstand repeated temperature and pressure cycles. To conserve ^{3}He it would be possible to find a non-conductive material to line the interior of the cup to displace liquid ^{3}He. This simple design change alone has the potential to increase the size of the NMR signal by an order of magnitude or more with no drawbacks other than the work involved to implement it.

A more ambitious improvement to the target might be to investigate new target materials and dopants based on new mechanisms of dynamic nuclear polarization which in recent years have led to the hope of creating polarized deuteron targets with polarizations exceeding 80%[34]. This might not be possible within the limited ability to prepare and

test such novel materials at TUNL.

5.3 Concluding Remarks

A number of suggestions to improve the measurement of $\Delta\sigma_L$ for the $\vec{n}-\vec{d}$ system have been presented. The objective of all suggestions are to ensure that experimental results are valid. The analysis of the experimental data presented was a key factor in the decision to upgrade the ^{3}He evaporation refrigerator to a ^{3}He-^{4}He dilution refrigerator. This modification alone should result in an increase in target polarization to approximately 30-40%[23], and as a result, reduce any systematic errors associated with the target.

Bibliography

[1] Kenneth S. Krane. *Introductory Nuclear Physics.* John Wiley and Sons, Inc., 1988.

[2] Samuel S. M. Wong. *Introductory Nuclear Physics.* John Wiley and Sons, Inc., 2nd edition, 1998.

[3] Amos deShalit and Herman Feshbach. *Theoretical Nuclear Physics: Nuclear Structure*, volume 1. John Wiley and Sons, Inc., 3rd edition, 1990.

[4] J. L. Friar. Three-nucleon forces for the new millennium. *Nucl. Phys. A*, 684:200–208, 2001.

[5] H. Witala, W. Gloeckle, D. Hueber, J. Golak, and H. Kamada. Cross section minima in elastic nd scattering: Possible evidence for three-nucleon force effects. *Phys. Rev. Lett.*, 81(6):1183–1186, 1998.

[6] D. Huber, H. Kamada, H. Witala, and W. Glockle. How to include a three-nucleon force into Faddeev equations for the 3N continuum: a new form. *Acta Phys. Polon.*, B28:1677–1686, 1997.

[7] Brian William Raichle. *A dynamically polarized proton target for measurement of the transverse spin-dependent total $\vec{n}-\vec{p}$ cross section difference, $\Delta\sigma_T$.* PhD thesis, North Carolina State University, 1997.

[8] Joseph Robb Walston. *Determination of the nucleon-nucleon tensor force through $\vec{n}-\vec{p}$ scattering measurements.* PhD thesis, North Carolina State University, 1998.

[9] V. G. J. Stoks, R. A. M. Klomp, C. P. F. Terheggen, and J. J. de Swart. Construction of high-quality NN potential models. *Phys. Rev. C*, 49(6):2950, 1994.

[10] R. B. Wiringa, V. G. J. Stoks, and R. Schiavilla. Accurate nucleon-nucleon potential with charge-independence breaking. *Phys. Rev. C*, 51(1):38, 1995.

[11] R. Machleidt, R. Sammarruca, and Y. Song. Nonlocal nature of the nuclear force and its impact on nuclear structure. *Phys. Rev. C*, 53(4):R1483, 1996.

[12] R. Machleidt. High-precision charge-dependent bonn nucleon-nucleon potential. *Phys. Rev. C*, 63:024001–1, 2001.

[13] R. Machleidt. The theory of nuclear forces: is the never-ending story coming to an end? In *18th International Conference on Few-Body Problems in Physics*, Santos, Brazil, August 2006.

[14] A. C. Phillips. Application of the Faddeev equations to the three-nucleon problem. *Phys. Rev.*, 142(4):984, 1966.

[15] J. L. Friar, G. L. Payne, V. G. J. Stoks, and J. J. de Swart. Triton calculations with the new Nijmegen potentials. *Phys. Lett.*, B53:4–8, 1993.

[16] John M. Blatt and Victor F. Weiskopf. *Theoretical Nuclear Physics*. Dover, 1st paperback edition, 1991.

[17] Donald H. Perkins. *Introduction to High Energy Physics*. Oxford University Press, 4th edition, 2000.

[18] P. F. Bedaque and U. van Kolck. Effective field theory for few-nucleon systems. *Ann. Rev. Nucl. Part. Sci.*, 52:339–396, 2002.

[19] B. Borasoy, editor. *Introduction to chiral Perturbation Theory*, Akyaka, Turkey, September 2006. summer school ISSSMB.

[20] Bastian Kubis, editor. *An introduction to chiral perturbation theory*, Shantiniketan, India, November 2006. Visva Bharati University.

[21] D. G. Crabb and W. Meyer. Solid polarized targets for nuclear and particle physics experiments. *Annu. Rev. Nucl. Part. Sci.*, 47:67–109, 1997.

[22] T. B. Clegg and et. al. A new atomic beam polarized ion source for the triangle universities nuclear laboratory: overview, operating experience, and performance. *Nuclear Instruments and Methods*, A357:200–211, 1995.

[23] R. D. Foster, C. R. Gould, D. G. Haase, D. M. Markoff, J. O. Poole, B. W. Raichle, W. Tornow, and J. R. Walston. Construction and operation of a dynamically polarized deuterium target. progress report XXXVIII, Triangle Universities Nuclear Laboratory, 1998-99.

[24] G. G. Ohlsen. Polarization transfer and spin correlation experiments in nuclear physics. *Reports on the Progress in Physics*, 35:717–801, 1972.

[25] T. B. Clegg, C. D. Roper, J. D. Dunham, and A. J. Mendez. Installation of an on-line lamb shift spin-filter polarimeter in the triangle nuclear laboratory atomic beam polarized ion source. *Rev. Sci. Instrum.*, 67(9):3073–3081, 1996.

[26] R. J. Van de Graaff, K. T. Compton, and L. C. Van Atta. The electrostatic production of high voltage for nuclear investigations. *Phys. Rev.*, 43(3):149, 1933.

[27] J. E. Bowsher. Babel. *computer code*, 1982.

[28] S. Manglos. Rkin. *computer code*, 1980.

[29] L. G. Holzweig, S. E. King, Y. C. Lau, R. V. Poore, N. R. Roberson, and S. A. Wender. The XSYS data acquisition system at triangle universities nuclear laboratory. *IEEE Trans. on Nucl. Sci.*, NS-28:3708–3714, 1981.

[30] B. van den Brandt, J. A. Konter, and S. Mango. A compact versatile dilution refrigerator with top loading capability. *Nuclear Instruments and Methods*, A289:526–531, 1990.

[31] Felix Sharipov. Rarefied gas flow through a long tube at any temperature ratio. *J. Vac. Sci. and Tech.*, A14(4):2627–2635, 1996.

[32] A. R. Cash and et. al. A transversely polarised deuteron target for kaon-nucleon interaction studies. *J. Phys. E: Sci. Inst.*, 13:182–191, 1980.

[33] E. I. Bunyatova. Free radicals and polarized targets. *Nuclear Instruments and Methods*, A526:22–27, 2004.

[34] B. van den Brandt, E. Bunyatova, P. Hautle, J. A. Konter, and A. Michels. Dynamic nuclear polarization with perchlorinated triphenylmethyl radicals. *PSI: NUM Prog. Rep.*, III, 2004.

[35] M. Krumpolc and J. Rocek. Synthesis of stable chromium(v) complexes of tertiary hydroxy acids. *J. Am. Chem. Soc.*, 101(12):3206–3209, 1979.

[36] C. D. Jeffries. Dynamic nuclear polarization in crystals. *Proc. of the Royal Soc. of London. Series A, Math. Phys. Sci.*, 283(1395):471–479, 1965.

[37] W. de Boer. Dynamic orientation of nuclei at low temperatures. *Journal of Low Temperature Physics*, A14(4):2627–2635, 1996.

[38] G. R. Court, D. W. Gifford, P. Harrison, W. G. Heyes, and M. A. Houlden. A high precision Q-meter for the measurement of proton polarization in polarized targets. *Nuclear Instruments and Methods*, A260:455–462, 1987.

[39] S. K. Dhawan. Understanding effect of teflon room temperature phase transition on coax cable delay in order to improve the measurement of TE signals of deuterated polarized targets. *IEEE Trans. Nucl. Sci.*, 39(5):1331–35, 1992.

[40] P. Hautle. A comparison of NMR concepts for polarization experiments. *Nuclear Instruments and Methods*, A526:76–80, 2004.

[41] Y. F. Kisselev, C. M. Dulya, and T. O. Niinikoski. Measurement of complex RF susceptibility using a series Q-meter. *Nuclear Instruments and Methods*, A354:249–261, 1995.

[42] Ryan Dean Foster. *A measurement of the longitudinal spin-dependent total cross section difference, $\Delta\sigma_L$, in the $\vec{n}$ - $\vec{d}$ system.* PhD thesis, North Carolina State University, 2004.

[43] O. Hamada, S. Hiramatsu, S. Isagawa, S. Ishimoto, A. Masaike, and K. Morimoto. Analysis of deuteron NMR spectrum in propaneiol for polarization measurement. *Nuclear Instruments and Methods*, 189:561–568, 1981.

[44] C. P. Slichter. *Principles of magnetic resonance.* Springer-Verlag, 3rd edition, 1990.

[45] J. Pearson. *PGPLOT Graphic Library version 5.2.0.* Cal. Inst. Tech., 1997. http://www.astro.caltech.edu/~tjp/pgplot/.

[46] E. Anderson, Z. Bai, C. Bischol, S. Blackford, J. Demmel, J. Dogarra, J. Du Croz, A. Greenbaum, S. Hammarling, A. McKenney, and D. Sorensen. *LAPACK Users' Guide.* Soc. Indust. Appl. Math., 3rd edition, 1999.

[47] J. J. More, B. S. Garbow, and K. E. Hillstrom. *User Guide for MINPACK-1*, volume ANL-80-74. Argonne Natl. Lab., 1980.

[48] F. Sperisen. Extracting the deuteron target polarization from the magnetic resonance signal line shape. *Nuclear Instruments and Methods*, A260:455–462, 1987.

[49] Philip R. Bevington and D. Keith Robinson. *Data reduction and error analysis for the physical sciences.* McGraw-Hill, Inc., 2nd edition, 1992.

[50] William H. Press, Saul A. Teukolsky, William T. Vetterling, and Brian P. Flannery. *Numerical recipes in Fortran 77: The art of scientific computing*, volume vol. 1. Cambridge University Press, 2001. online version available at http://www.nr.com.

[51] N. Horikawa, T. Kageya, B. van den Brandt, P. Hautle, J. A. Konter, S. Mango, T. Hagesgawa, T. Matsuda, T. Iinuma, T. Iwata, N. Maeda, Y. Miyachi, K. Mori, and N. Takabayashi. Polarization measurements in thin film foils of deuterated polyethylene. *Proc. of 13th Symposium on High Energy Spin Physics (SPIN98)*, pages 1–3, 1998.

Appendices

Appendix A

This appendix contains *examples* of the computer codes used for deuteron NMR lineshape analysis in Chapter 4. The Fortran 77 programs serve as the primary data analysis tool with Mathematica used for rapid prototyping as well as expert system validation of the numerical routines in the Fortran code.

The routines `qromo`, used for numerical integration, and `mrqmin`, which implements the Levenberg-Marquardt algorithm for non-linear least squares fitting, were based on code contained in Numerical Recipes in Fortran 77[50]. The naming and calling conventions have not been changed. The code for these routines is not included here but it can be found online, along with the entire text, at `http://www.nr.com`. The LAPACK linear least squares and MINPACK general least squares routines were also used to obtain fit parameters. Graphical output is generated by calls to PGPLOT library routines which can be found online at `http://www.astro.caltech.edu/~tjp/pgplot/`

```
|=====================================================================|
gosigma - script to compile and link sigma.f
|=====================================================================|

#!/bin/tcsh
set LIB_PGPLOT = "-L/usr/local/pgplot -L/usr/X11R6/lib64 -lX11
       -lpgplot -lg2c"
ifort -o sigma nrsubs.f sigma.f -L. -lminpack
      $LIB_PGPLOT |& tee error.out


|=====================================================================|
sigma.f - NL least squares fit to NMR spectra to extract model
          parameters and uncertainties
|=====================================================================|

c
      program nmrnlfit
c JP 09/18/2007
c non-linear least squares fit to NMR data
c requires Numerical Recipes routines in nrsubs.f
c (routines are named and called identically to published versions)
c usees MINPACK routines for non-linear least squares fit

      implicit none
c maximum number of data points and number of parameters
      integer NPTS, NMAX
      parameter(NPTS = 599, NMAX = 10)

      integer i, nloop

c variables for MINPACK lmdif1()
      integer m, n, info, lwa, iwa(NMAX)
      real*8 x(NMAX), fvec(NPTS), tol, wa(NPTS*NMAX+5*NMAX+NPTS)

      real*8 freq, val
      integer na, ia(NMAX)
      real*8 xdata(NPTS), ydata(NPTS), a(NMAX)
      common /fitdata/ xdata, ydata, a, ia, na
c establish error on sigma
      real*8 bfsigma, norm, chisq, rat

c temporary arrays for pgplot
      real*4 xpgtemp(NPTS), ypgtemp(NPTS), xmin, xmax, ymin, ymax
```

```
      logical showplot

      real*8 dpmpar, calcchisq
      integer pgopen, pgid
      external lmdif1, fcn, dpmpar, pgopen, calcchisq
c dptosp, plotrng

c m is the number of data points
c n is the number of parameters

c      open(unit=10,file="s1.dat")
      open(unit=10,file="nmr2_bkgsub.dat")
      open(unit=11,file="guess.dat")
      open(unit=12,file="fit.dat")
      showplot = .true.

c total number of parameters
      na = 9
c initial values of paramters to fit
c and values of those to remain fixed

c overall amplitude
c      a(1) = 1.856d-5
c      a(1) = 2.8159d-5
      a(1) = 9.8159d-5
c frequency offset
      a(2) = 1.2766d4
c quadrupole coupling constant C-D
      a(3) = 175.3d3
c quadrulole coupling constand O-D
c      a(4) = 215.0d3
      a(4) = 151.6d3
c sigma
      a(5) = 3.471d3
c eta C-D
      a(6) = 0.005
c eta O-D
      a(7) = 0.17
c fraction C-D bonds
      a(8) = 0.75d0
c ratio parameter where pz=(1-rat^2)/(1+rat+rat^2)
      a(9) = 0.806d0

c parameters to fit (fit=1, ignore=0)
      ia(1) = 1
```

```
      ia(2) = 0
      ia(3) = 0
      ia(4) = 0
      ia(5) = 1
      ia(6) = 0
      ia(7) = 0
      ia(8) = 0
      ia(9) = 1
      ia(10) = 0

c read in residual background subtracted data
      freq = 16.05d6
      do i=1,NPTS
         read(10,*) xdata(i), ydata(i)
         xdata(i) = sngl(freq)
         freq = freq + 1.0d3
      end do

      if (showplot) then
         pgid = pgopen("/xserve")
         if (pgid <= 0) then
            write(*,*) " problem opening pgplot device"
            stop
         end if

         call dptosp (xdata, ydata,  xpgtemp, ypgtemp, NPTS)
         call plotrng(NPTS, xpgtemp, xmin, xmax, 0.0)
         call plotrng(NPTS, ypgtemp, ymin, ymax, 0.1)
         call pgenv(xmin, xmax, ymin, ymax, 0, 0)
         call pgslw(10)
         call pgpnts(NPTS,xpgtemp,ypgtemp,-1,1)
         call pgslw(1)

         end if

c fit function evaluated at initial parameters
c         chisq = 0.0
c         freq = 16.05d6
c         do i=1,NPTS
c            call dnmrls(freq, a, na, val,0)
c            chisq = (ydata(i) - val)**2
c            write(11,*) freq, val
c            xpgtemp(i) = sngl(freq)
c            ypgtemp(i) = sngl(val)
c            freq = freq + 1.0d3
```

```
c         end do

c         write(*,*) "bf chisq = ", chisq
c         norm = NPTS/chisq
c         chisq = NPTS

c plot initial fit with data
c      if (showplot) then
c         call pgline(NPTS, xpgtemp, ypgtemp)
c         call pgclos
c      end if


c setup input parameters to lmdif1()
      m = NPTS
      tol = dsqrt(dpmpar(1))
      lwa = NPTS*NMAX + 5*NMAX + NPTS

c go into the loop
      chisq = -1.0d0
      nloop = 1
      norm = 1.0d0
c      call atox(x, n, a, ia, na)

      do while (chisq < NPTS+2.7)
c=======================================================================
      call atox(x, n, a, ia, na)
      call lmdif1(fcn,m,n,x,fvec,tol,info,iwa,wa,lwa)
      call xtoa(x, n, a, ia, na)

      write(*,*) "info = ", info
      do i=1,na
         if (ia(i) == 1) then
            write(*,*) a(i)
         end if
      end do

c calc chi^2 the long way (ignore fvec)
         chisq = 0.0
         freq = 16.05d6
         do i=1,NPTS
            call dnmrls(freq, a, na, val,0)
            chisq = chisq + (ydata(i) - val)**2
            write(11,*) freq, val
            xpgtemp(i) = sngl(freq)
```

```
            ypgtemp(i) = sngl(val)
            freq = freq + 1.0d3
         end do
         chisq = chisq*norm

c update user on status each iteration
         write(*,*) "chisq, sigma = ", chisq, a(5)

c plot initial fit with data
      if (showplot .and. (nloop ==1) ) then
         call pgline(NPTS, xpgtemp, ypgtemp)
         call pgclos
      end if

c on the first pass though loop
      if (nloop == 1) then
         norm = NPTS/chisq
         chisq = NPTS
c stop fitting sigma
         ia(5) = 0
         bfsigma = a(5)
         nloop = 2
      end if

c increase sigma by 10
      a(5) = a(5) + 10

      end do
c=====================================================================

      write(*,*) "bfsigma, sigma = ", bfsigma, a(5)
      rat = a(9)
      write(*,*) "pz = ", (1.0d0 - rat**2)/(1.0d0 + rat + rat**2)
      stop

c fit function evaluated at initial parameters
      freq = 16.05d6
      do i=1,NPTS
         call dnmrls(freq, a, na, val,0)
         write(11,*) freq, val
         xpgtemp(i) = sngl(freq)
         ypgtemp(i) = sngl(val)
         freq = freq + 1.0d3
      end do
```

```
      if (showplot) then
c         call dptosp(xdata, ydata,  xpgtemp, ypgtemp, NPTS)
         call pgline(NPTS,xpgtemp ,ypgtemp)
         call pgclos
      end if

      close(10)
      close(11)
      close(12)

      stop
      end

c*********************************************************************
c*********************************************************************

      subroutine fcn(m, n, x, fvec, iflag)
c*********************************************************************
c "driver" routine called by lmdif1() which handles the interface
c between

      implicit none
      integer m,n,iflag
      real*8 x(*), fvec(*)

      integer NPTS, NMAX, i, na
      parameter (NPTS = 599, NMAX=10)
      integer ia(NMAX)
      real*8 xdata(NPTS), ydata(NPTS), a(NMAX), val
c this comes from main program though "back door"
      common /fitdata/ xdata, ydata, a, ia, na

c copy parameters in x to a
c      write(*,*) "na = ", na
      call xtoa(x, n, a, ia, na)

      do i=1,m
         call dnmrls(xdata(i), a, na, val,0)
         fvec(i) = ydata(i) - val
      end do

      return
      end

      subroutine atox(x, n, a, ia, na)
```

```
c*******************************************************************
c copy parameters to vary from full parameter set _a_ to _x_
c model function gets all parameters from _a_

      implicit none
      real*8 a(*), x(*)
      integer n, na, ia(*)

      integer i, j

      j = 1
      n = 0
      do i=1,na
         if (ia(i) == 1) then
            x(j) = a(i)
            j = j + 1
            n = n + 1
         end if
      end do

      return
      end

      subroutine xtoa(x, n, a, ia, na)
c*******************************************************************
c copy parameters that vary from _x_ to full parameter set _a_
c model function gets all parameters from _a_

      implicit none
      real*8 a(*), x(*)
      integer n, na, ia(*)

      integer i, j, k

      j = 1
      k = 0
      do i=1,na
         if (ia(i) == 1) then
            a(i) = x(j)
            j = j + 1
            k = k + 1
         end if
      end do

      if (k /= n) then
```

```
          write(*,*) "error: xtoa parameter count incorrect"
          stop
       end if

       return
       end


       real*8 function calcchisq(fvec, npts)
c**********************************************************************
c calculate chisq after non-linear fit with lmdif1()
       implicit none

       real*8 fvec(*)
       integer npts

       integer i

       calcchisq = 0.0
       do i=1,npts
          calcchisq = calcchisq + fvec(i)**2
       end do

       return
       end

       subroutine dnmrls(freq,a,na,lsval,itype)
c**********************************************************************
c calculates the deteron NMR lineshape in partially (D6) and
c fully (D8) deuterated frozen 1,2-propanediol
c
c itype (only itype 0 is currently implemented)
c   0   full D8 lineshape
c   1   full D6 lineshape
c   2   F(x) for C-D bond
c   3   F(-x) for C-D bond
c   4   F(x) for O-D bond
c   5   F(-x) for O-D bond
c   6   F(x) for C-D and O-D bonds
c   7   F(-x) for C-D and O-D bonds
c

       implicit none
       integer NPTS, NMAX
       parameter (NPTS = 599, NMAX = 10)
```

```
      real*8 freq, a(*), lsval
      integer na, itype

      real*8 freqoff, ampl, rat, nuqcd, nuqod, FDEUT
c Larmor frequency for deuteron in 2.5T magnetic field
      parameter (FDEUT = 16.35d6)
      integer  j

      real*8 fraccd, fracod, beta, f1out, f2out, pi

      logical d8
      integer BONDCD, BONDOD, INT1, INT2
      parameter(BONDCD=0, BONDOD=1, INT1=1, INT2=2)

c common block internal to dnmrls
      real*8 etaod, etacd,sigmaod, sigmacd, rho, xfreq
      common /bondparam/ etaod, etacd, sigmaod, sigmacd, rho, pi, xfreq

      real*8 a1,a2,kconst,alpha,v0,r2,ulim,llim
      common /intparam/ a1,a2,kconst,alpha,v0,r2,ulim,llim

c external functions
      real *8 intfunc
      external intfunc, midpnt

      pi=3.1415926535897 93d0

c start by unpacking all parameters needed from "a" ...

c overall amplitude
      ampl = a(1)
c frequency offset
      freqoff = a(2)
c quadrupole coupling constant C-D
      nuqcd = 1.5d0*a(3)
c quadrulole coupling constant O-D
      nuqod = 1.5d0*a(4)
c sigma (built in potential for separate C-D and O-D but not used)
      sigmacd = 2.0d0*a(5)/nuqcd
c WARNING !!!
c       sigmaod = 2.0d0*a(5)/nuqod
      sigmaod = 2.0d0*a(5)/nuqcd
c      sigmaod = sigmacd
c eta C-D
      etacd = a(6)
```

```
c eta O-D
      etaod = a(7)
c fraction of C-D bonds
c D6 fraccd=3/4, fracod=1/4,  D8 fraccd=1, fracod=0
      fraccd = a(8)
      fracod = 1.0d0 - fraccd
c ratio of transition intensities, rat = I-/I+, where
c I- = (0 <-> -1) and I+ = (0 <-> +1)
c vector polarization pz = (1 - rat^2)/(1 + rat + rat^2)
      rat = a(9)

      rho = nuqcd/nuqod

      d8 = .true.

c alpha is real const > 1 which necessary for second variable
c substitution which deals with K(k) -> inf as k -> 1 at lower
c limits of both integrals
      alpha = 2.0d0

      lsval = 0.0d0
      beta = 1.0d0

c j=0 for F(x) and j=1 for F(-x)

      do j=0,1

         xfreq = 2.0d0*(freq+freqoff - FDEUT)/nuqcd

         if (j==1) then
             xfreq = -1.0d0*xfreq
             beta = rat
         end if

c calculate lineshape for C-D bonds
c initialize bond dependent parameters and first integrand
         call setparam(BONDCD,INT1)
         call qromo(intfunc,llim,ulim,f1out,midpnt)

c initialize bond dependent parameters and second integrand
         call setparam(BONDCD,INT2)
         call qromo(intfunc,llim,ulim,f2out,midpnt)

c for the deuteron, quadf > 0
         lsval = lsval + fraccd*beta*(f1out + f2out)
```

```
c         lsval = lsval + fraccd*beta*(f1out + f2out)

         if (d8) then
c calculate lineshape for O-D bonds
c WARNING !!!
            xfreq = 2.0d0*(freq+freqoff - FDEUT)/nuqod
c            xfreq = 2.0d0*(freq+freqoff - FDEUT)/nuqcd
            if (j==1) then
               xfreq = -1.0d0*xfreq
               beta = rat
            end if

c initialize bond dependent parameters and first integrand
            call setparam(BONDOD,INT1)
            call qromo(intfunc,llim,ulim,f1out,midpnt)
c initialize bond dependent parameters and second integrand
            call setparam(BONDOD,INT2)
            call qromo(intfunc,llim,ulim,f2out,midpnt)

            lsval = lsval + fracod*beta*(f1out + f2out)
         end if
      end do

      lsval = ampl*lsval

      end


      subroutine setparam(bondtype, intnum)
c*****************************************************************
c set global variables

      implicit none
      integer bondtype,intnum
      integer BONDCD, BONDOD, INT1, INT2
      parameter(BONDCD=0,BONDOD=1,INT1=1,INT2=2)

      real*8 a0,v1
      real*8 a1,a2,kconst,alpha,v0,r2,ulim,llim
c needed by the integrand function intfunc()
      common /intparam/ a1,a2,kconst,alpha,v0,r2,ulim,llim

c uses xfreq,etacd,etaod, sigmacd,sigmaod,rho
c sets r2, llim,ulim
      real*8 etaod, etacd,sigmaod, sigmacd, rho,pi,xfreq
```

```
      common /bondparam/ etaod, etacd, sigmaod, sigmacd, rho, pi, xfreq

      real*8 eta, sigma, vzzrat,p2,q2

c vzzrat = vzz(C-D)/vzz(O-D), b in the notation of Sperisen,
c rho in the notation of Hamada

      if (bondtype==BONDCD) then
         eta=etacd
         sigma=sigmacd
         vzzrat=1.0d0
      else if (bondtype==BONDOD) then
         eta=etaod
         sigma=sigmaod
         vzzrat=rho
      else
         write(*,*) "error: setparam() invalid parameter, bondtype = ",
     +              bondtype
      end if

      p2=2.0d0*eta
      q2=3.0d0-eta
      r2=3.0d0+eta

c does the requirement -0.5(1+eta) <= x <= 1 cause any concern?
c in practice x runs from approximately -2.0 to +2.0

      a0 = 4.0d0*sigma/pi/vzzrat**2
      a2 = 2.0d0*sigma/vzzrat

      if (intnum==INT1) then
         a1 = 2.0d0*(xfreq/vzzrat - 1.0d0)
         kconst = q2/p2
         v0 = datan((q2 + a1)/a2)/a2
      else if (intnum==INT2) then
         a1 = -2.0d0*xfreq/vzzrat -eta - 1.0d0
         kconst = p2/q2
         v0 = datan((p2 + a1)/a2)/a2
      else
         write(*,*) "error: setparam() invalid parameter, intnum = ",
     +              intnum
      end if

      llim=0.0d0
      v1 = datan((r2 + a1)/a2)/a2
```

```
      ulim=(v1 - v0)**(1.0d0/alpha)

      end

      real*8 function intfunc(w)
c*****************************************************************
c calculate integrand for the first and second integral

      implicit none
      real*8 w
c uses a1,a2,kconst,alpha,v0,r2
      real*8 a1,a2,kconst,alpha,v0,r2,ulim,llim
      common /intparam/ a1,a2,kconst,alpha,v0,r2,ulim,llim
      real*8 tw2, k2

      real*8 ellipk
      external ellipk

      tw2 = a2*dtan(a2*(w**alpha + v0)) - a1
      k2 = kconst*(r2/tw2 - 1.0d0)

c deal with k2=1 inside ellipk
      intfunc = ellipk(k2)*w**(alpha-1.0d0)/dsqrt(tw2)
      return
      end
      subroutine plotrng(npts,xdata,xmin,xmax,xscale)
c*****************************************************************
      implicit none
      integer npts
      real*4 xdata(*), xmin, xmax, xscale

      integer i
      real*4 diff

cc loop to figure out max and min y values for plotting
      do i=1,npts
         if(i==1) then
            xmax = xdata(i)
            xmin = xdata(i)
         else
            if (xdata(i) > xmax) xmax = xdata(i)
            if (xdata(i) < xmin) xmin = xdata(i)
         end if
      end do
```

```
cc add some space on the side
      diff=abs(xmax - xmin)

      xmin=xmin - xscale*diff
      xmax=xmax + xscale*diff

      return
      end


      subroutine dptosp(xdpin, ydpin, xspout, yspout, npts)
c*********************************************************************
c copy double precision arrays to single precision arrays

      real*8 xdpin(*), ydpin(*)
      real*4 xspout(*), yspout(*)
      integer npts

      integer i

      do i=1,npts
         xspout(i) = sngl(xdpin(i))
         yspout(i) = sngl(ydpin(i))
      end do

      return
      end
```

```
|=====================================================================|
gobulk - script to comile and link bulk.f
|=====================================================================|

#!/bin/tcsh
# compile and link Fortran programs with Intel Math Kernel Library
# (MKL) and PGPLOT library
#

set MKLROOT="/opt/intel/mkl/9.0"
set LIB_MKL_ALL="-lmkl_lapack -lmkl_em64t -lmkl -lvml -lguide
         -lpthread"
set LIB_PGPLOT = "-L/usr/local/pgplot -L/usr/X11R6/lib64 -lX11
         -lpgplot -lg2c"
ifort -o bulk nrsubs.f bulk.f -CB -openmp -B $MKLROOT
      -L ${MKLROOT}/lib/em64t $LIB_MKL_ALL  $LIB_PGPLOT



|=====================================================================|
bulk.f - bulk NMR data analysis code
|=====================================================================|

c
      program bulk
c JP 11/10/2007
c loop though bulk NMR data to determine quality
c needs Numerical Recipes routines contained in nrsubs.f !!
c (routines are named and called identically to published versions)

      implicit none
      integer npts, i, j, istat
      integer NMAX
      parameter (NMAX=599)
      real*8 nmrdata(NMAX), nmrfreq(NMAX)
      character*100 fname
      integer flen
c generic single precision arrays for calls to PGPLOT
      real*4 xdata(NMAX), ydata(NMAX), yfit(NMAX), coefs(10)
      real*4 bfampl, bfrat, z1, z2, z3, rat, bfchisq, bfpz, rchisq
      real*4 rmin, rmax, deltachisq, normchisq
      integer loopcnt

c maximum number of data sets
      integer DSMAX
```

```
      parameter (DSMAX = 1000)
      real*4 allchisq(DSMAX)
c, pz(DSMAX), chisqmin
      real*4 allarea(DSMAX), allsnr(DSMAX)
c      integer dschisqmin

      real*4 chisq, area, snr, calcpz
      external chisq, area, snr, calcpz

      istat = 0
c single space at end of path is critical
c      fpath = "ptdata/02_03_99/ "
c      fname = "d02071550.s25"

c      chisqmin = 999999.99d0

      open(unit=99, file="bulkpz.dat")
c dataset filenames come from a file called "edflist2.in"
      do i=1,643

c lenght of filname, including path, needs to be set manually
      read(*,"(A40)") fname
      flen=40

      call import(fname, nmrdata, nmrfreq, npts)

c for debugging purposes
c      open (unit=15, file ="checkout.dat")
c      do i=1,npts
c         write(15,"(I5, F10.4, F12.6)") i, nmrfreq(i), nmrdata(i)
c      end do
c      close(15)
      call dptosp(nmrfreq, nmrdata, xdata, ydata, npts)

c remove residual background with quadratic fit to wings
      call subquadbkg(xdata, ydata, coefs, npts)

c      open(unit=77,file="thurs.dat")
c      do j=1,NMAX
c         read(77,*) z1, z2, z3
c         ydata(j) = z2 + z3
c      end do
c      close(77)

c      istat = 0
```

```
c      call outplot (xdata, ydata, npts, fname(flen-13:flen), istat)
      istat = 2

c linear least squares fit to NMR lineshape function returns amplitude
c and ratio
      call llsfit (xdata, ydata, npts, bfrat, bfampl, yfit,0)
c      call outplot (xdata, yfit, npts, fname(flen-13:flen), istat)
      istat = 1

       bfchisq = chisq(ydata, yfit, npts)
       normchisq = NPTS/bfchisq
       bfpz = calcpz(bfrat)

c
c delta chisq = 2.6
c
       deltachisq = 2.6

       rat = bfrat
       rchisq = 0.0
       loopcnt = 0
c       write(*,*) "upper loop ..."
       do while ((rchisq < (NPTS+deltachisq)) .and. (loopcnt < 100))
          rat = rat + 0.02
          call llsfit (xdata, ydata, npts, rat, bfampl, yfit,1)
          rchisq = normchisq*chisq(ydata, yfit, npts)
c          write(*,*) "rchisq = ", rchisq
          loopcnt = loopcnt + 1
       end do
       rmax = rat

       rat = bfrat
       rchisq = 0.0
       loopcnt = 0
c       write(*,*) "lower loop ..."
       do while ((rchisq < (NPTS+deltachisq)) .and. (loopcnt < 100))
          rat = rat - 0.02
          call llsfit (xdata, ydata, npts, rat, bfampl, yfit,1)
          rchisq = normchisq*chisq(ydata, yfit, npts)
c          write(*,*) "rchisq = ", rchisq
          loopcnt = loopcnt + 1
       end do
       rmin = rat

c show progress ...
```

```
       write(*,*) "done dataset ", i
       write(99,"(I5, 3F10.5)") i, bfpz, calcpz(rmin), calcpz(rmax)


c1      allchisq(i) = chisq(ydata, yfit,npts)
c1      allarea(i) = area(npts,ydata)
c1      allsnr(i) = snr(npts, ydata, yfit)

c1      if (allchisq(i) < chisqmin) then
c1         chisqmin = allchisq(i)
c1      end if
c1      write(*,*) "chisq = ", allchisq(i)

c       call pgpage

      end do
      close(99)

c1      call pgclos

c1     write(*,*) "min chisq = ", chisqmin

c1    open(unit=99,file="bulk.dat")
c1     write(99,*) "# min chisq = ", chisqmin
c1      do i=1,400
c1         allchisq(i) = 599*(allchisq(i)/chisqmin)
c1         write(99,"(I5, F12.3)") i, allchisq(i), allarea(i), allsnr(i)
c1     end do
c1      close(99)

      stop
      end

c**********************************************************************
c**********************************************************************

      subroutine import(fname, nmrdata, nmrfreq, npts)
c**********************************************************************
c read nmr data directly from LabVIEW 4.0 binary data (datalog) files

c files follow an automated naming scheme in the format
c "nddddhhm.tss"
c
c n = nucleus (d = deuteron, p = proton)
c dddd = date, in the form of mmdd, where mm = month and dd = day
```

```
c hhmmss = time, hh = hour, mm = minute, and ss = second
c t = type of file (s = signal, b = background)

c this routine ignores most of the other data in the file
c offset (in 8 byte words, real*8 unless otherwise noted) in
c "scratch.dat"
c
c 68 base frequency (Hz)
c 69 gain
c 70 sweep width in channels (+1)
c 71 total number of sweeps
c 72 10T baratron
c 63 time (format unknown)
c 74 HW background subraction file (format unknown)
c 75 start of NMR data

c on exit, nrmdata contains 599 data points.  npts = 599 and -1 if this
c routine fails for any reason

      implicit none
      character*100 fpath
      character*100 fname
c      character*13 fname
      real*8 nmrdata(*), nmrfreq(*)
      integer npts

      integer NMAX
      parameter (NMAX=599)
      character*120 ffullname
      real*8 dpfloat, gain, fbase

      integer i, ii, j, k, bsize, boffset, fsize
      character bdata, wdata(8)

c file size, in bytes
      fsize = 10186
c changes the "endianess" of 2, 4 or 8 byte data
c all values are double precision floating point (8 bytes)
      bsize = 8
c throw away first to bytes of the file
      boffset = 2

c join path and filename
c      i = index(fpath, " ")
c      ffullname(1:i-1) = fpath(1:i-1)
```

```
c      ffullname(i:i+12) = fname
c      write(*,*) ffullname

c      open(unit=10, file=ffullname, form="binary",recl=1)
       open(unit=10, file=fname, form="binary",recl=1)
       open(unit=11, file="scratch.dat", form="binary",recl=1)

       j = 1
       do i=1, fsize
          read(10) bdata
c skip boffset bytes in file
          if (i > boffset) then
             wdata(j) = bdata
             if (j == bsize) then
c write out bytes in reverse order
                do k=bsize,1,-1
                   write(11) wdata(k)
                end do
                j = 0
             end if
             j = j + 1
          end if
       end do

       close(10)
       close(11)

c convert endianness by swapping bytes and then interpretting
c result as floating point numbers through an intermediate file

       open(unit=11, file="scratch.dat", form="binary",recl=1)

c debugging
c      open(unit=12, file="up.dat")
c      open(unit=13, file="down.dat")

       do i=1,(fsize-boffset)/bsize
          read(11) dpfloat

          ii = i-1

          if (ii == 68) then
             fbase = dpfloat
          else if (ii == 69) then
             gain = dpfloat
```

```
c            write(*,*) "gain = ", gain
         else if (ii == 70) then
            npts = NINT(dpfloat) - 1
c            write(*,*) "npts = ", npts
            k = npts
c         else if (ii == 71) then
c            write(*,*) "n sweeps = ", NINT(dpfloat)
         end if

c 75 is offset of NMR data
         if (ii >= 75) then
             j = ii-74
             if (j <= npts) then
                nmrdata(j) = dpfloat
c                write (12,*) j, dpfloat
             else
                nmrdata(k) = nmrdata(k) + dpfloat
c                write(13,*) k, dpfloat
                k = k - 1
             end if
          end if
      end do

      close(11)
c      close(12)
c      close(13)

c adjust for gain and factor of 2
      gain = 2*gain
      do i=1,npts
c frequency in MHz, channel spacing is 1KHz
         nmrfreq(i) = (fbase + (i-1))/1.0d+3
         nmrdata(i) = nmrdata(i)/gain
      end do

      if (npts /= 599) then
         write(*,*) "error: reading data from file failed"
         stop
      end if

      return
      end


      subroutine subquadbkg(xdata, ydata, coefs, npts)
```

```
c**********************************************************************

      implicit none
      real*4 xdata(*), ydata(*), coefs(*)
      integer npts

      integer NMAX
      parameter (NMAX=599)
      integer i,j, pgid
      real*4  xmin,xmax,ymin,ymax, diff,x, deltax
      real*4 PI
      parameter (PI=3.141592)

      integer NPOLY, WIDTH
c fit wings with a quadratic polynomial
      parameter (NPOLY=2, WIDTH=100)
      real*4 wleft, wright, xfit(2*WIDTH), yfit(2*WIDTH)
      real*4 a(2*WIDTH,NPOLY+1)
      real*4 s(2*WIDTH), rcond, rwork(2*WIDTH)
      integer rank, info
      real*4 quadfit(NMAX)

c      integer pgopen
c      external pgopen

c=====================================================================
c   PARAMETERS
c=====================================================================

c NPTS, number of data points, is set as a constant
c WIDTH, number of channels in each wing to fit residual background

c offset of wings from edges, in channels
      wleft = 10
      wright = 10

c=====================================================================

c      open(unit=10,file="nmr2.dat",status="OLD")

c      x = -2.0
c      x = 1.0
c      deltax = -2.0*x/(NPTS-1)
c      write(*,*) "deltax = ", deltax
c      deltax = 1.0
```

```
c      do i=1,NPTS
c         read (10,*) ydata(i)
c         xdata(i) = x
c         x= x + deltax
c      end do
c      close(10)

c generate a plot
c      call plotrng(NPTS, ydata, ymin, ymax, 0.1)
c      pgid = pgopen("labeltest.ps/vps")
c      pgid = pgopen("?")
c      if (pgid <= 0) then
c         write(*,*) " problem opening pgplot device"
c         stop
c      end if
c      call pgsubp(1,2)
c      call pgenv(-2.0, 2.0, ymin, ymax, 0, 0)
c      call pglab("freq", "voltage","")
cc try and label individual plots (a), (b), etc.
c      call pgmtxt("LV", -3.0 , 0.9 , 0.0, "(a)")
c      call pgline(NPTS, xdata,ydata)

cc construct arrays with wings to fit

      do i=1, WIDTH
         xfit(i) = xdata((i-1)+wleft)
         yfit(i) = ydata((i-1)+wleft)
      end do

      do i=1, WIDTH
         xfit(i+WIDTH) = xdata(i+(npts-wright-WIDTH))
         yfit(i+WIDTH) = ydata(i+(npts-wright-WIDTH))
      end do

c calculate design matrix (array of powers of x)
c a(i,j) where ith row corresponds to x_i
c              jth column corresonds to (x_i)^(j-1)


      do i=1,2*WIDTH
         x = 1.0
         do j=1,NPOLY+1
             a(i,j) = x
             x = x*xfit(i)
         end do
```

```
      end do


cc LAPACK routine to to linear least squares fit
      call sgelss(2*WIDTH, NPOLY+1, 1, a, 2*WIDTH, yfit, 2*WIDTH,
     +             s, -1.0, rank, rwork, 2*WIDTH, info)

c      write(*,*) "rank = ", rank

      if (info==0) then
c         write(*,*) (yfit(i), i=1,NPOLY+1)
      else
         write(*,*) "error: quadratic fit to wings failed"
         stop
      end if

c calculate quadratic background
      do i=1,NPTS
         x = 1.0
         quadfit(i) = 0.0
         do j=1,NPOLY+1
            quadfit(i) = quadfit(i) + yfit(j)*x
            x = x*xdata(i)
         end do
      end do

c superimpose generated quadratic fit on nmr signal
c      call pgline(NPTS, xdata,quadfit)
c draw horizontal lines to indicate channels fitted for bkg sub
c      xfit(1) = -2.0 + wleft*deltax
c      xfit(2) = -2.0 + (wleft+WIDTH)*deltax
c      yfit(1) = (1.0/1.1 + 0.05)*ymin
c      yfit(2) = (1.0/1.1 + 0.05)*ymin
c      call pgline(2, xfit,yfit)

c      xfit(1) = 2.0 - wright*deltax
c      xfit(2) = 2.0 - (wright+WIDTH)*deltax
c      call pgline(2, xfit,yfit)

c do background subraction
      do i=1,NPTS
          ydata(i) = ydata(i) - quadfit(i)
      end do

c generate a plot
```

```
c      call pgopen("?")
c      call plotrng(npts, ydata, ymin, ymax, 0.1)
c      call pgenv(-2.0, 2.0, ymin, ymax, 0, 0)
cc try and label individual plots (a), (b), etc.
c      call pgmtxt("LV", -3.0 , 0.9 , 0.0, "(b)")
c      call pglab("freq", "voltage","")
c      call pgline(NPTS, xdata,ydata)
c plot fitted quadratic background
c      call pgline(NPTS, xdata,quadfit)
cc plot just wings
cx      call pgline(width, xfit(1:width), yfit(1:width))
cx      call pgline(width, xfit(width+1:2*width), yfit(width+1:2*width))
c      call pgclos

c      stop
      return
      end

      subroutine plotrng(npts,xdata,xmin,xmax,xscale)
c*****************************************************************
      implicit none
      integer npts
      real*4 xdata(*), xmin, xmax, xscale

      integer i
      real*4 diff

cc loop to figure out max and min y values for plotting
      do i=1,npts
         if(i==1) then
            xmax = xdata(i)
            xmin = xdata(i)
         else
            if (xdata(i) > xmax) xmax = xdata(i)
            if (xdata(i) < xmin) xmin = xdata(i)
         end if
      end do

cc add some space on the side
      diff=abs(xmax - xmin)

      xmin=xmin - xscale*diff
      xmax=xmax + xscale*diff

      return
```

```
      end

      subroutine dptosp(xdpin, ydpin, xspout, yspout, npts)
c*********************************************************************
c copy double precision arrays to single precision arrays

      real*8 xdpin(*), ydpin(*)
      real*4 xspout(*), yspout(*)
      integer npts

      integer i

      do i=1,npts
         xspout(i) = sngl(xdpin(i))
         yspout(i) = sngl(ydpin(i))
      end do

      return
      end

      subroutine outplot (xdata, ydata, npts, fname, istat)
c*********************************************************************

      real*4 xdata(*), ydata(*)
      integer npts, istat
      character*13 fname

      real*4 xmin, xmax, ymin, ymax

      integer pgopen
      external pgopen

c new plot
      if (istat == 0) then
         pgid = pgopen("bulkall.ps/PS")
c         pgid = pgopen("/xserve")
         if (pgid <= 0) then
            write(*,*) "error: unable to open PGPLOT device"
            stop
         end if
cx       call pgask(.false.)
      end if

      if ((istat == 0) .or. (istat == 1)) then
         call plotrng(npts, xdata, xmin, xmax, 0.0)
```

```
         call plotrng(npts, ydata, ymin, ymax, 0.1)
         call pgenv(xmin, xmax,  ymin, ymax, 0, 0)
         call pglab("freq (MHz)", "voltage",fname)
      end if

cz      call plotrng(npts, xdata, xmin, xmax, 0.0)
cz      call plotrng(npts, ydata, ymin, ymax, 0.1)
cz     call pgenv(xmin, xmax,  ymin, ymax, 0, 0)
cz     call pglab("freq (MHz)", "voltage",fname)
c      call pgmtxt("LV", -3.0 , 0.9 , 0.0, fname)
      call pgline(npts, xdata,ydata)
      if (istat /= 0) then
c         call pgclos
      end if

      return
      end

      real*4 function chisq (ydata, yfit, npts)
c*****************************************************************
      implicit none

      real*4 ydata(*), yfit(*)
      integer npts

      integer i

      chisq = 0.0
      do i=1,npts
         chisq = chisq + (ydata(i) - yfit(i))**2
      end do

      return
      end

      real*4 function area(npts,ydata)
c*****************************************************************
c calculate "area" under signal by simple Riemann sum
      implicit none
      real*4 ydata(*)
      integer npts

      integer i

      area = 0.0
```

```
      do i=1,npts
         area = area + ydata(i)
      end do

      return
      end

      real*4 function snr(npts,ydata,yfit)
c*****************************************************************
      implicit none
      real*4 ydata(*), yfit(*)
      integer npts

      integer i
      real*4 spower, npower

      spower = 0.0
      npower = 0.0
      do i=1,npts
         spower = spower + yfit(i)**2
         npower = npower + (ydata(i) - yfit(i))**2
      end do

      snr = spower/npower

      return
      end


      real*4 function calcpz(ratio)
c*****************************************************************
c calculate pz from ratio fit parameter
      implicit none
      real*4 ratio

      calcpz = (1.0 - ratio**2)/(1.0 + ratio + ratio**2)

      return
      end
c
      subroutine llsfit(xdata, ydata, npts,fitratio,fitampl,yfit,switch)
c JP
      implicit none
      real*4 xdata(*), ydata(*), fitampl, fitratio, yfit(*)
      integer npts, switch
```

```
      integer NMAX
      parameter (NMAX=599)
      integer i,j
      real*4  xmin,xmax,ymin,ymax, diff,x, deltax

c*********************************************************************
c*********************************************************************

      real*4 s2(NMAX), rwork2(NMAX), rcond
      real*4 xfit2(NMAX), yfit2(NMAX)
      integer rank, info
      real*4 a2(NMAX,2), xrat
      real*4 azz(NMAX,2)

      integer na, jj
      real*8 pi
      parameter (pi=3.141592)

      real*8 xa(10), agen(10), dyda(10)
      real*8 etaod, etacd,sigmaod, sigmacd, rho
c*********************************************************************
      real*8 nmrdata(NPTS)
      real*4 dxdata(NPTS), dydata(NPTS)
      real*4 xxdata(NPTS), yydata(NPTS), ytemp(NPTS)

      integer NAMAX, counter
      parameter (NAMAX=10)
      integer ma(NAMAX)

      real*8 oldchisq, chisq, sig(NPTS), covar(NAMAX,NAMAX)
      real*8 alpha(NAMAX,NAMAX), alamda
      real*4 rplus, rminus

      integer chanoff
      real*8 fdeut, freq, fstart, fstep, xfreq(NPTS), deutls(NPTS)
      real*8 rat, pz, ampl, lscd, lsod, xfod, xfcd, quadfcd, quadfod
      real*8 quadf
      logical  d8, showplot

      external modls

      d8 = .false.
c quadruple shift will depend on bond (O-D, C-D)
c      quadf = 1.5d0*166.3d+3
```

```
       quadf = 1.5d0*180.3d+3
c      etacd = 0.03d0
      etacd = 0.005d0
c      sigmacd = 2.0d0*4.10d+3/quadf
      sigmacd = 2.0d0*4.10d+3/quadf

c      quadfod = 1.5d0*197.9d+3
      etaod = 0.17d0
      sigmaod = 2.0d0*4.88d+3/quadf

      rho = 0.840

c Larmor frequency (Hz) of deuteron in 2.5T magnetic field
      fdeut = 16.35d+6

c*********************************************************************
c number of channels
c     npts = 599
c frequency offset in channels
      chanoff = 0
c frequency channel spacing in Hz
      fstep = 1000.0d0
      fstart = (fdeut - ((npts-1)*fstep)/2.0d0) + chanoff*fstep
c rat is the model paramter directly proportional to vector pol, pz
c      rat = 0.85
      pz = (1.0d0 - rat**2)/(1.0d0 + rat + rat**2)
c      write(*,*) "deuteron vector polarizaton (pz) = ", pz

c      pz = 0.10
c      open (unit=28,file="d8pz20.txt")
c      sigmacd = 2.0d0*2.00d+3/quadf
      sigmacd = 2.0d0*2.48d+3/quadf
      ampl=1.30d-5
c      etacd = 0.030
      quadfcd = 1.5*175.3d+3
      quadfod = 1.5*215.0d+3

c      rplus =(-pz + sqrt(pz**2 - 4.0*(pz+1.0)*(pz-1.0)))/(2.0*(pz+1.0))
c      rminus =(-pz - sqrt(pz**2 - 4.0*(pz+1.0)*(pz-1.0)))/(2.0*(pz+1.0))

c      write(*,*) "r+ = ", rplus
c      write(*,*) "r- = ", rminus
c      rat = rplus
c       if (switch ==0) then
          rat = 1.0
```

```
          ampl=1.30d-5
c       else
c           rat = fitratio
c           ampl = fitampl*1.30d-5
c       end if

c      write(*,*) "deuteron vector polarizaton (pz) = ", pz

c       write(*,*) "sigma: "
c       read(*,*) sigmacd
c       sigmacd = 2.0*sigmacd/quadf

c       write(*,*) "V_Q(OD) (x 10^3): "
c       read(*,*) quadfod
c       quadfod = 1.5*quadfod*1000.0
c       write(*,*) "amplitude (x 10^-5) : "
c       read(*,*) ampl
c       ampl = ampl*1.0d-5

c start by designing parameter array "a" ...
c need to include quadcd/quadod in here?
c na is the max number of parameters in a
      na=9
c overall amplitude
      agen(1) = ampl
      xa(1) = 0.00006
c frequency offset
c      agen(2) = 8.50d-2
      agen(2) = -0.01d0
c      xa(2) = 0.030
c polarization ratio
      agen(3) = rat
      xa(3) = rat
c eta cd
      agen(4) = etacd
      xa(4) = etacd
c eta od
      agen(5) = etaod
      xa(5) = etaod
c sigma cd
      agen(6) = sigmacd
      xa(6) = sigmacd
c sigma od
      agen(7) = sigmaod
      xa(7) = sigmaod
```

```
c rho
      agen(8) = rho
      xa(8) = rho
c positive for d6, negative for d8
      if (d8) then
         agen(9) = -1.0
         xa(9) = -1.0
      else
         agen(9) = +1.0
         xa(9) = +1.0
      end if

c open output file
c      open(unit=10,file="nmrls.out")


      do jj=1,2
         do i=1,NPTS

            freq = fstart + (i-1)*fstep
            xfcd = 2.0d0*(freq - fdeut)/quadfcd
            agen(4) = etacd
            call modls(xfcd,agen, lscd,jj,na)

            xfod = 2.0d0*(freq - fdeut)/quadfod
            agen(4) = etaod
            call modls(xfod,agen,lsod,jj,na)

            deutls(i) = 1.1d0*(0.75d0*lscd + 0.25d0*lsod)

            xxdata(i) = sngl(xfcd)
            yydata(i) = sngl(deutls(i))

            a2(i,jj) = yydata(i)
            azz(i,jj) = yydata(i)
c         deutls(i) = deutls(i) + 0.001*(ran0(idum) -0.5)
c         write(10,*) xfreq(i), deutls(i)
         end do
      end do

c      open(unit=99, file="thurs.dat")
c      do i=1,NPTS
c         write(99,*) xxdata(i), a2(i,1), a2(i,2)
c      end do
c      close(99)
```

```
c      stop


cc LAPACK routine to to linear least squares fit
c      call sgelss(2*WIDTH, NPOLY+1, 1, a, 2*WIDTH, yfit, 2*WIDTH,
c     +             s, -1.0, rank, rwork, 2*WIDTH, info)

c      write(*,*) "before LAPACK call ..."

       do jj=1, NPTS
         ytemp(jj) = ydata(jj)
       end do

c%%%%%%%%%%%%%%%%%%%%%%%%%%%%%%%%%%%%%%%%%%%%%%%%%%%%%%%%%%%%%%%%%%%%%%%%%%%
       if (switch == 0) then
c      write(*,*) "before LAPACK call ..."
       call sgelss(NPTS, 2, 1, a2, NPTS, ytemp, NPTS,
     +             s2, -1.0, rank, rwork2, NPTS, info)

       write(*,*) "rank = ", rank

       if (info==0) then
          write(*,*) "fit to NMR LS succeeded, info = 0"
          write(*,*) ytemp(1), ytemp(2)
          fitratio = ytemp(1)/ytemp(2)
          xrat = fitratio
          fitampl = ytemp(2)
          write(*,*) "xrat = ", xrat
       pz = (1.0d0 - xrat**2)/(1.0d0 + xrat + xrat**2)
          write(*,*) "pz = ", pz
       else
          write(*,*) "error: fit failed to amplitude and ratio"
          stop
       end if

       end if
c%%%%%%%%%%%%%%%%%%%%%%%%%%%%%%%%%%%%%%%%%%%%%%%%%%%%%%%%%%%%%%%%%%%%%%%%%%%

       do jj=1,NPTS
          yfit(jj) = fitampl*(fitratio*azz(jj,1) + azz(jj,2))
       end do

c      open(unit=99, file="after.dat")
c      do i=1,NPTS
```

```
c         write(99,*) xxdata(i), a2(i,1), a2(i,2)
c      end do
c      close(99)

      return
      end

      subroutine nmrls(x,a,y,na,jj)
c*****************************************************************

      implicit none
c      real*8 inputxfreq, rat, deutls
      logical d8

      real*8 x, xoff, deutls, ampl, a(10), y, rat
      integer na, jj

      real*8 fraccd, fracod, beta, f1out, f2out, pi
      integer j

      integer BONDCD, BONDOD, INT1, INT2
      parameter(BONDCD=0, BONDOD=1, INT1=1, INT2=2)

c common block internal to nmrls
      real*8 etaod, etacd,sigmaod, sigmacd, rho, xfreq
      common /bondparam/ etaod, etacd, sigmaod, sigmacd, rho, pi, xfreq

      real*8 a1,a2,kconst,alpha,v0,r2,ulim,llim
      common /intparam/ a1,a2,kconst,alpha,v0,r2,ulim,llim

c functions
      real *8 intfunc
      external intfunc, midpnt

      pi=3.141592653589793d0

c start by designing parameter array "a" ...

c overall amplitude
      ampl = a(1)
c frequency offset
      xoff = a(2)
c polarization ratio
      rat = a(3)
c eta cd
```

```
      etacd = a(4)
c eta od
      etaod = a(5)
c sigma cd
      sigmacd = a(6)
c sigma od
      sigmaod = a(7)
c rho
      rho = a(8)
c positive for d6, negative for d8
      if (a(9) >= 0.0) then
         d8 = .false.
      else
         d8 = .true.
      end if

c alpha is real const > 1 which necessary for second variable
c substitution which deals with K(k) -> inf as k -> 1 at lower
c limits of both integrals
      alpha = 2.0d0

      xfreq = x + xoff

c D6 fraccd=3/4, fracod=1/4,  D8 fraccd=1, fracod=0
      if (d8) then
         fraccd = 3.0d0/4.0d0
         fracod = 1.0d0/4.0d0
      else
         fraccd = 1.0d0
         fracod = 0.0d0
      endif

      deutls = 0.0d0
      beta = 1.0d0

c j=0 for F(x) and j=1 for F(-x)

      if (jj==1) then
         j = 0
      else
         j = 1
      end if
c      do j=0,1

         if (j==1) then
```

```
            xfreq = -1.0d0*xfreq
            beta = rat
         end if

c calculate lineshape for C-D bonds
c initialize bond dependent parameters and first integrand
         call setparam(BONDCD,INT1)
         call qromo(intfunc,llim,ulim,f1out,midpnt)

c initialize bond dependent parameters and second integrand
         call setparam(BONDCD,INT2)
         call qromo(intfunc,llim,ulim,f2out,midpnt)

c for the deuteron, quadf > 0
         deutls = deutls + fraccd*beta*(f1out + f2out)
         deutls = deutls + fraccd*beta*(f1out + f2out)

         if (d8) then
c calculate lineshape for O-D bonds
c initialize bond dependent parameters and first integrand
            call setparam(BONDOD,INT1)
            call qromo(intfunc,llim,ulim,f1out,midpnt)
c initialize bond dependent parameters and second integrand
            call setparam(BONDOD,INT2)
            call qromo(intfunc,llim,ulim,f2out,midpnt)

            deutls = deutls + fracod*beta*(f1out + f2out)
         end if
c      end do

      y = ampl*deutls

      end


      subroutine setparam(bondtype, intnum)
c*****************************************************************
c set global variables

      implicit none
      integer bondtype,intnum
      integer BONDCD, BONDOD, INT1, INT2
      parameter(BONDCD=0,BONDOD=1,INT1=1,INT2=2)

      real*8 a0,v1
```

```
      real*8 a1,a2,kconst,alpha,v0,r2,ulim,llim
c needed by the integrand function intfunc()
      common /intparam/ a1,a2,kconst,alpha,v0,r2,ulim,llim

c uses xfreq,etacd,etaod, sigmacd,sigmaod,rho
c sets r2, llim,ulim
      real*8 etaod, etacd,sigmaod, sigmacd, rho,pi,xfreq
      common /bondparam/ etaod, etacd, sigmaod, sigmacd, rho, pi, xfreq

      real*8 eta, sigma, vzzrat,p2,q2

c vzzrat = vzz(C-D)/vzz(O-D), b in the notation of Sperisen,
c rho in the notation of Hamada

      if (bondtype==BONDCD) then
         eta=etacd
         sigma=sigmacd
         vzzrat=1.0d0
      else if (bondtype==BONDOD) then
         eta=etaod
         sigma=sigmaod
         vzzrat=rho
      else
         write(*,*) "error: setparam() invalid parameter, bondtype = ",
     +              bondtype
      end if

      p2=2.0d0*eta
      q2=3.0d0-eta
      r2=3.0d0+eta

c does the requirement -0.5(1+eta) <= x <= 1 cause any concern?
c in practice x runs from approximately -2.0 to +2.0
c     if ((xfreq <= -0.5d0*(1.0d0+eta)) .or. (xfreq >= 1.0d0)) then
c        write(*,*) "warning: xfreq = ", xfreq, "outside range."
c     end if

      a0 = 4.0d0*sigma/pi/vzzrat**2
      a2 = 2.0d0*sigma/vzzrat

      if (intnum==INT1) then
         a1 = 2.0d0*(xfreq/vzzrat - 1.0d0)
         kconst = q2/p2
         v0 = datan((q2 + a1)/a2)/a2
      else if (intnum==INT2) then
```

```
         a1 = -2.0d0*xfreq/vzzrat -eta - 1.0d0
         kconst = p2/q2
         v0 = datan((p2 + a1)/a2)/a2
      else
         write(*,*) "error: setparam() invalid parameter, intnum = ",
     +              intnum
      end if

      llim=0.0d0
      v1 = datan((r2 + a1)/a2)/a2
      ulim=(v1 - v0)**(1.0d0/alpha)

      end

      real*8 function intfunc(w)
c*****************************************************************
c calculate integrand for the first and second integral

      implicit none
      real*8 w
c uses a1,a2,kconst,alpha,v0,r2
      real*8 a1,a2,kconst,alpha,v0,r2,ulim,llim
      common /intparam/ a1,a2,kconst,alpha,v0,r2,ulim,llim
      real*8 tw2, k2

      real*8 ellipk
      external ellipk

c      write(*,*) "inside intfunc, w = ", w
      tw2 = a2*dtan(a2*(w**alpha + v0)) - a1
      k2 = kconst*(r2/tw2 - 1.0d0)

cc deal with k2=1 inside ellipk
      intfunc = ellipk(k2)*w**(alpha-1.0d0)/dsqrt(tw2)
      return
      end
```

Appendix B

This appendix includes the 599 data points used to obtain the "best fit" in Chapter 4. The data is listed as a table with the channel number in the first column followed by the NMR voltage in the second column. The frequency of channel 1 is 16.05MHz and increases by 1KHz per channel.

chan	voltage	chan	voltage	chan	voltage	chan	voltage
1	-0.016530	41	-0.015990	81	-0.015320	121	-0.014910
2	-0.016440	42	-0.015920	82	-0.015340	122	-0.014820
3	-0.016510	43	-0.015990	83	-0.015490	123	-0.014820
4	-0.016460	44	-0.015940	84	-0.015270	124	-0.014860
5	-0.016450	45	-0.015870	85	-0.015370	125	-0.014780
6	-0.016520	46	-0.015730	86	-0.015290	126	-0.014740
7	-0.016390	47	-0.015930	87	-0.015290	127	-0.014690
8	-0.016490	48	-0.015850	88	-0.015230	128	-0.014710
9	-0.016430	49	-0.015790	89	-0.015390	129	-0.014750
10	-0.016370	50	-0.015750	90	-0.015170	130	-0.014790
11	-0.016400	51	-0.015780	91	-0.015100	131	-0.014810
12	-0.016460	52	-0.015740	92	-0.015190	132	-0.014720
13	-0.016300	53	-0.015780	93	-0.015120	133	-0.014690
14	-0.016380	54	-0.015650	94	-0.015180	134	-0.014790
15	-0.016440	55	-0.015680	95	-0.015210	135	-0.014700
16	-0.016460	56	-0.015530	96	-0.015190	136	-0.014570
17	-0.016310	57	-0.015630	97	-0.015190	137	-0.014710
18	-0.016370	58	-0.015640	98	-0.015190	138	-0.014590
19	-0.016210	59	-0.015570	99	-0.015270	139	-0.014630
20	-0.016180	60	-0.015570	100	-0.015250	140	-0.014610
21	-0.016110	61	-0.015580	101	-0.015250	141	-0.014720
22	-0.016190	62	-0.015600	102	-0.015200	142	-0.014660
23	-0.016080	63	-0.015590	103	-0.015060	143	-0.014680
24	-0.016140	64	-0.015540	104	-0.015180	144	-0.014680
25	-0.016000	65	-0.015440	105	-0.015210	145	-0.014600
26	-0.015910	66	-0.015580	106	-0.015060	146	-0.014550
27	-0.016090	67	-0.015660	107	-0.015070	147	-0.014600
28	-0.016000	68	-0.015590	108	-0.015110	148	-0.014490
29	-0.016130	69	-0.015490	109	-0.015180	149	-0.014720
30	-0.016010	70	-0.015570	110	-0.015090	150	-0.014880
31	-0.016060	71	-0.015650	111	-0.015130	151	-0.014650
32	-0.016050	72	-0.015540	112	-0.015160	152	-0.014540
33	-0.015960	73	-0.015540	113	-0.015020	153	-0.014350
34	-0.015950	74	-0.015590	114	-0.014960	154	-0.014420
35	-0.016040	75	-0.015590	115	-0.015040	155	-0.014410
36	-0.015860	76	-0.015500	116	-0.014990	156	-0.014140
37	-0.016000	77	-0.015520	117	-0.014970	157	-0.014100
38	-0.015890	78	-0.015550	118	-0.015020	158	-0.014140
39	-0.015810	79	-0.015480	119	-0.014960	159	-0.014120
40	-0.015880	80	-0.015400	120	-0.014960	160	-0.014070

chan	voltage	chan	voltage	chan	voltage	chan	voltage
161	-0.013900	201	-0.012680	241	-0.009470	281	-0.010310
162	-0.013940	202	-0.012720	242	-0.009530	282	-0.010350
163	-0.013880	203	-0.012620	243	-0.009590	283	-0.010360
164	-0.013850	204	-0.012630	244	-0.009660	284	-0.010310
165	-0.013850	205	-0.012760	245	-0.009680	285	-0.010320
166	-0.013790	206	-0.012550	246	-0.009720	286	-0.010330
167	-0.013800	207	-0.012610	247	-0.009740	287	-0.010290
168	-0.013810	208	-0.012520	248	-0.009840	288	-0.010250
169	-0.013720	209	-0.012530	249	-0.010050	289	-0.010340
170	-0.013830	210	-0.012530	250	-0.009930	290	-0.010310
171	-0.013810	211	-0.012490	251	-0.009840	291	-0.010280
172	-0.013710	212	-0.012430	252	-0.009980	292	-0.010290
173	-0.013770	213	-0.012400	253	-0.009920	293	-0.010300
174	-0.013730	214	-0.012240	254	-0.009950	294	-0.010310
175	-0.013730	215	-0.012020	255	-0.010030	295	-0.010100
176	-0.013720	216	-0.012080	256	-0.009960	296	-0.010380
177	-0.013650	217	-0.011830	257	-0.009940	297	-0.010210
178	-0.013660	218	-0.011600	258	-0.009930	298	-0.010240
179	-0.013700	219	-0.011000	259	-0.010090	299	-0.010330
180	-0.013610	220	-0.010310	260	-0.010110	300	-0.010270
181	-0.013600	221	-0.009410	261	-0.010130	301	-0.010190
182	-0.013600	222	-0.008440	262	-0.010120	302	-0.010410
183	-0.013460	223	-0.007760	263	-0.010140	303	-0.010450
184	-0.013570	224	-0.007190	264	-0.010100	304	-0.010330
185	-0.013550	225	-0.007160	265	-0.010250	305	-0.010300
186	-0.013500	226	-0.007000	266	-0.010200	306	-0.010270
187	-0.013350	227	-0.007000	267	-0.010230	307	-0.010340
188	-0.013380	228	-0.007330	268	-0.010360	308	-0.010340
189	-0.013380	229	-0.007370	269	-0.010210	309	-0.010450
190	-0.013420	230	-0.007530	270	-0.010300	310	-0.010270
191	-0.013330	231	-0.007820	271	-0.010390	311	-0.010250
192	-0.013180	232	-0.007960	272	-0.010380	312	-0.010300
193	-0.013130	233	-0.008330	273	-0.010350	313	-0.010250
194	-0.013250	234	-0.008500	274	-0.010270	314	-0.010170
195	-0.013100	235	-0.008710	275	-0.010370	315	-0.010130
196	-0.013030	236	-0.008870	276	-0.010430	316	-0.010150
197	-0.012910	237	-0.009010	277	-0.010370	317	-0.010180
198	-0.012860	238	-0.009150	278	-0.010360	318	-0.010160
199	-0.012820	239	-0.009180	279	-0.010330	319	-0.010070
200	-0.012910	240	-0.009330	280	-0.010370	320	-0.009940

chan	voltage	chan	voltage	chan	voltage	chan	voltage
321	-0.009970	361	-0.011730	401	-0.012930	441	-0.014450
322	-0.010100	362	-0.011730	402	-0.012990	442	-0.014350
323	-0.009920	363	-0.011750	403	-0.012980	443	-0.014300
324	-0.009760	364	-0.011900	404	-0.013050	444	-0.014500
325	-0.009990	365	-0.011960	405	-0.013220	445	-0.014360
326	-0.009760	366	-0.011840	406	-0.013180	446	-0.014430
327	-0.009840	367	-0.012130	407	-0.013250	447	-0.014430
328	-0.009800	368	-0.011910	408	-0.013230	448	-0.014430
329	-0.009750	369	-0.012040	409	-0.013360	449	-0.014310
330	-0.009730	370	-0.012170	410	-0.013300	450	-0.014370
331	-0.009640	371	-0.012080	411	-0.013380	451	-0.014430
332	-0.009760	372	-0.012320	412	-0.013360	452	-0.014530
333	-0.009680	373	-0.012320	413	-0.013400	453	-0.014600
334	-0.009570	374	-0.012170	414	-0.013430	454	-0.014590
335	-0.009480	375	-0.012410	415	-0.013540	455	-0.014500
336	-0.009480	376	-0.012290	416	-0.013560	456	-0.014460
337	-0.009420	377	-0.012430	417	-0.013750	457	-0.014510
338	-0.009280	378	-0.012400	418	-0.013770	458	-0.014670
339	-0.009300	379	-0.012600	419	-0.013780	459	-0.014390
340	-0.009110	380	-0.012650	420	-0.013920	460	-0.014510
341	-0.009000	381	-0.012640	421	-0.013880	461	-0.014490
342	-0.008910	382	-0.012640	422	-0.013910	462	-0.014530
343	-0.008750	383	-0.012670	423	-0.014130	463	-0.014500
344	-0.008480	384	-0.012680	424	-0.014040	464	-0.014570
345	-0.008350	385	-0.012740	425	-0.014040	465	-0.014480
346	-0.008120	386	-0.012880	426	-0.013930	466	-0.014620
347	-0.007860	387	-0.012740	427	-0.013990	467	-0.014640
348	-0.007700	388	-0.012770	428	-0.014090	468	-0.014630
349	-0.008570	389	-0.012770	429	-0.014010	469	-0.014700
350	-0.008480	390	-0.012830	430	-0.013970	470	-0.014650
351	-0.007560	391	-0.012850	431	-0.013980	471	-0.014900
352	-0.007810	392	-0.012830	432	-0.014060	472	-0.014660
353	-0.008090	393	-0.012750	433	-0.014180	473	-0.014700
354	-0.008570	394	-0.012800	434	-0.014220	474	-0.014880
355	-0.009280	395	-0.012840	435	-0.014200	475	-0.014690
356	-0.010160	396	-0.012760	436	-0.014240	476	-0.014830
357	-0.010790	397	-0.012960	437	-0.014340	477	-0.014750
358	-0.011260	398	-0.012810	438	-0.014300	478	-0.014870
359	-0.011470	399	-0.013050	439	-0.014300	479	-0.014900
360	-0.011550	400	-0.012850	440	-0.014330	480	-0.014840

chan	voltage	chan	voltage	chan	voltage
481	-0.014930	521	-0.015290	561	-0.015810
482	-0.014680	522	-0.015310	562	-0.016040
483	-0.014860	523	-0.015400	563	-0.015990
484	-0.014830	524	-0.015350	564	-0.015940
485	-0.014990	525	-0.015280	565	-0.016040
486	-0.014930	526	-0.015400	566	-0.015820
487	-0.014980	527	-0.015340	567	-0.015940
488	-0.014940	528	-0.015320	568	-0.015880
489	-0.014860	529	-0.015280	569	-0.016040
490	-0.014850	530	-0.015470	570	-0.016200
491	-0.014920	531	-0.015430	571	-0.016260
492	-0.014840	532	-0.015350	572	-0.016150
493	-0.014880	533	-0.015440	573	-0.016280
494	-0.014800	534	-0.015470	574	-0.016250
495	-0.014940	535	-0.015540	575	-0.016330
496	-0.015000	536	-0.015560	576	-0.016310
497	-0.014930	537	-0.015650	577	-0.016330
498	-0.015030	538	-0.015710	578	-0.016370
499	-0.015030	539	-0.015630	579	-0.016410
500	-0.015090	540	-0.015610	580	-0.016360
501	-0.014970	541	-0.015670	581	-0.016400
502	-0.015120	542	-0.015730	582	-0.016410
503	-0.015140	543	-0.015730	583	-0.016300
504	-0.015110	544	-0.015720	584	-0.016420
505	-0.015100	545	-0.015760	585	-0.016380
506	-0.015180	546	-0.015770	586	-0.016450
507	-0.015310	547	-0.015740	587	-0.016450
508	-0.015110	548	-0.016000	588	-0.016400
509	-0.015260	549	-0.015730	589	-0.016620
510	-0.015210	550	-0.015710	590	-0.016400
511	-0.015270	551	-0.015970	591	-0.016600
512	-0.015280	552	-0.015920	592	-0.016390
513	-0.015280	553	-0.015780	593	-0.016510
514	-0.015340	554	-0.015920	594	-0.016500
515	-0.015280	555	-0.015770	595	-0.016540
516	-0.015350	556	-0.015810	596	-0.016560
517	-0.015300	557	-0.015650	597	-0.016460
518	-0.015290	558	-0.015790	598	-0.016580
519	-0.015390	559	-0.015850	599	-0.016740
520	-0.015310	560	-0.015880		

Appendix C

This appendix contains the results of bulk data analysis on 643 sets of data taken sequentially over a period of 5 days during February 1999. The details of the procedure used to generate these plots is discussed in Chapter 4. Key features to note are the large uncertainties on much of the data (compare with "best data" used to understand the lineshape fit) which lead to the conclusion that 81% of the data is not of sufficiently high quality to reliably establish target polarization.

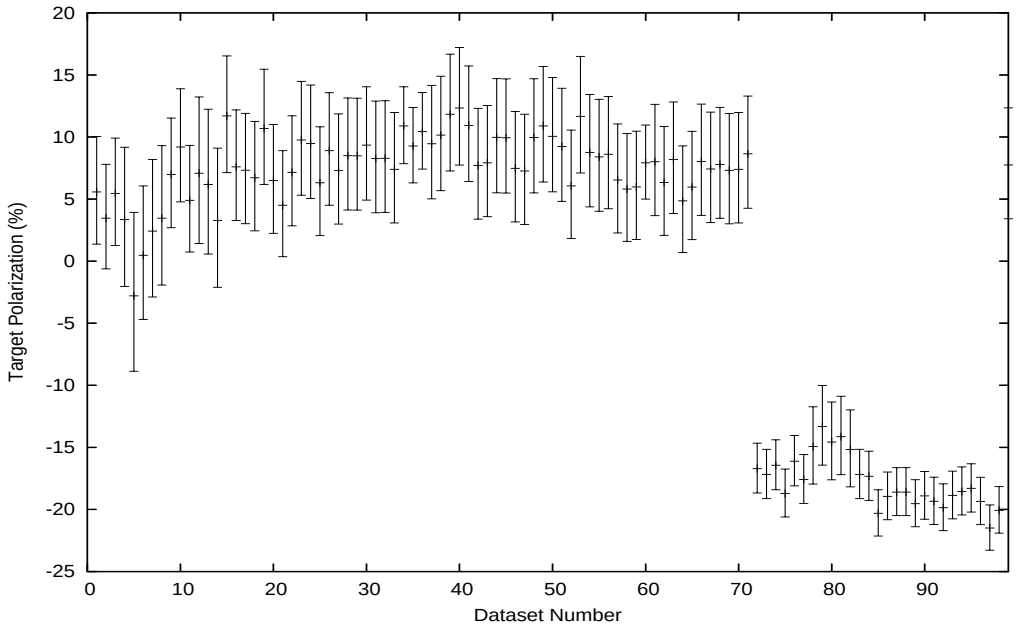

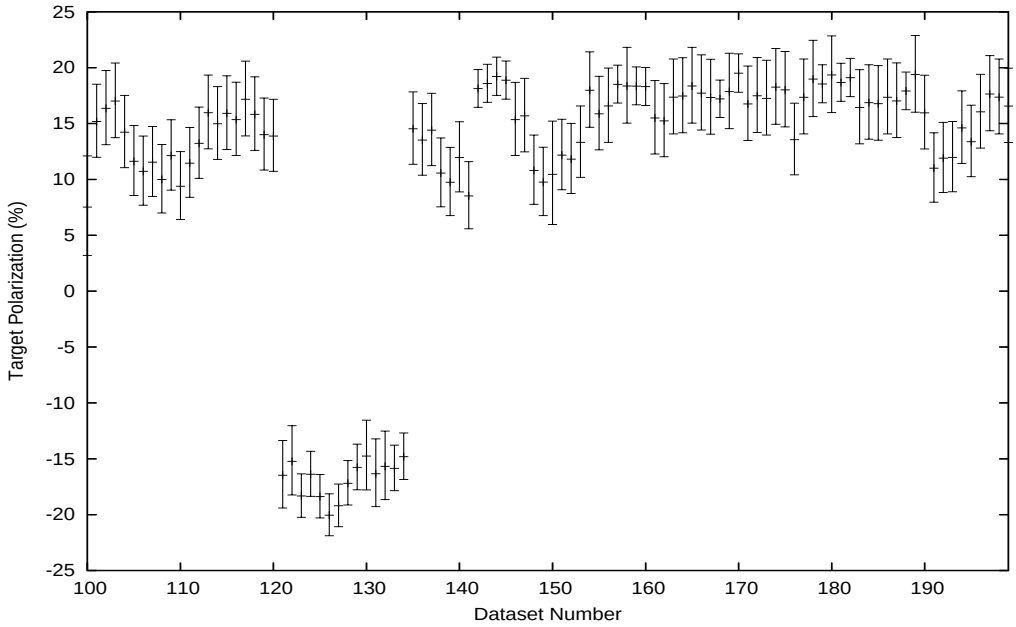
Target Polarization (%)
Dataset Number
25
20
15
10
5
0
-5
-10
-15
-20
-25
100
110
120
130
140
150
160
170
180
190

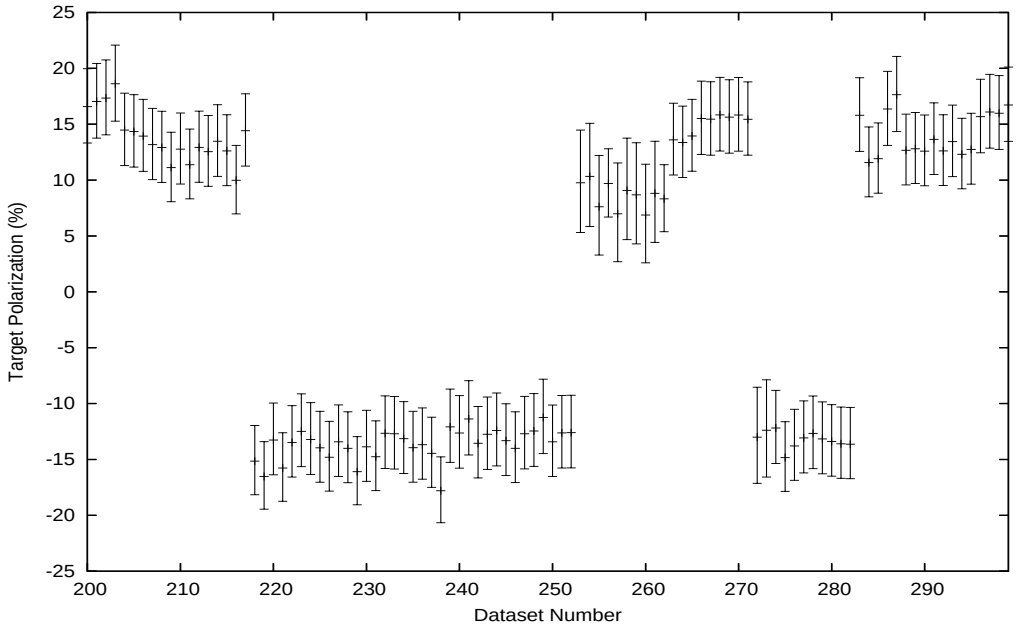
Target Polarization (%)
Dataset Number
25
20
15
10
5
0
-5
-10
-15
-20
-25
200
210
220
230
240
250
260
270
280
290

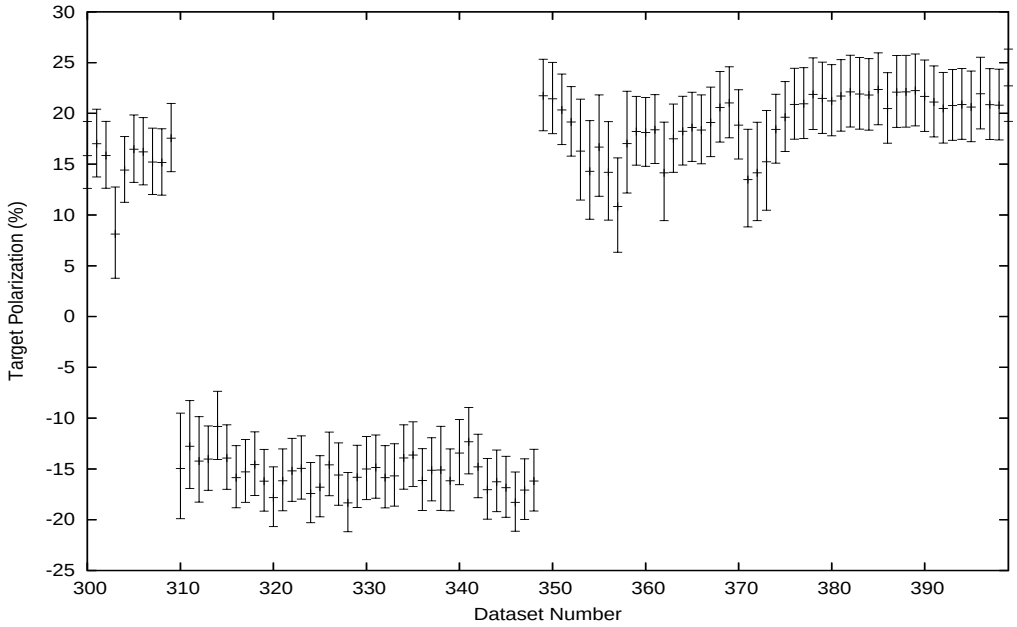
Target Polarization (%)
Dataset Number
30
25
20
15
10
5
0
-5
-10
-15
-20
-25
300
310
320
330
340
350
360
370
380
390

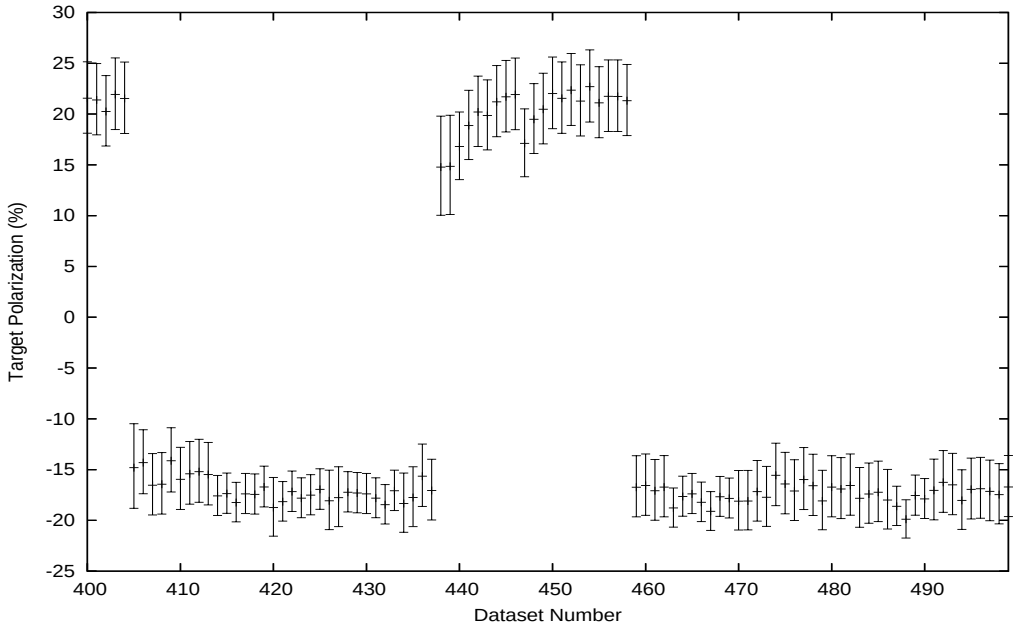
Target Polarization (%)
Dataset Number
30
25
20
15
10
5
0
-5
-10
-15
-20
-25
400
410
420
430
440
450
460
470
480
490

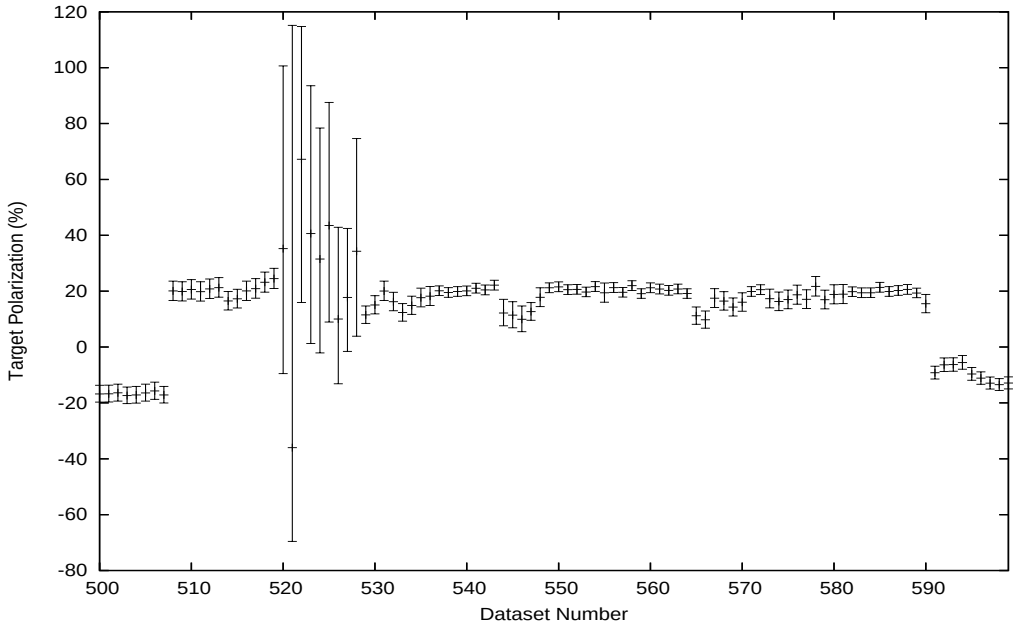
Target Polarization (%)
Dataset Number
120
100
80
60
40
20
0
-20
-40
-60
-80
500
510
520
530
540
550
560
570
580
590

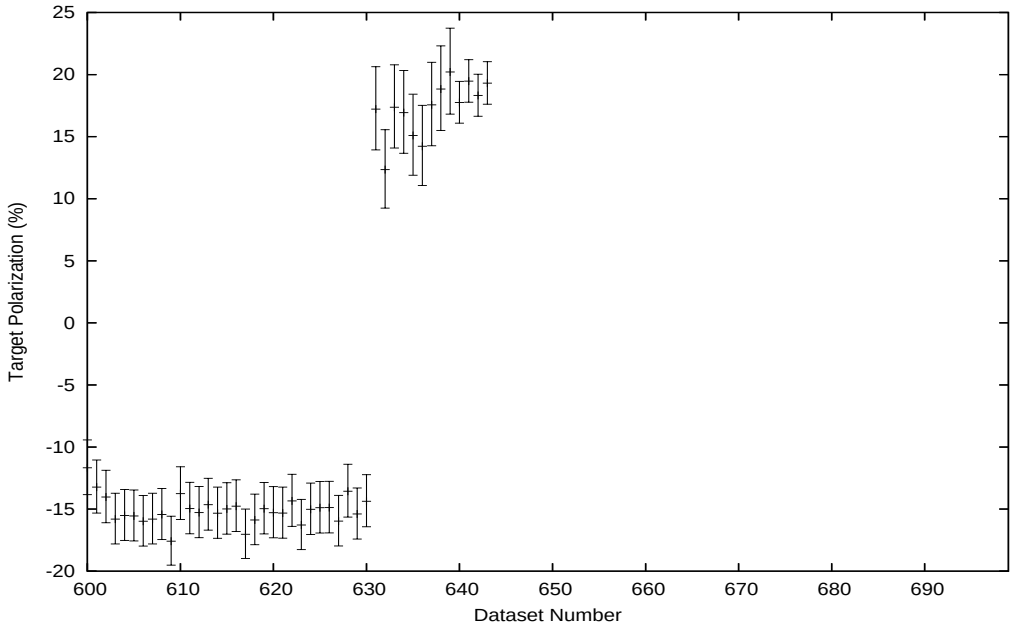
Target Polarization (%)
Dataset Number
25
20
15
10
5
0
-5
-10
-15
-20
600
610
620
630
640
650
660
670
680
690